

REPORT DOCUMENTATION PAGE			Form Approved OMB No. 0704-0188	
Public reporting burden for this collection of information is estimated to average 1 hour per response, including the time for reviewing instructions, searching existing data sources, gathering and maintaining the data needed, and completing and reviewing the collection of information. Send comments regarding this burden estimate or any other aspect of this collection of information, including suggestions for reducing this burden, to Washington Headquarters Services, Directorate for Information Operations and Reports, 1215 Jefferson Davis Highway, Suite 1204, Arlington, VA 22202-4302, and to the Office of Management and Budget, Paperwork Reduction Project (0704-0188), Washington, DC 20503.				
1. AGENCY USE ONLY (Leave blank)	2. REPORT DATE 3.Nov.99	3. REPORT TYPE AND DATES COVERED THESIS		
4. TITLE AND SUBTITLE AN INTERCOMPARISON OF HURRICANE FORECASTS USING SSM/I AND TRMM RAIN RATE ALGORITHM(S)		5. FUNDING NUMBERS		
6. AUTHOR(S) CAPT TIBBETTS ROBERT T				
7. PERFORMING ORGANIZATION NAME(S) AND ADDRESS(ES) FLORIDA STATE UNIVERSITY		8. PERFORMING ORGANIZATION REPORT NUMBER		
9. SPONSORING/MONITORING AGENCY NAME(S) AND ADDRESS(ES) THE DEPARTMENT OF THE AIR FORCE AFIT/CIA, BLDG 125 2950 P STREET WPAFB OH 45433		10. SPONSORING/MONITORING AGENCY REPORT NUMBER FY99-405		
11. SUPPLEMENTARY NOTES				
12a. DISTRIBUTION AVAILABILITY STATEMENT Unlimited distribution In Accordance With AFI 35-205/AFIT Sup 1			12b. DISTRIBUTION CODE	
13. ABSTRACT (Maximum 200 words)				
<div style="display: flex; justify-content: space-between; align-items: center;"> <div style="text-align: center;"> DISTRIBUTION STATEMENT A Approved for Public Release Distribution Unlimited </div> <div style="font-size: 2em; font-weight: bold;">19991117 085</div> </div>				
14. SUBJECT TERMS			15. NUMBER OF PAGES 126	
			16. PRICE CODE	
17. SECURITY CLASSIFICATION OF REPORT	18. SECURITY CLASSIFICATION OF THIS PAGE	19. SECURITY CLASSIFICATION OF ABSTRACT	20. LIMITATION OF ABSTRACT	

DTIC QUALITY INSPECTED 4

AN INTERCOMPARISON OF HURRICANE FORECASTS USING SSM/I AND TRMM RAIN RATE ALGORITHM(S)

Name: R. Thomas Tibbetts
Department: Meteorology
Major Professor: Dr. T.N. Krishnamurti
Degree: Master of Science
Term Degree Awarded: Summer Semester, 1999

Three different Special Sensor Microwave Imager (SSM/I) rain rate algorithms are evaluated as a means of improving both the physical initialization and the hurricane forecast output of the Florida State University Global Spectral Model (FSU GSM). These SSM/I rain rate algorithms are known as Cal/Val, NESDIS, and GPROF 4.0. In addition, the Tropical Rainfall Measuring Mission (TRMM) TMI – 2A12 rain rate algorithm is validated, and its impact on the FSU GSM is also studied.

Validation results of the Cal/Val rain rate algorithm show a bias toward gross underestimation. Both the NESDIS and GPROF 4.0 algorithms produce robust rain rates, in agreement with surface based observations. However, the NESDIS SSM/I rain rate algorithm proves to be the most consistent and accurate in this study. While the TRMM satellite has been described as vastly superior to the SSM/I platforms, this research has concluded the TRMM / TMI – 2A12 rain rate algorithm is in need of modification.

The impact of different magnitudes of rain on the FSU GSM is significant. This thesis has shown that the use of NESDIS SSM/I rain rates in the physical initialization of the

FSU GSM provides the most accurate hurricane track forecasts. In addition, a small improvement in forecast hurricane wind intensity has been achieved. Finally, use of the GPROF algorithm yields a notable improvement in forecast minimum central pressure.

ABSTRACT

Three different Special Sensor Microwave Imager (SSM/I) rain rate algorithms are evaluated as a means of improving both the physical initialization and the hurricane forecast output of the Florida State University Global Spectral Model (FSU GSM). These SSM/I rain rate algorithms are known as Cal/Val, NESDIS, and GPROF 4.0. In addition, the Tropical Rainfall Measuring Mission (TRMM) TMI – 2A12 rain rate algorithm is validated, and its impact on FSU GSM hurricane forecasts is also studied.

Validation results of the Cal/Val rain rate algorithm show a bias toward gross underestimation. Both the NESDIS and GPROF 4.0 algorithms produce robust rain rates, in agreement with surface based observations. However, the NESDIS SSM/I rain rate algorithm proves to be the most consistent and accurate in this study. While the TRMM satellite has been described as vastly superior to the SSM/I platforms, this research has concluded the TRMM / TMI – 2A12 rain rate algorithm is in need of modification.

The impact of different magnitudes of rain on the FSU GSM is significant. This thesis has shown that the use of NESDIS SSM/I rain rates in the physical initialization of the FSU GSM provides the most accurate hurricane track forecasts. In addition, a small improvement in forecast hurricane wind intensity has been achieved. Finally, use of the GPROF algorithm yields a notable improvement in forecast minimum central pressure.

THE FLORIDA STATE UNIVERSITY

COLLEGE OF ARTS AND SCIENCES

**AN INTERCOMPARISON OF HURRICANE FORECASTS
USING SSM/I AND TRMM RAIN RATE ALGORITHM(S)**


By

R. THOMAS TIBBETTS

A thesis submitted to the
Department of Meteorology
in partial fulfillment of the
requirements for the degree of
Master of Science

Degree Awarded:
Summer Semester, 1999

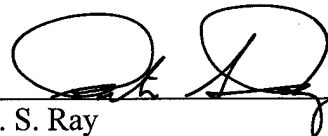
The members of the Committee approve the thesis of R. Thomas Tibbetts defended
on July 1st, 1999.



T. N. Krishnamurti
Professor Directing Thesis



N. E. LaSeur
Committee Member



P. S. Ray
Committee Member

This thesis is dedicated to my wife, Kristen, who supported me wholeheartedly throughout my masters degree program. Without her love and support at home, this research would not have been completed. Seven years ago Kristen convinced me to pursue an education in meteorology. I owe my past and future accomplishments in the weather career field to her.

My research is equally dedicated to my two year old son, Nathan. The countless hours I spent completing this experiment certainly came at the expense of our time together. Despite this, Nathan's expressions of love and excitement each day I returned home from school kept me motivated until the end. I can't wait, Nathan, until you are old enough to learn about the wonders of weather.

ACKNOWLEDGMENTS

Dr. T. N. Krishnamurti deserves recognition for his leadership and support, both of which were instrumental to the success of my research project. Two years ago, Dr. Krishnamurti extended me the opportunity to join his laboratory and study cutting-edge research in hurricane prediction. It is for his trust in me that I am most grateful.

Special thanks go to both Dr. N. E. LaSeur and Dr. P. S. Ray for serving as committee members throughout the course of my research. The knowledge I learned from them regarding synoptic scale weather and cloud physics greatly contributed to my understanding of numerical weather prediction.

Major Ed Bensman is due the utmost respect and admiration for his continuous assistance throughout my entire master's degree program. Ed Bensman's keen knowledge of meteorology, plus his personal commitment to aid those in need, contribute to the outstanding Air Force weather officer he represents each and every day. I owe the successful completion of both this thesis *and* my entire master's degree program to the professional relationship we have developed over the last two years.

While the entire "Krish" lab contributed support to my research, certain individuals deserve special recognition. First, I give thanks for Eric Williford's continuous assistance and patience as I learned the tools necessary to manipulate the FSU GSM.

Eric's knowledge of the FSU GSM is outstanding. Dr. Krishnamurti's lab continues to benefit from his services daily. Second, Curtis Knox is due thanks for all the times he breathed life back into the computer systems I crashed, especially when he was the only one around at 0730 hours each day. Third, Ricardo Correa-Torres and Brian Mackey deserve recognition for answering all the small but significant questions I pestered them with over the last year. Last but certainly not least, Dr. C. M. Kishtawal was extremely helpful in the acquisition of TRMM / TMI data.

Finally, the United States Air Force must be acknowledged for its sponsorship of my master's degree program. This research would not have been accomplished without the support of the AFIT/CI graduate program in meteorology. The knowledge acquired in the last two years will certainly benefit both Air Force Weather and myself.

TABLE OF CONTENTS

List of Tables	viii
List of Figures	xi
Abstract	xvi

<u>Chapter</u>	<u>Page</u>
1. Special Sensor Microwave Imager (SSM/I) Rain Rate Retrieval	1
1.1 SSM/I overview	1
1.2 Overview of the Navy Cal/Val SSM/I algorithm	7
1.3 Overview of the Navy third generation NOAA/NESDIS SSM/I algorithm ...	11
1.3.1 NESDIS scattering algorithm	15
1.3.2 NESDIS emission algorithm	17
1.4 Overview of the GPROF 4.0 SSM/I algorithm	19
2. SSM/I Rain Rate Algorithm Validation & Comparison	26
2.1 Global rain rate averages	26
2.2 Case studies of the Cal/Val, NESDIS, and GPROF rain rate algorithms	27
2.3 SSM/I rain rate comparison studies	28
2.3.1 Case 1: July 13, 1998 (Julian Day 194)	28
2.3.2 Case 2: October 29, 1998 (Julian Day 302)	32
2.3.3 Case 3: September 21-22, 1998 (Julian Days 264-265)	35
2.3.4 Case 4: August 26-27, 1998 (Julian Days 238-239)	38
2.4 NEXRAD – SSM/I rain rate comparison	41
2.5 SSM/I algorithm comparison synopsis	45
3. FSU Global Spectral Model (FSU GSM)	
Physical Initialization	46
3.1 Brief description of the FSU Global Spectral Model (FSU GSM)	46
3.2 The use of rainfall rates within the physical initialization process	48
3.3 Reverse similarity theory	51

<u>Chapter</u>	<u>Page</u>
3.4 Reverse cumulus parameterization	55
3.5 Outgoing longwave radiation (OLR) merging	56
3.6 Newtonian relaxation	58
4. FSU Global Spectral Model: Hurricane Forecasts	60
4.1 Overview	60
4.2.1 Hurricane Bonnie (72 hour forecast)	61
4.2.2 Hurricane Bonnie (48 hour forecast)	67
4.3.1 Hurricane Danielle (72 hour forecast)	70
4.3.2 Hurricane Danielle (48 hour forecast)	74
4.4.1 Hurricane Georges (72 hour forecast)	78
4.5.1 Hurricane Mitch (72 hour forecast)	81
4.5.2 Hurricane Mitch (48 hour forecast)	85
5. Tropical Rainfall Measuring Mission (TRMM)	
TMI – 2A12 Rain Rate Algorithm	89
5.1 TRMM overview	89
5.2 TRMM microwave imager (TMI)	90
5.3 TRMM / TMI – 2A12 rain rate algorithm	92
5.4 TMI – 2A12 rain rate validation	94
5.4.1 Case 1: July 13, 1998 (Julian Day 194)	94
5.4.2 Case 2: October 29, 1998 (Julian Day 302)	95
5.4.3 Case 3: September 21-22, 1998 (Julian Days 264-265)	95
5.5 TRMM / TMI – 2A12 hurricane forecasts	97
5.6.1 Hurricane Bonnie (72 hour forecast)	97
5.6.2 Hurricane Bonnie (48 hour forecast)	101
5.7.1 Hurricane Danielle (72 hour forecast)	104
5.7.2 Hurricane Danielle (48 hour forecast)	107
5.8.1 Hurricane Georges (72 hour forecast)	110
5.9.1 Hurricane Mitch (72 hour forecast)	113
5.9.2 Hurricane Mitch (48 hour forecast)	116
6. Conclusions	119
References	123
Biographical Sketch	126

LIST OF TABLES

<u>Table</u>	<u>Page</u>
4-1.1 Forecast track deviations for Hurricane Bonnie (3 day forecast)	64
4-2.1 Forecast wind intensity deviations for Hurricane Bonnie (3 day forecast)	65
4-3.1 Minimum central pressure deviations for Hurricane Bonnie (3 day forecast)	66
4-4.1 Forecast track deviations for Hurricane Bonnie (2 day forecast)	68
4-5.1 Forecast wind intensity deviations for Hurricane Bonnie (2 day forecast)	68
4-6.1 Minimum central pressure deviations for Hurricane Bonnie (2 day forecast)	69
4-7.1 Forecast track deviations for Hurricane Danielle (3 day forecast)	72
4-8.1 Forecast wind intensity deviations for Hurricane Danielle (3 day forecast) ..	73
4-9.1 Minimum central pressure deviations for Hurricane Danielle (3 day forecast)	73
4-10.1 Forecast track deviations for Hurricane Danielle (2 day forecast)	75
4-11.1 Forecast wind intensity deviations for Hurricane Danielle (2 day forecast) ..	76
4-12.1 Minimum central pressure deviations - Hurricane Danielle (2 day forecast)	77
4-13.1 Forecast track deviations for Hurricane Georges (3 day forecast)	79
4-14.1 Forecast wind intensity deviations for Hurricane Georges (3 day forecast) ..	79
4-15.1 Minimum central pressure deviations for Hurricane Georges (3 day forecast)	80
4-16.1 Forecast track deviations for Hurricane Mitch (3 day forecast)	83
4-17.1 Forecast wind intensity deviations for Hurricane Mitch (3 day forecast)	83

<u>Table</u>	<u>Page</u>
4-18.1 Minimum central pressure deviations for Hurricane Mitch (3 day forecast)	84
4-19.1 Forecast track deviations for Hurricane Mitch (2 day forecast)	86
4-20.1 Forecast wind intensity deviations for Hurricane Mitch (2 day forecast)	87
4-21.1 Minimum central pressure deviations - Hurricane Mitch (2 day forecast) ...	88
5-7.1 Forecast track deviations for Hurricane Bonnie (3 day forecast)	98
5-8.1 Forecast wind intensity deviations for Hurricane Bonnie (3 day forecast) ..	99
5-9.1 Minimum central pressure deviations for Hurricane Bonnie (3 day forecast)	100
5-10.1 Forecast track deviations for Hurricane Bonnie (2 day forecast)	102
5-11.1 Forecast wind intensity deviations for Hurricane Bonnie (2 day forecast) ..	102
5-12.1 Minimum central pressure deviations for Hurricane Bonnie (2 day forecast)	102
5-13.1 Forecast track deviations for Hurricane Danielle (3 day forecast)	105
5-14.1 Forecast wind intensity deviations for Hurricane Danielle (3 day forecast)	105
5-15.1 Minimum central pressure deviations for Hurricane Danielle (3 day forecast)	105
5-16.1 Forecast track deviations for Hurricane Danielle (2 day forecast)	108
5-17.1 Forecast wind intensity deviations for Hurricane Danielle (2 day forecast)	108
5-18.1 Minimum central pressure deviations - Hurricane Danielle (2 day forecast)	108
5-19.1 Forecast track deviations for Hurricane Georges (3 day forecast)	111
5-20.1 Forecast wind intensity deviations for Hurricane Georges (3 day forecast)	111
5-21.1 Minimum central pressure deviations for Hurricane Georges (3 day forecast)	111
5-22.1 Forecast track deviations for Hurricane Mitch (3 day forecast)	114

<u>Table</u>	<u>Page</u>
5-23.1 Forecast wind intensity deviations for Hurricane Mitch (3 day forecast) ...	114
5-24.1 Minimum central pressure deviations for Hurricane Mitch (3 day forecast)	114
5-25.1 Forecast track deviations for Hurricane Mitch (2 day forecast)	117
5-26.1 Forecast wind intensity deviations for Hurricane Mitch (2 day forecast) ...	117
5-27.1 Minimum central pressure deviations - Hurricane Mitch (2 day forecast)	117
6-1.1 Average forecast track deviations for a total of four hurricanes and seven different experiments	120
6-2.1 Average forecast wind intensity deviations for a total of four hurricanes and seven different experiments	120
6-3.1 Average forecast minimum central pressure deviations for a total of four hurricanes and seven different experiments	121

LIST OF FIGURES

<u>Figure</u>	<u>Page</u>
1-1 SSM/I orbit and scan geometry	3
1-2 Cal/Val SSM/I rain rate algorithm flow chart	11
1-3 NESDIS SSM/I rain rate algorithm flow chart	19
1-4 GPROF 4.0 SSM/I rain rate algorithm flow chart	21
2-1 SSM/I rainfall for three different algorithms (August 24 th , 1998)	29
2-2 Cal/Val SSM/I rain rates, July 13 th , 1998 (mm/day)	30
2-3 NESDIS SSM/I rain rates, July 13 th , 1998 (mm/day)	30
2-4 GPROF 4.0 SSM/I rain rates, July 13 th , 1998 (mm/day)	31
2-5 Cal/Val SSM/I rain rates for Hurricane Mitch, October 29 th , 1998	33
2-6 NESDIS SSM/I rain rates for Hurricane Mitch, October 29 th , 1998	33
2-7 GPROF 4.0 SSM/I rain rates for Hurricane Mitch, October 29 th , 1998	34
2-8 Cal/Val SSM/I rain rates for Hurricane Georges, Sep 21 st – 22 nd , 1998	35
2-9 NESDIS SSM/I rain rates for Hurricane Georges, Sep 21 st – 22 nd , 1998	36
2-10 GPROF SSM/I rain rates for Hurricane Georges, Sep 21 st – 22 nd , 1998	38
2-11 Cal/Val SSM/I rain rates for Hurricane Bonnie, August 26 th – 27 th , 1998	39
2-12 NESDIS SSM/I rain rates for Hurricane Bonnie, August 26 th – 27 th , 1998 ...	40

<u>Figure</u>	<u>Page</u>
2-13 GPROF SSM/I rain rates for Hurricane Bonnie, August 26 th – 27 th , 1998	41
2-14 NEXRAD storm total precipitation (units = inches) – Hurricane Georges	42
2-15 Cal/Val SSM/I rain rates (units = inches) – Hurricane Georges	43
2-16 NESDIS SSM/I rain rates (units = inches) – Hurricane Georges	43
2-17 GPROF 4.0 SSM/I rain rates (units = inches) – Hurricane Georges	44
3-1 Rainfall estimation from a mix of outgoing longwave radiation (OLR) and SSM/I	57
3-2 The physical initialization procedure	59
4-1 72-hour track forecast(s) using three SSM/I rain rate algorithms for Hurricane Bonnie. Forecast tracks are compared to the official, NHC observed “best track” positions at 6 hour intervals	62
4-2 FSU GSM wind intensity output using three different SSM/I algorithms	65
4-3 FSU GSM minimum central pressure output using three different SSM/I algorithms	66
4-4 48-hour track forecast(s) using three SSM/I rain rate algorithms for Hurricane Bonnie. Forecast tracks are compared to the official, NHC observed “best track” positions at 6 hour intervals	67
4-5 FSU GSM wind intensity output using three different SSM/I algorithms	69
4-6 FSU GSM minimum central pressure output using three different SSM/I algorithms	70
4-7 72-hour track forecast(s) using three SSM/I rain rate algorithms for Hurricane Danielle. Forecast tracks are compared to the official, NHC observed “best track” positions at 6 hour intervals	71
4-8 FSU GSM wind intensity output using three different SSM/I algorithms	72

<u>Figure</u>	<u>Page</u>
4-9 FSU GSM minimum central pressure output using three different SSM/I algorithms	74
4-10 48-hour track forecast(s) using three SSM/I rain rate algorithms for Hurricane Danielle. Forecast tracks are compared to the official, NHC observed "best track" positions at 6 hour intervals	75
4-11 FSU GSM wind intensity output using three different SSM/I algorithms	76
4-12 FSU GSM minimum central pressure output using three different SSM/I algorithms	77
4-13 72-hour track forecast(s) using three SSM/I rain rate algorithms for Hurricane Georges	78
4-14 FSU GSM wind intensity output using three different SSM/I algorithms	80
4-15 FSU GSM minimum central pressure output using three different SSM/I algorithms	81
4-16 72-hour track forecast(s) using three SSM/I rain rate algorithms for Hurricane Mitch	82
4-17 FSU GSM wind intensity output using three different SSM/I algorithms	84
4-18 FSU GSM minimum central pressure output using three different SSM/I algorithms	85
4-19 48-hour track forecast(s) using three SSM/I rain rate algorithms for Hurricane Mitch	86
4-20 FSU GSM wind intensity output using three different SSM/I algorithms	87
4-21 FSU GSM minimum central pressure output using three different SSM/I algorithms	88
5-1 TRMM satellite orbit	90

<u>Figure</u>	<u>Page</u>
5-2 TMI scan geometry	91
5-3 TRMM TMI – 2A12 rain rate algorithm flow chart	92
5-4 TMI – 2A12 rain rates, July 13 th , 1998 (mm/day)	94
5-5 TMI – 2A12 rain rates for Hurricane Mitch, October 29 th , 1998	96
5-6 TMI – 2A12 rain rates for Hurricane Georges, Sep 21 st – 22 nd , 1998	96
5-7 72-hour track forecast using TRMM/NESDIS blended rain rates. SSM/I based model experiments are included for comparison purposes	98
5-8 FSU GSM wind intensity output using TRMM/NESDIS blended rain rates. SSM/I based forecasts are included for comparison purposes	99
5-9 FSU GSM minimum central pressure output using TRMM/NESDIS blended rain rates. SSM/I based forecasts are included for comparison purposes	100
5-10 48-hour track forecast using TRMM/NESDIS blended rain rates. SSM/I based model experiments are included for comparison purposes	101
5-11 FSU GSM wind intensity output using TRMM/NESDIS blended rain rates. SSM/I based forecasts are included for comparison purposes	103
5-12 FSU GSM minimum central pressure output using TRMM/NESDIS blended rain rates. SSM/I based forecasts are included for comparison purposes	103
5-13 72-hour track forecast using TRMM/NESDIS blended rain rates. SSM/I based model experiments are included for comparison purposes	104
5-14 FSU GSM wind intensity output using TRMM/NESDIS blended rain rates. SSM/I based forecasts are included for comparison purposes	106
5-15 FSU GSM minimum central pressure output using TRMM/NESDIS blended rain rates. SSM/I based forecasts are included for comparison purposes	106
5-16 48-hour track forecast using TRMM/NESDIS blended rain rates. SSM/I based model experiments are included for comparison purposes	107

<u>Figure</u>	<u>Page</u>
5-17 FSU GSM wind intensity output using TRMM/NESDIS blended rain rates. SSM/I based forecasts are included for comparison purposes	109
5-18 FSU GSM minimum central pressure output using TRMM/NESDIS blended rain rates. SSM/I based forecasts are included for comparison purposes	109
5-19 72-hour track forecast using TRMM/NESDIS blended rain rates. SSM/I based model experiments are included for comparison purposes	110
5-20 FSU GSM wind intensity output using TRMM/NESDIS blended rain rates. SSM/I based forecasts are included for comparison purposes	112
5-21 FSU GSM minimum central pressure output using TRMM/NESDIS blended rain rates. SSM/I based forecasts are included for comparison purposes	112
5-22 72-hour track forecast using TRMM/NESDIS blended rain rates. SSM/I based model experiments are included for comparison purposes	113
5-23 FSU GSM wind intensity output using TRMM/NESDIS blended rain rates. SSM/I based forecasts are included for comparison purposes	115
5-24 FSU GSM minimum central pressure output using TRMM/NESDIS blended rain rates. SSM/I based forecasts are included for comparison purposes	115
5-25 48-hour track forecast using TRMM/NESDIS blended rain rates. SSM/I based model experiments are included for comparison purposes	116
5-26 FSU GSM wind intensity output using TRMM/NESDIS blended rain rates. SSM/I based forecasts are included for comparison purposes	118
5-27 FSU GSM minimum central pressure output using TRMM/NESDIS blended rain rates. SSM/I based forecasts are included for comparison purposes	118

ABSTRACT

Three different Special Sensor Microwave Imager (SSM/I) rain rate algorithms are evaluated as a means of improving both the physical initialization and the hurricane forecast output of the Florida State University Global Spectral Model (FSU GSM). These SSM/I rain rate algorithms are known as Cal/Val, NESDIS, and GPROF 4.0. In addition, the Tropical Rainfall Measuring Mission (TRMM) TMI – 2A12 rain rate algorithm is validated, and its impact on FSU GSM hurricane forecasts is also studied.

Validation results of the Cal/Val rain rate algorithm show a bias toward gross underestimation. Both the NESDIS and GPROF 4.0 algorithms produce robust rain rates, in agreement with surface based observations. However, the NESDIS SSM/I rain rate algorithm proves to be the most consistent and accurate in this study. While the TRMM satellite has been described as vastly superior to the SSM/I platforms, this research has concluded the TRMM / TMI – 2A12 rain rate algorithm is in need of modification.

The impact of different magnitudes of rain on the FSU GSM is significant. This thesis has shown that the use of NESDIS SSM/I rain rates in the physical initialization of the FSU GSM provides the most accurate hurricane track forecasts. In addition, a small improvement in forecast hurricane wind intensity has been achieved. Finally, use of the GPROF algorithm yields a notable improvement in forecast minimum central pressure.

CHAPTER 1

SPECIAL SENSOR MICROWAVE IMAGER (SSM/I)

RAIN RATE RETRIEVAL

1.1 SSM/I Overview

Since the late 1980's, the Special Sensor Microwave Imager (SSM/I) has made significant contributions to the remote sensing of global precipitation. The precipitation estimates derived from the SSM/I have been and continue to be utilized for various meteorological applications, including numerical weather prediction (NWP). In data sparse regions such as the oceans, the SSM/I has proven itself to be an immensely valuable tool to obtain daily precipitation values in such areas where ground and radar based observations are not available. This constitutes a key element in the physical initialization of certain numerical weather prediction models, including the Florida State University Global Spectral Model (FSU GSM). Without accurate estimates of daily, global precipitation, real-time physical modeling of weather systems of all scales is difficult to achieve. The following paragraphs will emphasize the important role of the SSM/I in obtaining reliable rain rate estimates, to include the operation of the microwave imager and various algorithms used to calculate global rain rates.

The SSM/I is a seven-channel, four frequency, linearly polarized, passive microwave

radiometer which measures radiation emitted from the earth at 19.35, 22.235, 37.0, and 85.5 GHz. The seven separate total-power radiometers simultaneously measure the microwave emission originating from the earth's surface and the intervening atmosphere. The SSM/I receives both horizontally and vertically linearly polarized radiation at 19, 37, and 85 GHz. The 22 GHz frequency only receives vertically polarized radiation. Vertical and horizontal polarizations will be subsequently referred to as V and H, respectively.

The Defense Meteorological Satellite Program (DMSP) is responsible for the launch, maintenance, and operation of the polar orbiting satellite(s) which host the SSM/I. The first SSM/I instrument was launched on June 19th, 1987, aboard the DMSP Block 5D-2 Spacecraft F-8. This and subsequent SSM/I satellites are commonly referred to by their "F" identifier, such as F-8. Since the SSM/I satellites are subject to a limited operational lifespan, only three SSM/I satellites currently remain operational: F-11, F-13, and F-14. The data utilized in this study is a combination of all three of these operational satellites. Data for time periods prior to November 28th, 1991, can only be obtained from the F-8 and F-10 satellites. According to Ferraro and Marks (1995), the DMSP satellites operate in a sun-synchronous, near-polar orbit with an orbital period of about 101 minutes. Since the DMSP satellites are in sun-synchronous orbit, the ascending equatorial crossing time remains relatively constant with respect to the local time throughout the lifetime of the satellite. Earth observations are taken during a 102.4° segment of a circular rotation at an earth incidence angle of 53.1°. The 102.4° arc is centered on the satellite subtrack and corresponds to a 1400 km wide swath on the earth's surface, which results in 24 hour

global coverage. The 19, 22, and 37 GHz channels sample every 25 km in both the scan direction and satellite direction. The 85 GHz channel, on the other hand, samples the earth every 12.5 km. Figure 1-1 depicts the SSM/I orbit and scan geometry.

According to Wentz (1991), the SSM/I uses an offset parabolic reflector to collect the microwave radiation. The reflector, dimensioned 61 x 66 cm, focuses the radiation into a corrugated, broad-band, 7-port feedhorn. The rotation period of the reflector-feedhorn unit is 1.9 seconds. During each SSM/I scan, the 85 GHz channels are sampled 128 times over the 102.4° scan region. The integration period for a single sample is 3.89 ms.

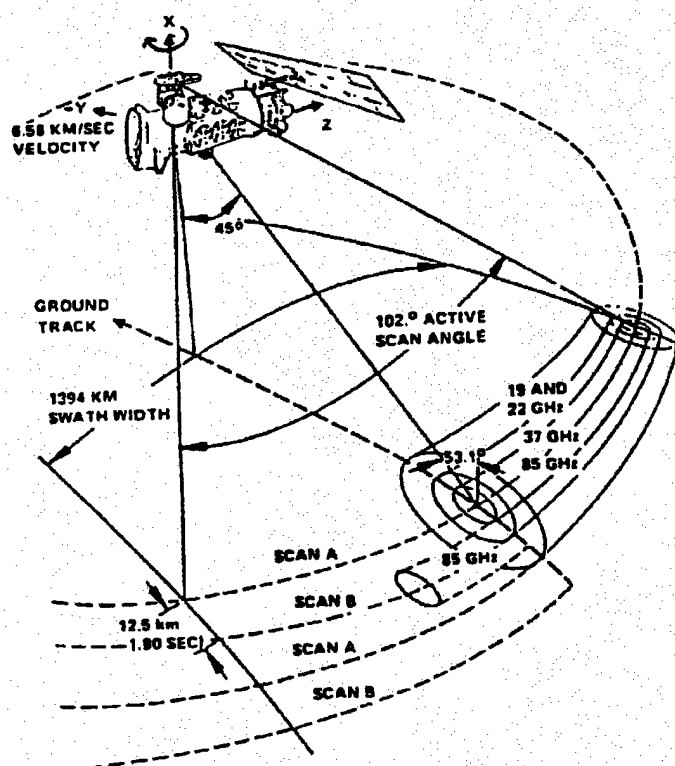


Figure 1-1: SSM/I orbit and scan geometry

This results in 128 uniformly spaced, vertically polarized footprints and 128 horizontally polarized footprints. Observations at the 19, 22, and 37 GHz channels are only taken every other scan. 'A-scans' refer to the sampling of the lower channels, while 'B-scans' refer to 85 GHz sampling. During an A-scan, the 19, 22, and 37 GHz channels are sampled 64 times with an integration period of 7.95 ms.

Both SSM/I antenna temperature (T_a) and SSM/I brightness temperature (T_b) calculations must be performed before rain rate algorithms can be applied to the data. According to Wentz (1991), SSM/I antenna temperature computations are based upon the assumption that the radiometer output voltage is linearly related to the input power at the mixer/preamplifier. The output voltage, V_i , is converted to counts by applying a scaling factor and a constant offset such that:

$$C_i = \omega V_i - P \quad (1)$$

where the subscript i denotes either a cold-space observation ($i = C$), a hot-load observation ($i = H$), or an earth observation ($i = E$).

As mentioned earlier, the variable V_i in equation (1) is termed the radiometer output voltage. This *output* voltage is linearly related to the *input* power, which is expressed in terms of radiation temperature according to:

$$V_i = ck\beta g(T_{Ai} + T_N) \quad (2)$$

where T_{Ai} is the radiation temperature entering the feedhorn, T_N is the radiometer noise temperature, c is the detector constant, k is the Boltzmann constant, β is the receiver predetection bandwidth, and g is the receiver gain. Both g and T_N are assumed to be

the same for cold-space, hot-load, and earth observations. Nonlinear effects are assumed to be negligible.

By combining (1) and (2) for $i = C, H$, and E , the following relationships are achieved:

$$T_{AE} = AC_E + B \quad (3)$$

$$A = (T_{AH} - T_{AC}) / (C_H - C_C) \quad (4)$$

$$B = (T_{AC}C_H - T_{AH}C_C) / (C_H - C_C) \quad (5)$$

where:

$$T_{AH} = T_{oH} + 0.01(T_{oP} - T_{oH}) \quad (6)$$

and T_{oH} , T_{oP} are the physical temperatures of the hot load and the radiator plate facing the hot load. T_{AC} , the cold-space antenna temperature, is set to 2.7 Kelvin for all channels. Using the values for each of the variables contained in the above equations, the A-scan and B-scan coefficients can quickly be computed according to (4) and (5). Using these A-scan and B-scan coefficients, T_{AE} can be computed according to (3), which then can be used in equation (2) to obtain the relationship between input power and radiation temperature. This relationship is integral to further calculations since antenna temperature is a measure of the radiant power entering the SSM/I feedhorn. By integrating over the gain pattern of the parabolic reflector and feedhorn assembly, the antenna temperature(s) can be computed according to:

$$T_A = \int d\Omega (G_{vp} T_{Bv} + G_{hp} T_{Bh}) \quad (7)$$

where: $d\Omega$ is the differential solid angle and the integral is over the entire 4π steradians of a sphere; G is the antenna gain in the direction $d\Omega$ for vertically and horizontally polarized radiation received by port p ; and T_B refers to the vertically and horizontally polarized brightness temperatures coming from the $d\Omega$ direction. In order for rain rate estimation algorithms to be applied to the SSM/I data, antenna temperatures must be converted to brightness temperatures. The conversion method is discussed next.

An ocean brightness temperature model developed by Wentz (1991) is used to compute the polarized brightness temperatures. This model computes T_{Bv} and T_{Bh} over the entire SSM/I, 860 km altitude field of view. A system of two linear equations is inverted to express brightness temperature in terms of antenna temperature according to:

$$T_{Bv} = A_{vv}T_{Av} + A_{hv}T_{Ah} + 2.7A_{ov} \quad (8)$$

$$T_{Bh} = A_{hh}T_{Ah} + A_{vh}T_{Av} + 2.7A_{oh} \quad (9)$$

where the factor 2.7 is the temperature of cold-space. The A coefficients are functions of the spillover factor δ and the cross-polarization factor χ_p according to:

$$A_{vv} = (1 + \chi_v) / [(1 - \chi_v\chi_h)(1 - \delta)] \quad (10)$$

$$A_{hv} = -\chi_v(1 + \chi_h) / [(1 - \chi_v\chi_h)(1 - \delta)] \quad (11)$$

$$A_{hh} = (1 + \chi_h) / [(1 - \chi_v\chi_h)(1 - \delta)] \quad (12)$$

$$A_{vh} = -\chi_h(1 + \chi_v) / [(1 - \chi_v\chi_h)(1 - \delta)] \quad (13)$$

$$A_{ov} = A_{oh} = -\delta / (1 - \delta) \quad (14)$$

Least-squares regression expressing T_B as a function of T_A provides the final relationship:

$$T_{Bv} = 1.01993T_{Av} + 1.994 \quad (15)$$

which happens to be an example of the regression formula valid only at 22 GHz.

Separate but similar regression formulae exist for each of the other channels. It is important to note that over land, brightness temperatures are depolarized according to:

$$T_{Bv} = T_{Av} / (1 - \delta) - 2.7\delta / (1 - \delta) \quad (16)$$

Using the above relationships to obtain antenna temperatures and brightness temperatures for each of the seven channels, estimations of the global rain rate field can subsequently be computed using various SSM/I *rain rate algorithms*. These algorithms will be highlighted in the following paragraphs.

1.2 Overview of the Navy Cal/Val SSM/I Algorithm

The Cal/Val algorithm is the United States Navy's second generation precipitation retrieval algorithm. Developed by the Calibration/Validation group in the early 1990's, it replaced the Navy's D-Matrix algorithm for operational use. It is important to note that prior to this study, the Cal/Val algorithm served as the *primary* SSM/I rain rate algorithm used in the physical initialization of the FSU Global Spectral Model. Since 1991, SSM/I rain rates based upon the Cal/Val algorithm have been merged with Outgoing Longwave Radiation (OLR) data to produce a first guess, global rain rate field.

The Cal/Val algorithm is based upon the statistical regression of SSM/I brightness temperatures against collocated surface radar measurements of rain rate (Berg *et al.*, 1998). In other words, it can be called a statistical rain map. This algorithm is described by Olson et al. (1991) in Volume II of the Cal/Val Final Report (Cal/Val 1991). Training

data sets from radar-derived rain rates created at Kwajalein Atoll and Darwin, Australia, were used to develop this algorithm. The radar-derived rain rates were used in a regression expression relating the log of the rain rate to five of the seven SSM/I brightness temperatures over the ocean, but only to the 85 GHz vertical and horizontal brightness temperatures for land areas (Smith *et al.*, 1998).

The rainfall rate, R , is a function of the collocated SSM/I brightness temperature measurements. By regressing the brightness temperatures against rainfall rate in a stepwise multiple linear regression procedure, a retrieval formula of the type represented by equation (17) was determined.

$$R = a_0 + \sum_{i=1}^N a_i TB_i \quad (17)$$

Limited cloud radiative transfer modeling experiments proved that the nonlinear relationship between brightness temperature and rainfall rate could be expressed by regressing brightness temperatures against $\ln(R + c)$, where c is a constant (Berg *et al.*, 1998). This retrieval formula is represented by equation (18).

$$R = \exp[a_0 + \sum_{i=1}^N a_i TB_i] - c \quad (18)$$

According to Berg *et al.* (1998), this regression formula allows for a better fit to the data than a linear fit. This is due to the fact that the response of the SSM/I channels to changes in rainfall rate generally diminishes with increasing rain rate. A total of 342 collocated observations over land and 1365 observations over the ocean were utilized to obtain the above regression formulae.

The Cal/Val algorithm tests SSM/I pixels to determine if they represent land or water according to the landscape descriptor "isfc" (Wentz "isfc" flag). The designating landscape descriptors are as follows:

0 = land
 1 = land with vegetation cover
 5 = water

If "isfc" equals 0 or 1, then the rain rate is calculated according to a land-based algorithm. On the other hand, if "isfc" equals 5, the rain rate is calculated according to an ocean-based algorithm. A more detailed description of the Cal/Val algorithm follows:

isfc = landscape descriptor
TB = brightness temperature
v = vertical polarization
h = horizontal polarization
ichk85 = 85 GHz channel usability check
 00 = usable
 01 = unusable
PCP = rain

For rainfall over the land

```

if (isfc.eq.0.or.isfc.eq.1) then
  if (ichk85.eq.00) then
     $PCP = \exp(3.29716 - 0.01290 * TB_{85v} + 0.0087 * TB_{85h}) - 8.0 \text{ (mm/hr)}$ 
  else
    if (ichk85.eq.01) then
       $PCP = \exp(-17.76849 - 0.09612 * TB_{37v} + 0.15678 * TB_{19v}) - 1.0 \text{ (mm/hr)}$ 
    endif
  endif
else

```

For rainfall over the ocean

```

if (isfc.eq.5) then
  if (ichk85.eq.00) then

```

```

PCP = exp(3.06231 - 0.0056036 * TB85v + 0.0029478 * TB85h - 0.0018119 *
        TB37v - 0.00750 * TB22v + 0.0097550 * TB19v) - 8.0 (mm/hr)
else
  if (ichk85.eq.01) then
    PCP = exp(5.10196 - 0.05378 * TB37v + 0.02766 * TB37h + 0.01373 * TB19v)
        - 2.0 (mm/hr)
  endif
endif

if (PCP.lt.0.0) PCP = 0.0

```

It is important to note that the Cal/Val algorithm checks to see if the 85 GHz channel is usable or unusable. This adaptation was in response to the fact that the DMSP F-8, 85v GHz channel became increasingly noisy beginning in January of 1988, and ultimately became unusable by May of 1988. To solve this problem, a stepwise linear regression scheme was developed by the Hughes Aircraft Company to “synthesize” the 85v GHz channel using the other available channels (*i.e.* 19 and 37 GHz). It is necessary to include the 85 GHz “check” feature if data from the DMSP F-8 satellite is used. This is not a factor for this study, however, since the SSM/I data has been obtained from the three remaining and currently active DMSP satellites (F-11, F-13, F-14).

As various figures in this study will indicate, the Cal/Val algorithm exhibits a major weakness. The original radar-derived, collocated “training” datasets *did not* include any high intensity rain events. In fact, Berg et al. (1998) states that nearly all of the radar-derived area-averaged rain rates were less than 6 mm/hr. Consequently, a bias towards underestimation exists in the algorithm. Precipitation intercomparison projects have concluded that the Cal/Val algorithm underestimates rain rates by an approximate factor of two. However, this study has produced underestimations as large as a factor of four.

It is this weakness which causes the Cal/Val algorithm to perform poorly in almost all intercomparisons, especially for intense storm systems. As a result, the Cal/Val SSM/I algorithm was retired in favor of the NESDIS SSM/I algorithm for “real time” runs of the FSU Global Spectral Model, beginning with the 1998 hurricane season. Figure 1-2 depicts a flow chart of the Cal/Val SSM/I rain rate algorithm.

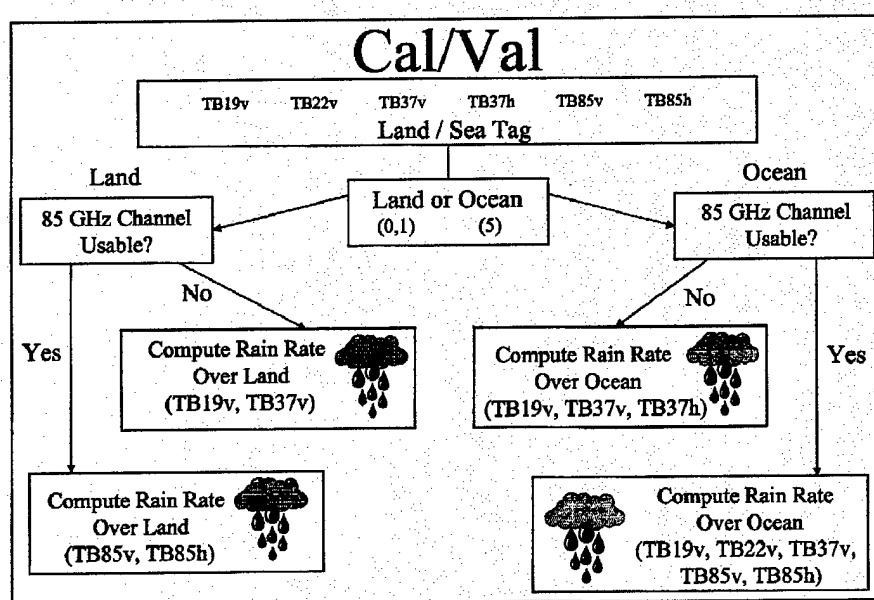


Figure 1-2: Cal/Val SSM/I rain rate algorithm flow chart.

1.3 Overview of the Navy Third Generation NOAA/NESDIS SSM/I Algorithm

The NESDIS SSM/I rain rate algorithm is the Navy's third generation algorithm developed by the National Environmental Satellite, Data, and Information System (Ferraro and Marks 1995). The algorithm used in this research is the most recent version of NESDIS, which includes an emission component. Older versions only used the 85 GHz scattering.

The NESDIS algorithm bases its rain rates on non-linear regression between the 85 GHz scattering index used in both a screening procedure and operational radar measurements (Ferraro *et al.*, 1994; Ferraro and Marks 1995). The radar data used in the algorithm's original validation study was obtained from three worldwide sites: the 22 platform Japanese Meteorological Agency AMEDAS system; the 14 platform U.K. Meteorological Office FRONTIERS system; and the 13 platform U.S. National Weather Service RADAP-II system (Smith *et al.*, 1998). From these radar measurements, rain rate retrieval coefficients were empirically derived for use in the algorithm.

Similar in nature to the Cal/Val algorithm, the NESDIS algorithm separates land and ocean areas. This distinction is in response to the greater microwave emissivity of land surfaces compared to ocean surfaces. An 85 GHz scattering based algorithm is used over land, and a combined 85 GHz scattering and 19/37 GHz emission based algorithm is used over the ocean. These algorithms have been calibrated with ground based radar data as described by Ferraro and Marks (1995). Power laws are used in the ocean-land relationship, with exponents for the scattering indexes of approximately 2.0. The algorithm tests SSM/I pixels to determine if they represent land or water according to the landscape descriptor "isfc" (Wentz "isfc" flag). The designating landscape descriptors are as follows:

- 0 = land
- 1 = land with vegetation cover
- 3 = permanent ice
- 4 = water with possible sea ice
- 5 = water
- 6 = coast

If "isfc" equals 0, 1, or 6, then the rain rate is calculated according to a land-based algorithm. As a result, the NESDIS algorithm expands the coast. According to Ferraro (1997), in order to avoid contamination by coastlines, the coastline is stretched by two SSM/I A-scan measurements (50 km) in all directions from the current observation point. If land or coast is present in any one of the "footprints" in the 5 by 5 matrix of SSM/I measurements, the measurement is considered to be over land. In other words, if any pixel within two beam positions and two scan lines is defined as coast or land, the pixel is defined solely as land, and the land-based algorithm is applied. This minimizes the effect of "footprint" averaging on the emission algorithm, which can result in false rain along the coasts (Ferraro *et al.*, 1998). On the other hand, if "isfc" equals 3, 4, or 5, the rain rate is calculated according to an ocean-based algorithm. A more detailed description of the NESDIS algorithm follows:

isfc = landscape descriptor
SI85 = 85 GHz scattering index
TB = brightness temperature
v = vertical polarization
h = horizontal polarization
PCP = rain

parameter (*RT2* = 285.0)
 if (*isfc.eq.6.or.isfc.eq.0.or.isfc.eq.1*) then *PCP*=0.0

Check for rain

Compute 85 GHz scattering index. If greater than 10, rain possible

if (*TB19v.ge.100.0.and.TB19v.le.300.0.and.TB85v.ge.80.0.and.TB85v.le.300.0*) then
 $SI85 = 451.9 - (0.44 * TB19v) - (1.775 * TB22v) + (0.00574 * TB22v * TB22v) - TB85v$
 if (*SI85.ge.10.0*) then
 $PCP = 0.00513 * (SI85 ** 1.9468)$

Special care must be taken to remove false rain signatures due to snow cover, deserts, and semi-arid land (Ferraro *et al.*, 1998).

Tests for snow cover

$TT = 175.0 + (0.49 * TB85v)$
if $(TB22v .lt. 264.0 .and. TB22v .lt. TT)$ $PCP = 0.0$

Tests for desert

$PD19 = TB19v - TB19h$
if $(PD19 .gt. 20.0)$ $PCP = 0.0$

Tests for semi-arid regions

if $(TB85v .gt. 253.0 .and. PD19 .gt. 7.0)$ $PCP = 0.0$
else
 $PCP = 0.0$
endif

Conversion from SI85 to rain rate uses a power fit. This power fit produces lower rain rates than a linear fit for rain rates less than 15 mm/hr. It also produces higher rain rates than a linear fit for rain rates in excess of 15 mm/hr. Since this relationship tends to accelerate toward high rain rate values for extreme scattering cases, rain rate is maximized to 35 mm/hr.

if $(PCP .gt. 35.0)$ *then* $PCP = 35.0$
else
 $PCP = -999.0$
endif
else

Compute 85 GHz scattering index developed for oceanic use only

if $(TB19v .ge. 100.0 .and. TB19v .le. 300.0 .and. TB85v .ge. 80.0 .and. TB85v .le. 300.0)$ *then*
 $SI85 = -174.4 + (0.715 * TB19v) + (2.439 * TB22v) - (0.00504 * TB22v * TB22v) - TB85v$
 $PCP = 0.0$

Compute parameters used for sea-ice filters

$TT = 44.0 + (0.85 * TB19v)$

If SI85 is 10.0 or greater, rain or sea-ice is present. Compute rain rate and check for sea-ice.

if $(SI85 .ge. 10.0)$ *then*
 $PCP = 0.00115 * (SI85 ** 2.16832)$

```

if (isfc .eq. 4) then
  if (TB22v .le. TT) PCP = 0.0
  if (TB22v .gt. 264.0 .and. (TB22v - TB19v) .lt. 2.0) PCP = 0.0
endif
else

```

Check for emission component if no scattering is found. This is comparable to combining the PIP-2 Alishouse/Grody algorithm with the Ferraro algorithm (scattering).

```

if (TB19v .lt. RT2 .and. TB22v .lt. RT2) then
  Q19 = -2.70*(ALOG(290.0 - TB19v) - 2.84 - (0.40*ALOG(290.0 - TB22v)))
endif
if (Q19 .ge. 0.60) then
  PCP = 0.001707*((Q19*100.0)**(1.7359))
else
  if (TB37v .lt. RT2 .and. TB22v .lt. RT2) then
    Q37 = -1.15*(ALOG(290.0 - TB37v) - 2.99 - (0.32*ALOG(290.0 - TB22v)))
  endif
  if (Q37 .ge. 0.20) PCP = 0.001707*((Q37*100.0)**(1.7359))
endif
endif
If (PCP .gt. 35.0) then PCP = 35.0
else
  PCP = -999.0
endif
endif

```

1.3.1 NESDIS Scattering Algorithm

Ice particles most often found in raining clouds reflect upwelling radiation back to the surface. This lowers the observed brightness temperatures. Kummerow et al. (1996) states that as microwave frequencies increase, so does the amount of scattering due to ice. The 85 GHz channel exhibits the most scattering due to ice, with brightness temperature depressions as high as 150K over convective updrafts. This relationship, where precipitation is inferred based upon a measure related to the ice content of a cloud, is the backbone of any scattering algorithm.

The NESDIS algorithm has recently been updated to include many improvements from its original version. The algorithm currently incorporates enhanced sensitivity to oceanic scattering, plus improved screening for anomalous scattering features such as frozen ground and non-vegetated land. While the older version used antenna temperatures, the latest version uses coefficients derived for brightness temperatures (Ferraro and Marks 1995).

Almost all precipitation systems contain both water and ice particles. Cloud physics guarantees that the size and density of these particles will vary. SSM/I temperature measurements at 37 GHz will be depressed by scattering if the ice particles increase in size to approximately 8 mm. At 85 GHz, measurement depression will occur around 4 mm. The original version of the NESDIS algorithm used a scattering index (SI) developed by Grody (1991). This scattering index measured the temperature depression at 85 GHz, which is more sensitive to smaller ice particles. As the previous algorithm description indicates, other scattering media such as snow, desert, and sea-ice are removed. According to Hakkarinen and Adler (1988), the scattering technique is best suited for land-based precipitation systems since the ice layer in a cloud is typically thicker over land. However, since many ocean-based weather systems also contain ice, the scattering index can also be applied in these cases (Ferraro and Marks 1995).

As previously written, the scattering index used in this most recent version of the NESDIS algorithm is an improvement over the original index developed by Grody (1991). The improvement is due to different indexes for land and ocean:

Land

$$SI_{85} = 451.9 - (0.44 \cdot TB_{19v}) - (1.775 \cdot TB_{22v}) + (0.00574 \cdot TB_{22v} \cdot TB_{22v}) - TB_{85v}$$

Ocean

$$SI_{85} = -174.4 + (0.715 \cdot TB_{19v}) + (2.439 \cdot TB_{22v}) - (0.00504 \cdot TB_{22v} \cdot TB_{22v}) - TB_{85v}$$

Grody (1991) found that a scattering index greater than 10.0 degrees Kelvin is a good global indicator of rain. It is possible to lower this threshold for regional applications. This, however, will cause very light rain rates over a larger geographical area. Moreover, lowering the threshold will introduce false rain signatures globally (Ferraro 1997).

1.3.2 NESDIS Emission Algorithm

According to Kummerow et al. (1996), the oceans radiate microwave energy equivalent to ϵT_s , where ϵ is the surface emissivity. For typical microwave frequencies, $\epsilon \approx 0.5$. As a result, the ocean surface appears uniformly cold for passive microwave observations. On the other hand, raindrops increase the observed brightness temperatures since they absorb and re-emit radiation at their own thermodynamic temperature. This relationship defines emission-based algorithms. Since land exhibits high surface emissivities on the order of ≈ 0.9 , this obscures the emission signal. Consequently, the NESDIS emission algorithm can only be applied to ocean surfaces.

If rain is not first detected using the NESDIS *ocean-based* scattering index threshold of 10 K, a liquid water emission technique is applied. Ferraro (1997) states that this emission technique is necessary since an ice-scattering signature may not be present in many mid and high latitude rain systems, or in warm, tropical air. Additional rain

retrievals are made by using the 19 and 37 GHz components of the cloud liquid water algorithm of Weng and Grody (1994). Q19 and Q37 denote atmospheric liquid water in the NESDIS algorithm. The 19 and 37 GHz channels are better suited for the emission algorithm. According to Ferraro and Marks (1995), the 19 and 37 GHz frequencies are used since they are the least sensitive to scattering. The longer wavelengths (due to the 19 and 37 GHz frequencies) tend to “saturate” at higher rainfall rates and therefore are less sensitive to the effects of ice scattering. At these two frequencies the brightness temperature variations are mainly due to clouds, water vapor, and rain. The contributions due to water vapor are removed using the 22 GHz channel (Ferraro *et al.*, 1992). Since the 37 GHz channel is prone to saturate at low rain rates and is influenced by ice scattering, the 19 GHz liquid water measurement is superior over the global oceans:

$$Q19 = -2.70*(ALOG(290.0 - TB19v) - 2.84 - (0.40*ALOG(290.0 - TB22v)))$$

The NESDIS algorithm uses an empirical threshold to distinguish clouds from rain. A global threshold of 0.20 mm of liquid water is used to separate non-precipitating clouds from rain, although this value is highly dependent upon the height of the freezing level and the depth of the rain column (Wentz 1990). By examining several global datasets, Ferraro and Marks (1995) concluded that rain is almost always present if $Q > 0.40$ mm. The NESDIS algorithm uses this value in global applications to represent rain which is heavier than drizzle.

Stated simply, the emission algorithm is based on the retrieval of cloud liquid water. Since the Q19 and Q37 algorithm estimates are valid over different ranges of liquid water, rain is detected if either $Q19 > 0.60$ mm or if $Q37 > 0.20$ mm. Similar to the

scattering portion of the NESDIS algorithm, the maximum retrieved rain rate is set to 35 mm/hr. Figure 1-3 depicts a flow chart of the NESDIS SSM/I rain rate algorithm.

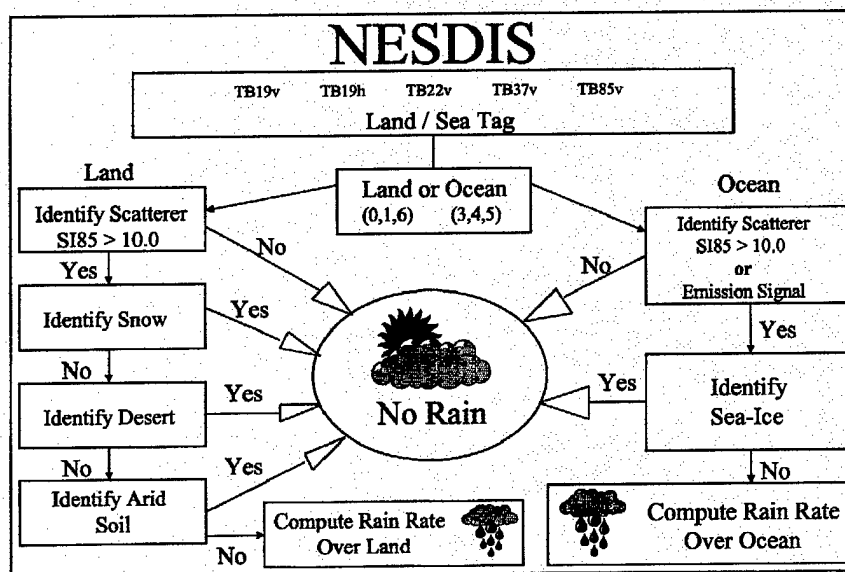


Figure 1-3: NESDIS SSM/I rain rate algorithm flow chart.

1.4 Overview of the GPROF 4.0 SSM/I Algorithm

While the Cal/Val and NESDIS SSM/I rain rate algorithms can be categorized as *statistical rain maps*, the GPROF 4.0 SSM/I rain rate algorithm can be described as a *physical profile* algorithm. In general, physical profile algorithms retrieve the vertical structure of various hydrometeor categories. These categories can include both precipitating and suspended hydrometeors, in both liquid and frozen states. After the retrieval process, surface rain rates are computed from the hydrometeor profiles (Smith *et al.*, 1998).

GPROF stands for "Goddard Profiling" algorithm. The algorithm version used for this study is identified as GPROF 4.0 for SSM/I. It must be referred to in such a specific manner because separate versions of the GPROF algorithm exist for use in the Tropical Rainfall Measuring Mission (TRMM). In fact, GPROF 4.0 for SSM/I was originally developed in anticipation of its adaptation to the future, operational applications of TRMM. Kummerow et al. (1996) states that GPROF 4.0 was primarily designed with the operational goals of TRMM in mind. To create an operationally viable algorithm which could be adapted to the Tropical Rainfall Measuring Mission, two requirements needed fulfillment. The first requirement was that GPROF be computationally inexpensive. In other words, the algorithm needed to be modest enough that it could be computed on a midsize workstation. Kummerow et al. (1996) claims that this requirement has been achieved by eliminating explicit radiative transfer computations from inside the retrieval scheme. The disadvantage of this procedure, however, is the fact that it can hamper the algorithm's ability to obtain an ideal match between observed and modeled brightness temperatures. The second requirement was that GPROF be structured to provide clearly separated, individual processes. This design was implemented to make each process in the algorithm individually quantifiable, thereby allowing easier refinement for future use in TRMM.

Similar in nature to both the Cal/Val and NESDIS algorithms, the GPROF 4.0 algorithm also tests SSM/I pixels to determine if they represent land or water according to the landscape descriptor "isfc" (Wentz "isfc" flag). The designating landscape descriptors specific to GPROF 4.0 are as follows:

0 = land
 3 = permanent ice
 5 = water
 6 = coast

Each surface type is handled independently. Surface types 1 and 4, which *were* used in the NESDIS algorithm, are *not* considered in the GPROF 4.0 algorithm. GPROF 4.0 “thickens” the coastline by setting all pixels that border a coastline pixel equal to six. Due to the complex nature and extreme length of the GPROF 4.0 computer code, which includes multiple subroutines, it is not prudent to present a detailed Fortran code description of the algorithm in this chapter. A more definitive understanding of the GPROF 4.0 rain rate algorithm is presented in the following paragraphs. In addition, a highly simplified flow chart of the algorithm can be found in Figure 1-4.

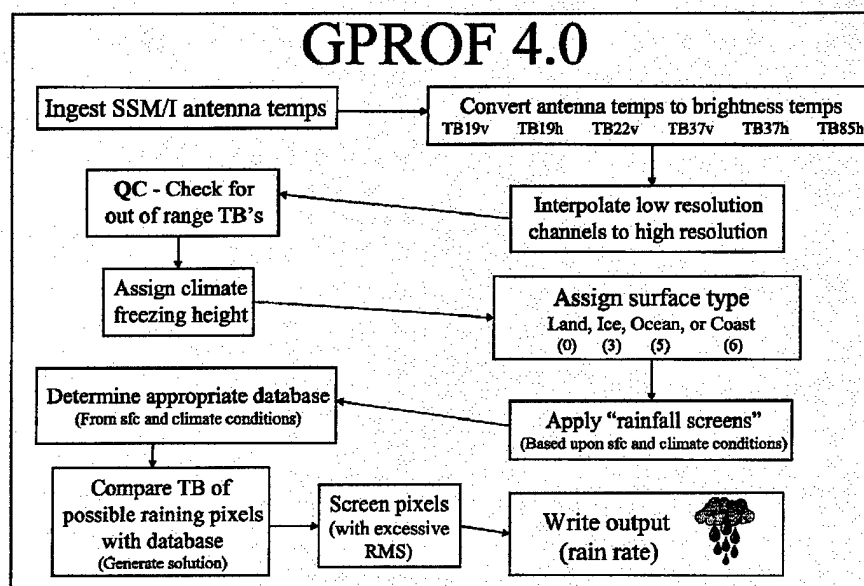


Figure 1-4: GPROF 4.0 SSM/I rain rate algorithm flow chart.

As stated earlier, the GPROF 4.0 SSM/I rain rate algorithm explicitly accounts for the vertical structure of precipitation within a cloud. The algorithm accomplishes this feat by taking advantage of the fact that response functions for the different SSM/I channels peak at different depths within the raining column. GPROF 4.0 "profiles" the relationship between raindrops and radiation through the variation of an assumed rain structure, which serves to minimize the difference between the observed and modeled radiances (Kummerow *et al.*, 1996). The necessary radiative transfer calculations are evaluated by the GPROF 4.0 *retrieval method*, which is presented in the following paragraphs.

Radiative transfer equations must address the effects of both absorptivity and emissivity. The GPROF 4.0 algorithm uses the model of Wilheit (1979) to compute water surface emissivity as a function of near-surface wind speed. Over land, the GPROF algorithm assigns an emissivity value of 0.9 for moderately dry, bare soil (Kummerow *et al.*, 1996). Factors such as vegetation and soil moisture are not generally known for the entire globe and therefore emissivities for these parameters cannot be defined in the context of this model.

The radiative transfer of the GPROF algorithm addresses water vapor, oxygen, and cloud water as atmospheric absorbers of microwave radiation. Both water vapor absorption as well as oxygen absorption are calculated from Liebe (1985). Since the size of non-precipitating cloud droplets ($< 100 \mu\text{m}$) is much smaller than typical microwave wavelengths (3 cm at 10 GHz to 3.5 mm at 85 GHz), the Rayleigh approximation is used to calculate the absorption due to cloud water (Olson *et al.*, 1996). Mie theory is

employed to address the larger raindrops produced by collision/coalescence, with the assumption that these droplets are spherical in nature.

With the radiative characteristics of the surface and atmosphere now known using the models and approximations discussed above, the GPROF 4.0 algorithm empowers the backward Monte Carlo scheme to compute the upwelling radiances. According to Kummerow et al. (1996), photons are started at the point at which the brightness temperature is to be computed, in the direction opposite to that in which they would physically propagate inside the medium. Each photon is then traced backward through the medium following probabilistic interaction laws until the photon is absorbed. Absorbed photons are treated as being emitted at the point of absorption, x , with the brightness temperature equal to the physical temperature of the medium at that point $T(x)$. Using the Monte Carlo scheme allows for computations on smaller, mid-sized computer workstations, thereby decreasing the total cost of obtaining upwelling radiances. A more extensive description of the Monte Carlo scheme can be found in Roberti et al. (1994).

With the aid of computer model based brightness temperature fields, the GPROF 4.0 algorithm simulates the radiances as they would be measured from a downviewing microwave sensor. According to Kummerow et al. (1996), this is achieved by convolving the brightness temperature field with the antenna gain function. For each channel, v , the measured temperature $Tb(s_0)$ may be expressed as:

$$Tb(s_0) = \int G_v(s_0, s) Tb_v(s) dA \quad (19)$$

where $G_v(s_0, s)$ is the antenna gain function for channel v at position s relative to antenna boresight position, s_0 , and $Tb_v(s)$ is the high-resolution brightness temperature

calculated from a cloud microphysical model known as the Goddard Cumulus Ensemble model. A detailed description of this cloud model can be found in Tao and Simpson (1993).

The final step in the *retrieval method* of the GPROF 4.0 algorithm utilizes statistical applications to compare calculated parameters to the set of sensor observations. The output generated from the Goddard Cumulus Ensemble model and radiative transfer equations within the *retrieval method* produces a large database of atmospheric profiles and associated brightness temperatures. These modeled brightness temperatures are compared to the set of observed SSM/I brightness temperatures, and a minimum variance solution is obtained according to:

$$W_i = \exp\left\{-\frac{1}{2} \sum_j^{All\ channels} (TB_j(R_{model_i}) - TB_{obs_j})^2 / \sigma_j^2\right\} \quad (20)$$

where σ_j^2 represents the error variance of the model plus the observational error.

Based on the deviation(s) from the observed SSM/I brightness temperatures, a probability density function is used to obtain weighted rainfall profiles. This probability density function is an extension of Bayes theorem. Bayes theorem states: Given a brightness temperature vector, **TB**, the probability of a particular profile of vertically distributed hydrometeors, **R**, can be written as

$$\Pr(\mathbf{R}|\mathbf{TB}) = \Pr(\mathbf{R}) \times \Pr(\mathbf{TB}|\mathbf{R}) \quad (21)$$

where $\Pr(\mathbf{R})$ is the probability with which a particular profile of **R** will be observed and $\Pr(\mathbf{TB}|\mathbf{R})$ is the probability of observing **TB**, given rain profile **R**. $\Pr(\mathbf{R})$ is derived using the Goddard Cumulus Ensemble model and therefore taken from the cloud profile

database. $\text{Pr}(\mathbf{TB}|\mathbf{R})$ is obtained using both the radiative transfer calculations and the brightness temperature convolution scheme highlighted earlier. This term is the gaussian weight, which depends upon the RMS difference between the observed and computed brightness temperatures. The end result of this Bayesian approach is a rainfall solution profile based upon the weighted database profiles:

$$R \sim \sum_i^{\text{All profiles}} R_{\text{model}_i} \cdot W_i \quad (22)$$

This rainfall output is a measure of the surface rainfall only, which can be easily verified using rain gauge observations.

CHAPTER 2

SSM/I RAIN RATE ALGORITHM VALIDATION & COMPARISON

2.1 Global Rain Rate Averages

Global rain rate averages were computed for the daily rain totals calculated by the Cal/Val, NESDIS, and GPROF 4.0 algorithms. A cosine weighted average of the latitudes was incorporated to account for the curvature of the earth and the associated smaller grid boxes at higher and lower latitudes. Based upon 84 days of calculated rain rates from June 16th, 1998, to November 5th, 1998, the mean global rain rate average for the Cal/Val algorithm proved to be **1.89 mm/day**. As expected, the NESDIS algorithm produced a higher mean global rain rate average of **2.44 mm/day**. In addition, the GPROF 4.0 algorithm produced a mean global rain rate average of **2.51 mm/day**.

The meteorology research community commonly accepts global rain rate averages between 2 to 3 mm/day to be valid. This is known as the evaporation baseline and/or global moisture balance. More specifically, Manabe et al. (1965) states that the global precipitation mean is approximately 1 meter per year, which converts to 2.74 mm/day. It must be noted that both the NESDIS and GPROF 4.0 global rain rate averages computed in this study are in accordance with the evaporation baseline of 2 to 3 mm/day. The Cal/Val mean global rain rate average, however, is significantly lower.

2.2 Case Studies of the Cal/Val, NESDIS, and GPROF Rain Rate Algorithms

SSM/I rain rate data has been analyzed on a daily basis for the purpose of establishing the similarities and differences between the Cal/Val, NESDIS, and GPROF 4.0 rain rate algorithms. Rain rates were calculated using all three algorithms for 84 days between the period June 16th, 1998, to November 5th, 1998. The calculations compile rain rates in units of millimeters per day (mm/day), and the figures which follow depict rain at T170 resolution (global grid of 512 longitude points by 256 latitude points).

At first inspection of the graphed rain rates, only minor differences between the Cal/Val, NESDIS, and GPROF 4.0 rain rate calculations are apparent. However, closer inspection reveals significant differences in surface rain rate totals for broad, synoptic scale rain events and intense storm systems. In certain cases the Cal/Val algorithm underestimates the daily rain rate total by as much as a factor of four. This is demonstrated in various figures which follow in this chapter. It is important to note that recent precipitation intercomparison projects, such as PIP-2, also indicate a gross underestimation of rain rates by the Cal/Val algorithm. In addition, the algorithm was documented to be bias towards detection of overly broad regions of precipitation (Berg *et al.* 1998). For example, the Cal/Val algorithm will often exhibit larger rain bands within high latitude oceanic frontal systems when compared to the rain bands from other SSM/I algorithms. As further study will show, incorporation of the NESDIS and GPROF 4.0 rain rate algorithms into the FSU Global Spectral Model, in place of the existing Cal/Val algorithm, will result in largely different hurricane track, wind intensity, and minimum central pressure forecasts.

2.3 SSM/I Rain Rate Comparison Studies

Figure 2-1 depicts SSM/I global surface rain rates as calculated by the Cal/Val, NESDIS, and GPROF 4.0 algorithms, respectively, for the 24 hours of August 24th, 1998. While it is difficult to determine exact numerical values of rainfall from this figure due to limited detail, this initial figure is provided for a specific purpose. The main purpose of Figure 2-1 is to contrast and to compare the *spatial coverage* as calculated by each of the individual SSM/I rain rate algorithms. Figure 2-1 shows that the spatial orientation of rain presented by each SSM/I algorithm is very similar throughout the globe, to include both the tropics and the middle latitudes. Moreover, storm systems (such as the cold frontal induced rain band in the middle Atlantic ocean, tropical convection over central Africa, and Hurricane Bonnie off the east coast of Florida) are highlighted by each of the three algorithms in a similar fashion. While it is clearly evident that the Cal/Val, NESDIS, and GPROF 4.0 algorithms depict global rain over an almost identical spatial scale, huge differences in magnitude can exist for synoptic rain events. These variations in magnitude are presented in the following case studies. These case studies present further evidence of the Cal/Val algorithm's tendency toward underestimation.

2.3.1 Case 1: July 13, 1998 (Julian Day 194)

After three months of extreme heat and unprecedented drought throughout the state of Florida, afternoon thunderstorms returned to north Florida with a vengeance on July 13th, 1998. Over four inches of rain filled the rain gauge at the Tallahassee airport, and other locations, such as the FSU campus, received over six inches of precipitation in three short

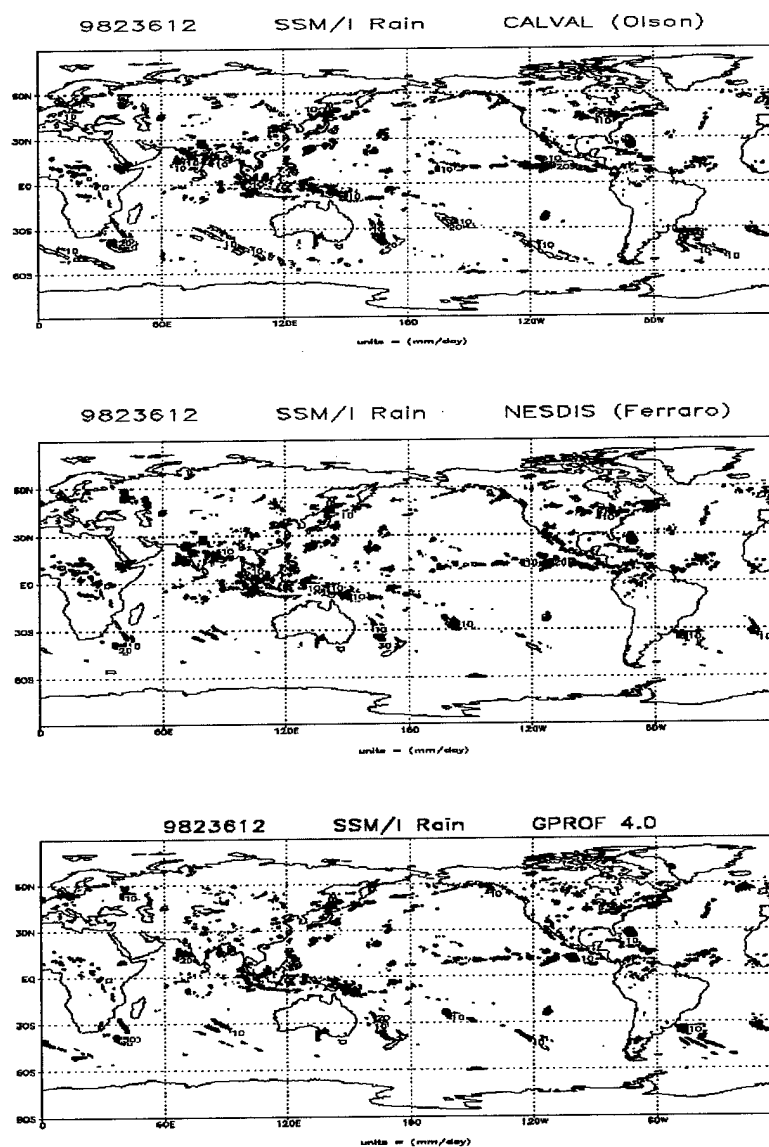


Figure 2-1: SSM/I rainfall for three different algorithms (August 24th, 1998).

hours. Figure 2-2 shows SSM/I estimated rain rates for the 13th of July using the Cal/Val algorithm. With the maximum contour only indicating 20 mm/day (0.8 inches) in the vicinity of Tallahassee, a gross underestimation of the rain is evident when compared to the observed values of four to six inches (100 to 150 mm).

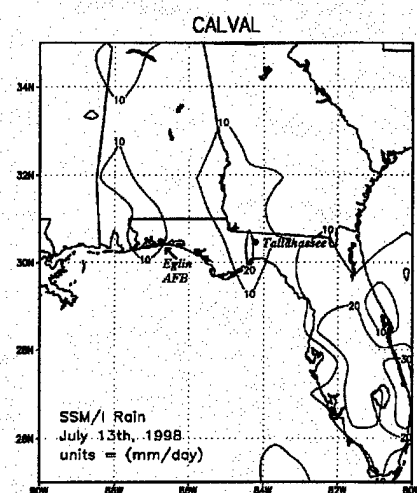


Figure 2-2: Cal/Val SSM/I rain rates, July 13th, 1998 (mm/day)

Figure 2-3 shows SSM/I estimated rain rates for Tallahassee using the NESDIS algorithm. Much more realistic rain rates are depicted. An impressive bulls-eye centered on Tallahassee shows an inner contour of 80 mm/day (3.2 inches). While this SSM/I

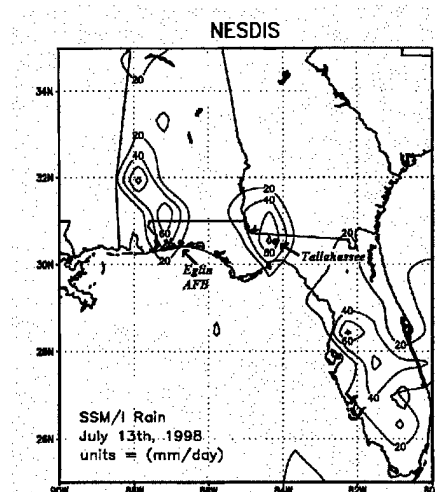


Figure 2-3: NESDIS SSM/I rain rates, July 13th, 1998 (mm/day)

based value is still slightly less than the official, observed value of 110.75 mm (4.43 inches), it nevertheless represents a huge improvement when compared to the Cal/Val estimated rain rate.

Figure 2-4 shows SSM/I estimated rain rates for Tallahassee using the GPROF 4.0 algorithm. While not as low as the Cal/Val estimate, the GPROF 4.0 estimate of 40 mm/day (1.6 inches) is still much less than the observed value. However, the GPROF 4.0

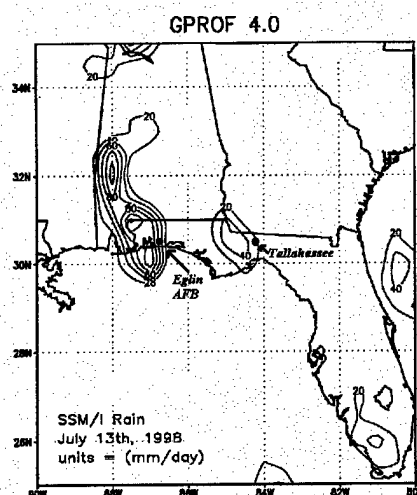


Figure 2-4: GPROF 4.0 SSM/I rain rates, July 13th, 1998 (mm/day)

algorithm performs quite well in estimating the rain rates for the thunderstorms a few hundred miles west of Tallahassee. The official observation at Eglin Air Force Base for the same period was 43.25 mm (1.73 inches). Figure 2-4 shows that the GPROF 4.0 algorithm produces the closest estimate of the three rain rate codes for Eglin AFB, with a contour of 40 mm.

2.3.2 Case 2: October 29, 1998 (Julian Day 302)

Hurricane Mitch has been described as the strongest hurricane to plague the Atlantic basin in the past decade, and the first to reach Category 5 on the Saffir/Simpson scale in the past nine years. Due to the massive destruction caused by Hurricane Mitch, and due to the fact that Honduras is a third world nation, very few surface rainfall measurements were taken and/or published after the storm slammed the Honduran mainland. The only reliable, published rainfall observations can be credited to Mr. Jon Hellin of the United Kingdom, who spent time in Honduras working on his Ph.D. in soil and water conservation in association with the Corporacion Hondurena de Desarrollo Forestal. Mr. Hellin's study site was approximately 11 km from Choluteca (87 deg 04 min West, 13 deg 17 min North, 100 m altitude).

Despite the fact that his study site was destroyed by heavy rains, Mr. Hellin published rainfall measurements from October 28th through November 3rd, 1998. The total amount of rain for this period was an astonishing 933 mm. Figure 2-5 depicts the Cal/Val SSM/I rain rates for the 24 hours of October 29th, 1998, for the Honduran mainland. For this case study, Jon Hellin's rain totals were summed for the 24 hour period from 00Z to 00Z on October 29th. Once again, the Cal/Val SSM/I rain rate algorithm grossly underestimates the observed, 24 hour rain total of 108.45 mm, producing only a 23 mm estimate.

Figure 2-6 shows the NESDIS SSM/I rain rates for this same 24 hour period. It is readily apparent that the NESDIS algorithm does a much better job of portraying the intense convection in southern Honduras. The NESDIS rain rate algorithm estimated 110

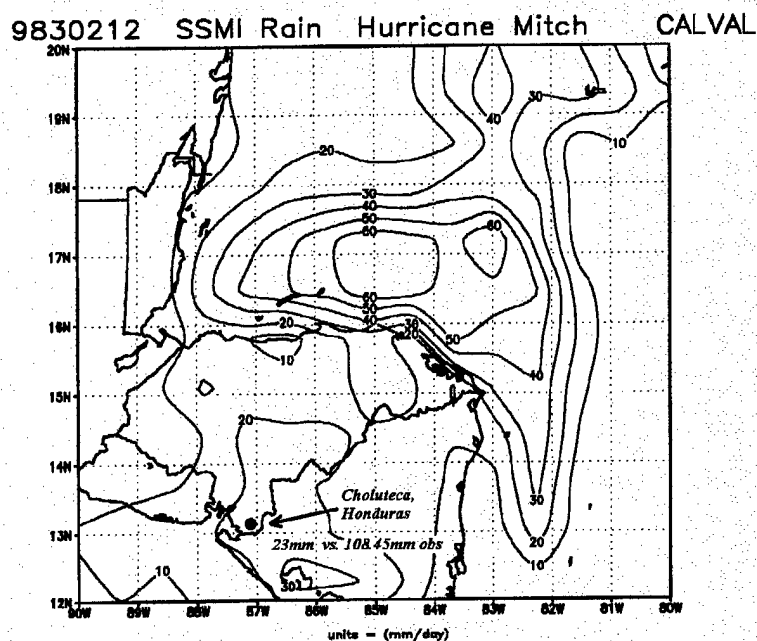


Figure 2-5: Cal/Val SSM/I rain rates for Hurricane Mitch, October 29th, 1998.

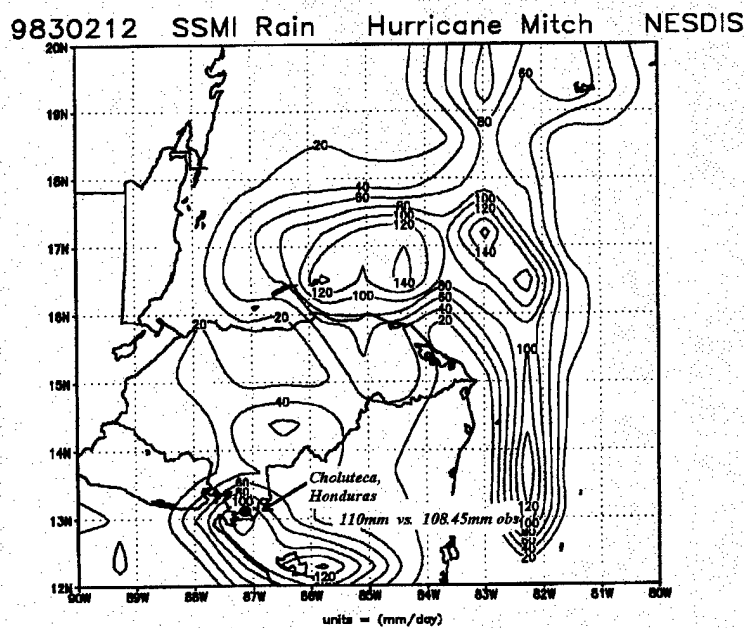


Figure 2-6: NESDIS SSM/I rain rates for Hurricane Mitch, October 29th, 1998.

mm of rain reached the ground in the vicinity of Choluteca. This compares remarkably close to the official observation of 108.45 mm.

Figure 2-7 shows the rain rate estimate as calculated by the GPROF 4.0 SSM/I algorithm. The GPROF algorithm also depicts the hurricane-induced convection in southern Honduras very well. However, the 60 mm of rain for the Choluteca vicinity underestimates the 108.45 mm observed value. On the other hand, the GPROF algorithm exhibits a bias towards overestimation of oceanic rainfall, as is indicated in Figure 2-7 to the north and east of Honduras. While this bias cannot be proven for this particular case study since no oceanic, surface rain rates were available for verification, it is at least

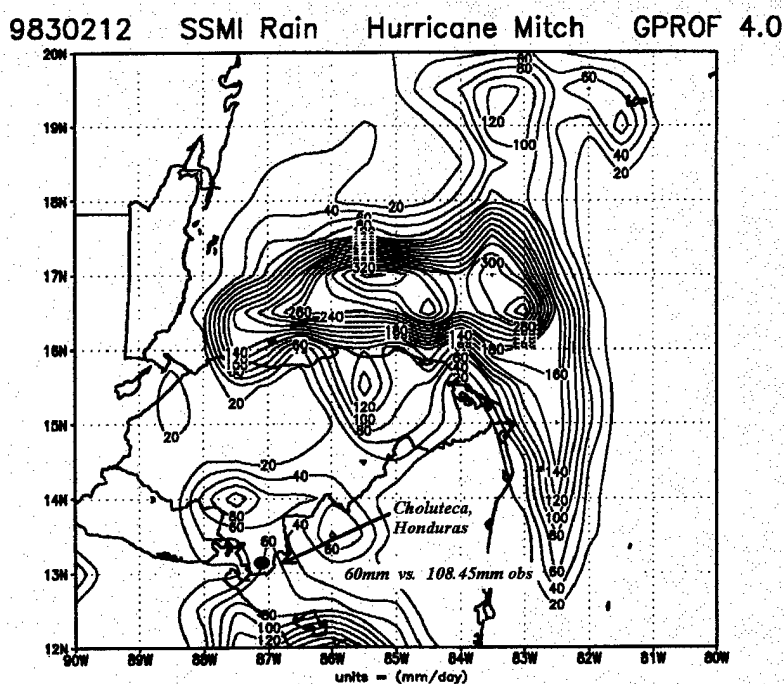


Figure 2-7: GPROF 4.0 SSM/I rain rates for Hurricane Mitch, October 29th, 1998.

worth noting the 24 hour rain totals exceeding 300 mm over the open water. Referring back to Figure 2-6, the NESDIS algorithm estimates a maximum of only 160 mm for the same oceanic area.

2.3.3 Case 3: September 21-22, 1998 (Julian Days 264-265)

Hurricane Georges struck Puerto Rico and the surrounding islands of St. Thomas and St. Croix on September 21st – 22nd, 1998. With surface-based oceanic rain rate data scarce and difficult to obtain, official observations from tiny island areas can serve as validation tools for the accuracy of the *ocean*-based portions of each of the three SSM/I rain rate algorithms. Figure 2-8 represents a two day (48 hour) accumulation of SSM/I rain rates as estimated by the Cal/Val algorithm for Hurricane Georges as it passed over

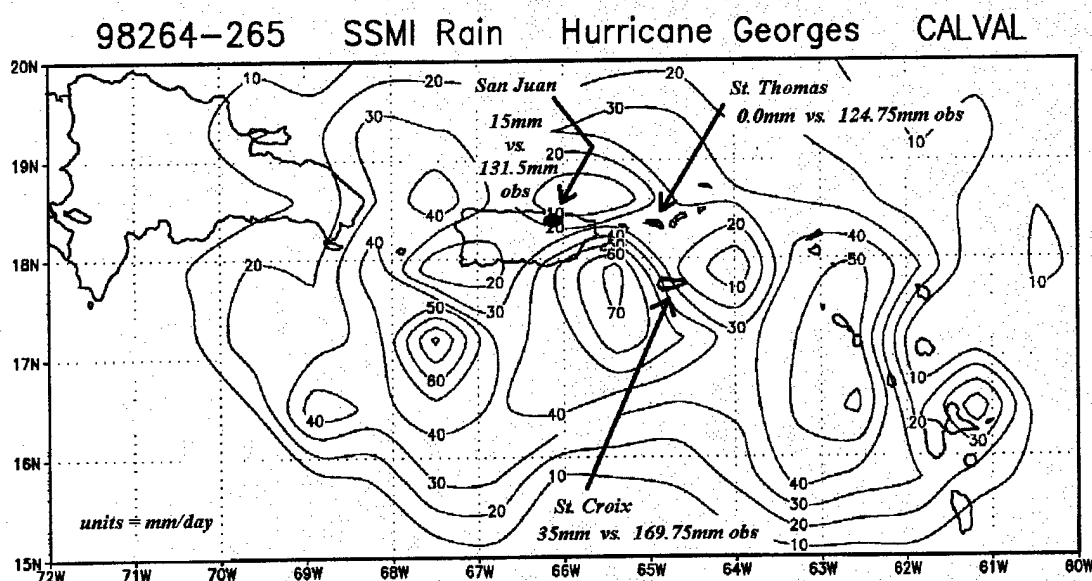


Figure 2-8: Cal/Val SSM/I rain rates for Hurricane Georges, Sep 21st – 22nd, 1998.

St. Croix, St. Thomas, and San Juan, Puerto Rico. Official rain rate observation totals for these three locations (for the same 48 hour period) are annotated on the figure. It is clear from Figure 2-8 that both the land-based *and* ocean-based portions of the Cal/Val algorithm are performing poorly, with official rainfall observations being on the order of 125 mm greater than the SSM/I estimation at all three locations. Moreover, the Cal/Val SSM/I algorithm completely failed to initialize *any* surface rain at St. Thomas, in comparison to the official observation of 124.75 mm at this island location.

Figure 2-9 shows NESDIS calculated rain rates for the same location and period. A remarkable improvement in the SSM/I estimated rain rates is evident when comparing the NESDIS result to the Cal/Val product. Both the land-based and ocean-based portions

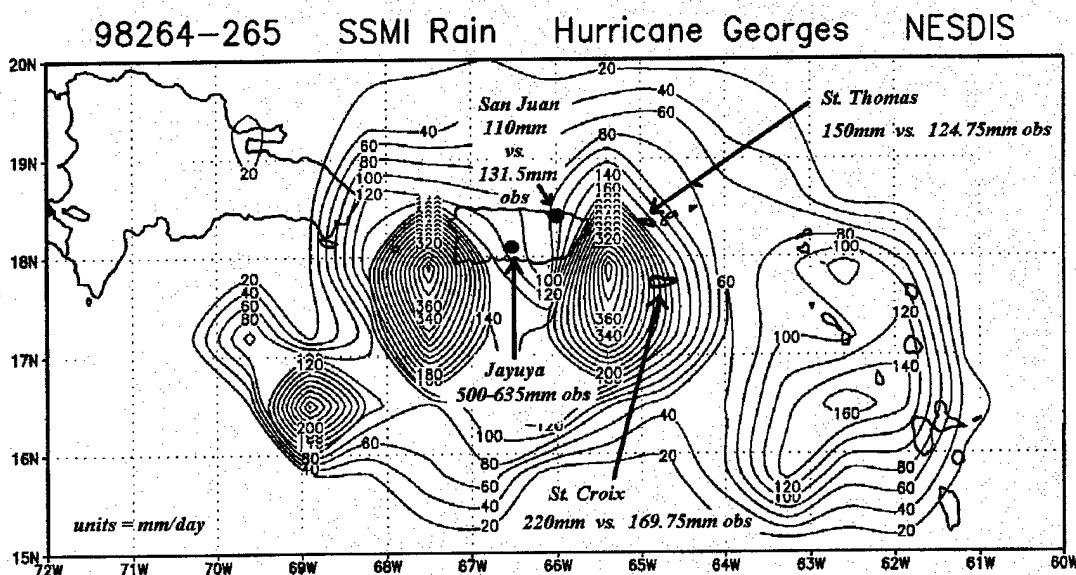


Figure 2-9: NESDIS SSM/I rain rates for Hurricane Georges, Sep 21st – 22nd, 1998.

of the NESDIS algorithm perform quite well in this case study, with only a 25 mm differential between the observed and SSM/I at St. Thomas, and only a 21 mm differential at San Juan. In addition, it is interesting to note that the NESDIS algorithm concentrates most of the surface rain from Hurricane Georges in two very distinct areas over the water: to the southeast and southwest of Puerto Rico. This is in stark contrast to Figure 2-8 and Figure 2-10, in which both the Cal/Val and the GPROF 4.0 algorithms do not initialize the surface rainfall in such a manner. Finally, Figure 2-9 is indicative of a limitation characteristic of *all* SSM/I based rain rate algorithms. This limitation is the fact that SSM/I rain rate algorithms do not account for topography. Figure 2-9 shows that a mountain community known as Jayuya, Puerto Rico, received 500 to 635 mm of rainfall. This massive concentration of rain was due to intense orographic processes, none of which is handled by SSM/I rain rate algorithms. The estimated rain rates for all three algorithms in this study do not even come close to matching the actual, recorded surface rainfall.

Figure 2-10 depicts GPROF 4.0 SSM/I rain rates for the same case study. While certainly not as low as the Cal/Val based rain rates, the GPROF based rain rates also underestimate the official observations. However, the GPROF algorithm does produce reasonable yet robust rain rates over the ocean to the southeast of St. Croix and southwest of Puerto Rico. Moreover, the large scale surface rain distribution in Figure 2-10 closely resembles the spatial distribution of the NESDIS product described earlier.

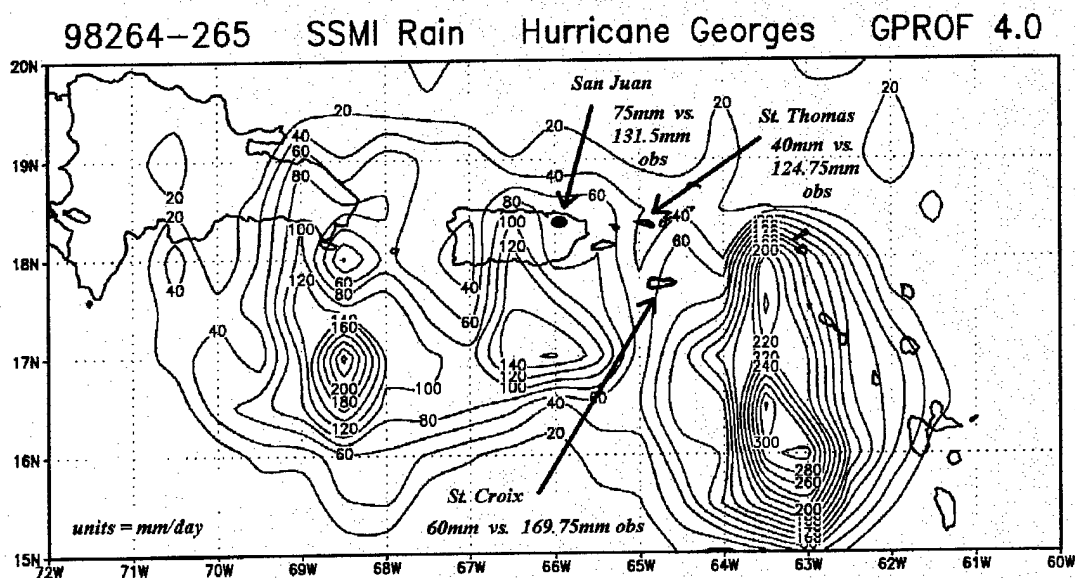


Figure 2-10: GPROF SSM/I rain rates for Hurricane Georges, Sep 21st – 22nd, 1998.

2.3.4 Case 4: August 26-27, 1998 (Julian Days 238-239)

The eye of Hurricane Bonnie reached Cape Fear, North Carolina on the afternoon of August 26th, 1998. Hurricane Bonnie then assumed a northeasterly course, skirting the coastal communities of North Carolina until it exited the state near Nag's Head around 00Z on August 28th. The potential for both inland and coastal flooding was great; however, the majority of the heavy rainfall associated with the hurricane remained offshore. The heavy concentration of rain just off the coast of North Carolina can be seen in the following three figures (2-11, 2-12, 2-13).

Figure 2-11 shows a two day accumulation of rainfall as estimated by the Cal/Val SSM/I algorithm. For the 48 hours of August 26th – 27th, 1998, Seymour-Johnson AFB,

98238-239 SSM/I Rain Hurricane Bonnie CALVAL

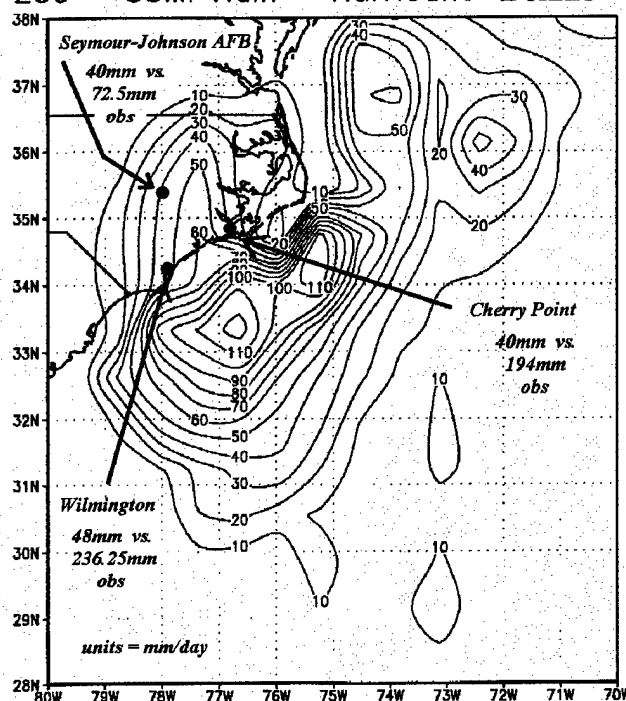


Figure 2-11: Cal/Val SSM/I rain rates for Hurricane Bonnie, August 26th – 27th, 1998.

Cherry Point Marine Air Station, and Wilmington, NC, provided reliable, official rain rate observations. As Figure 2-11 indicates, the Cal/Val algorithm is once again severely underestimating the actual, measured surface rain rates. The largest difference between the observed rain and the SSM/I rain is apparent at the coastal sites of Cherry Point and Wilmington. However, the land-based portion of the Cal/Val algorithm seems to be performing slightly better at Seymour-Johnson AFB, with only a 32 mm differential.

Figure 2-12 depicts the rain rates from Hurricane Bonnie as calculated by the NESDIS algorithm. In this case the NESDIS algorithm *overestimates* the inland station, Seymour-

98238-239 SSM/I Rain Hurricane Bonnie NESDIS

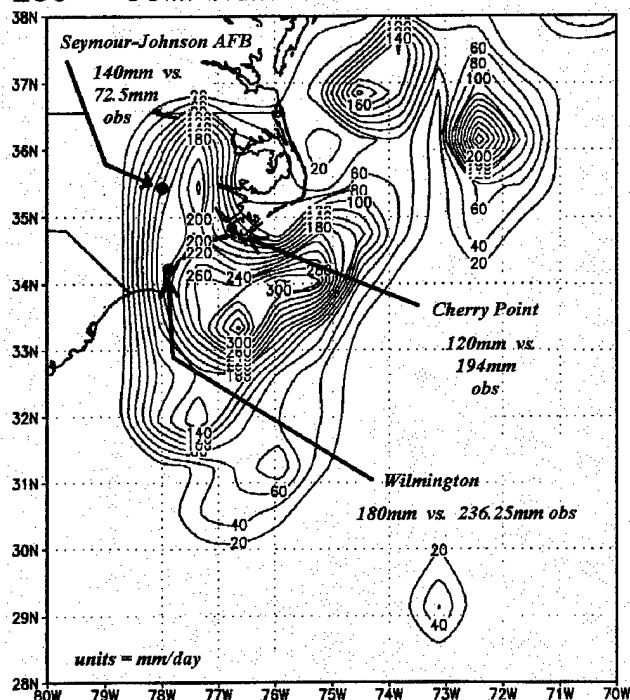


Figure 2-12: NESDIS SSM/I rain rates for Hurricane Bonnie, August 26th – 27th, 1998.

Johnson AFB, by a factor of two. On the other hand, the SSM/I rain totals from the coastal stations of Cherry Point and Wilmington are as much as 74 mm *less* than the observed values. While not as impressive or conclusive as in the prior three case studies, the performance of the NESDIS algorithm in this case is still superior to the Cal/Val performance exhibited in Figure 2-11.

Figure 2-13 shows SSM/I rain rates as calculated by the GPROF 4.0 algorithm. This case study is by far the best GPROF performance highlighted in this paper. The

98238-239 SSM/I Rain Hurricane Bonnie GPROF 4.0

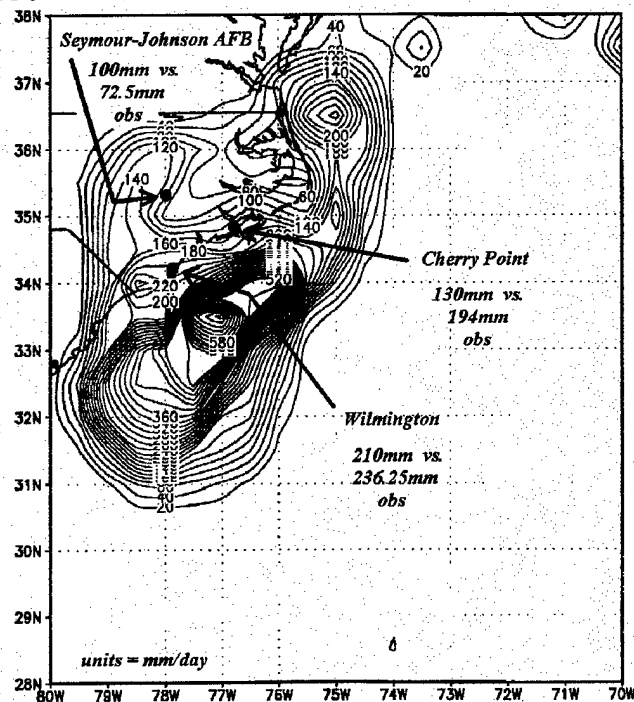


Figure 2-13: GPROF SSM/I rain rates for Hurricane Bonnie, August 26th – 27th, 1998.

difference between the SSM/I and observed rain rate values is only 26 mm at Wilmington, and only 28 mm at Seymour-Johnson AFB. When compared to the Cal/Val and NESDIS estimations, the GPROF algorithm produces the most accurate representation of rain rates for this two day period.

2.4 NEXRAD – SSM/I Rain Rate Comparison

In addition to ground-based rainfall observations, evaluation of SSM/I rain rates can be achieved using Next Generation Radar (NEXRAD) precipitation data. It must be asserted that NEXRAD storm total precipitation data is an *estimation* of surface rainfall

derived from other radar measurements. Therefore, comparing NEXRAD rain to SSM/I rain constitutes comparison of two *estimated* quantities. Consequently, SSM/I validation is not the goal of this section (2.4). The purpose of this section is to simply compare the estimated rain rates of an *active* sensor (NEXRAD) to the estimated rain rates of a *passive* sensor (SSM/I).

Figure 2-14 depicts NEXRAD storm total precipitation for Hurricane Georges as the storm slammed Mobile, Alabama. NEXRAD estimated rain rates for the two day period

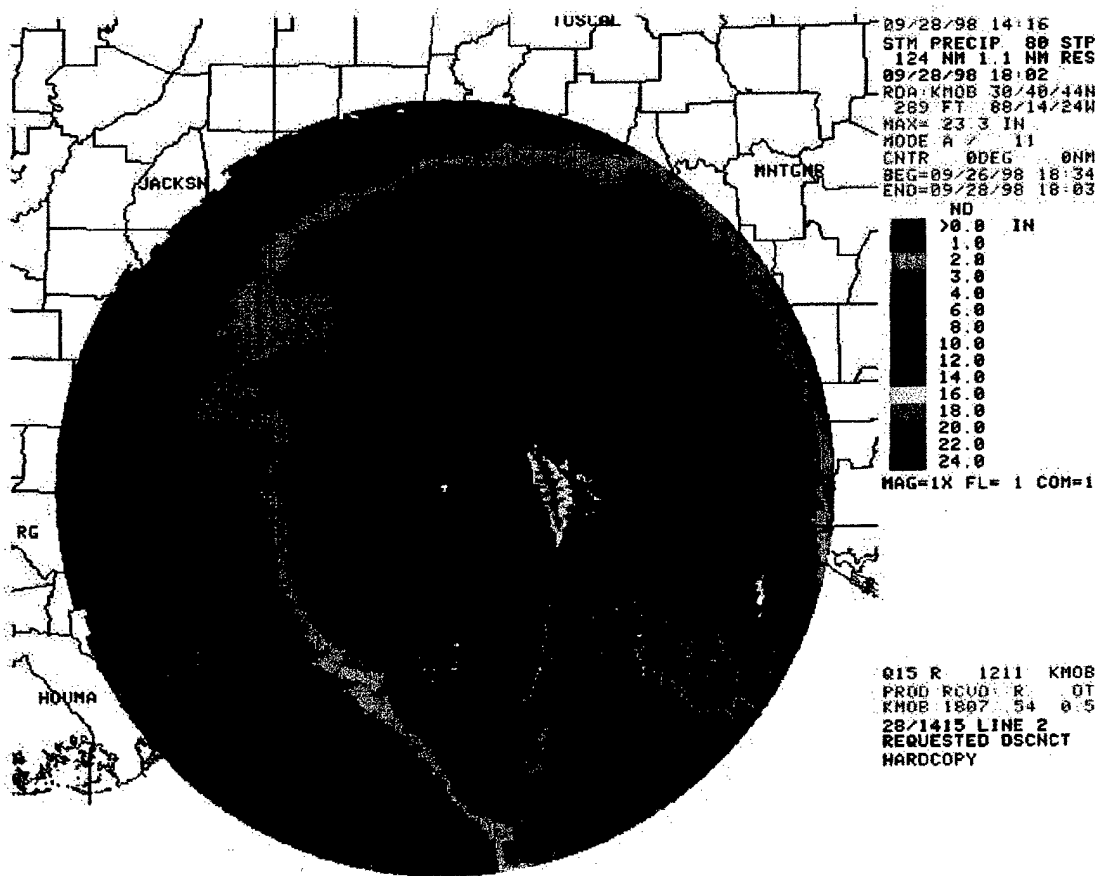


Figure 2-14: NEXRAD storm total precipitation (units = inches) – Hurricane Georges.

exceed 20 inches just east of Mobile Bay. Figures 2-15, 2-16, and 2-17 show the Cal/Val, NESDIS, and GPROF 4.0 SSM/I estimated rain rates for the same period.

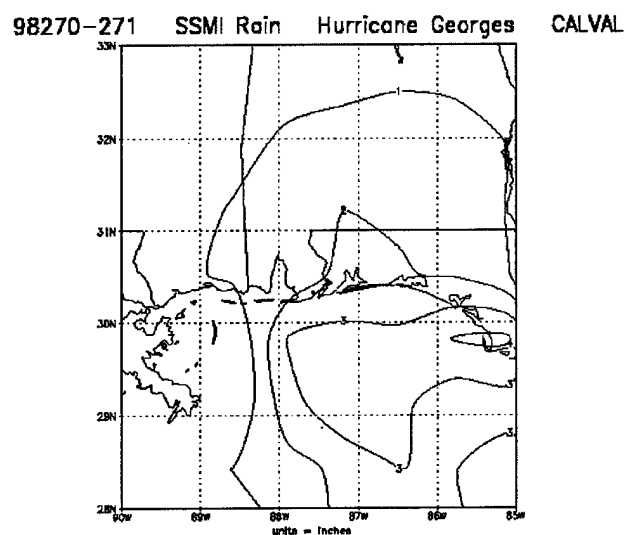


Figure 2-15: Cal/Val SSM/I rain rates (units = inches) – Hurricane Georges.

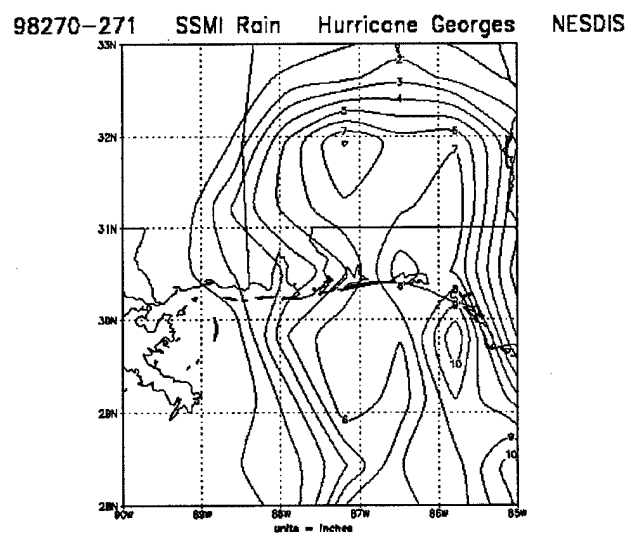


Figure 2-16: NESDIS SSM/I rain rates (units = inches) – Hurricane Georges.

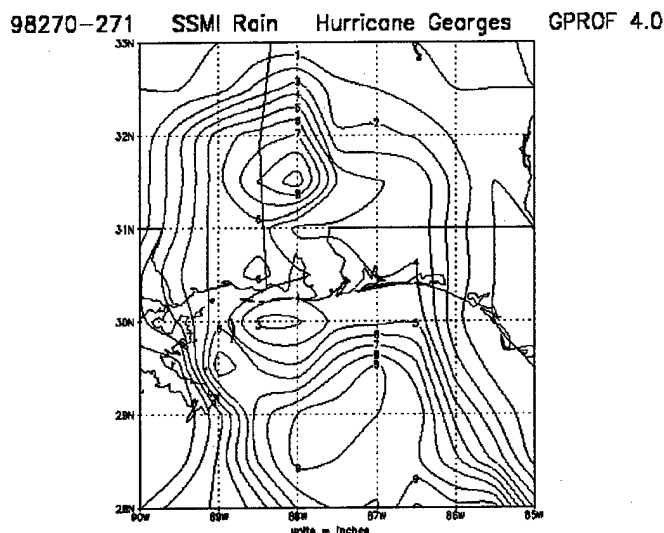


Figure 2-17: GPROF 4.0 SSM/I rain rates (units = inches) – Hurricane Georges.

The maximum rain rate in the vicinity of Mobile Bay is only 2 inches using the Cal/Val algorithm. Both the NESDIS and GPROF algorithms estimate an accumulation of 5 inches for the same area. These values, however, are much less than the 10-20 inches of rain estimated by NEXRAD (Figure 2-14).

On the other hand, the NESDIS algorithm closely agrees with the NEXRAD product just south of Panama City Beach, Florida. NEXRAD estimates 16 inches of rain associated with a rain band just off the coast, while the NESDIS algorithm estimates a maximum of 10 inches for the same area. In addition, both NEXRAD and the GPROF algorithm similarly depict another oceanic rain band south of Pensacola, Florida. While the NEXRAD estimation equals 10 inches in this area, the GPROF algorithm calculates 9 inches of rain.

2.5 SSM/I Algorithm Comparison Synopsis

The main purpose of the four case studies highlighted in this chapter is to validate the accuracy of the three SSM/I rain rate algorithms when compared to official, ground-based observations. While it *has been* proven that the Cal/Val SSM/I algorithm has serious limitations, it *has not been* fully proven that the NESDIS algorithm is superior to the GPROF algorithm for *all* possible storm systems on any given day. While the NESDIS algorithm did indeed produce the best results for three of the four case studies highlighted in this paper, the GPROF algorithm still produces rain rates of a large enough magnitude to be considered valid. In addition, the lower rain rates typical of the Cal/Val algorithm might be of considerable value for use in certain climate prediction models not requiring robust rain rates. The final test of SSM/I algorithm validity is presented in the remainder of this paper. Specifically, all three algorithms will be used in the physical initialization of the FSU Global Spectral Model, to determine which algorithm produces the most reliable hurricane track, wind intensity, and minimum central pressure forecasts.

CHAPTER 3

FSU GLOBAL SPECTRAL MODEL (FSU GSM)

PHYSICAL INITIALIZATION

3.1 Brief Description of the FSU Global Spectral Model (FSU GSM)

The NWP model used in this study is the Florida State University Global Spectral Model (FSU GSM). The FSU GSM is a high resolution, multi-level global model based on primitive meteorological equations. Vorticity (ζ), divergence (D), temperature (T), dewpoint depression (S), and the log of the surface pressure ($\ln P_s$) comprise the model's *dependent* variables. The model's *independent* variables include latitude, longitude, sigma in the vertical (σ), and time.

The FSU GSM atmosphere includes the vorticity equation, the divergence equation, the First Law of Thermodynamics, the pseudo vertical velocity equation, the mass continuity equation, the hydrostatic equation, and the moisture conservation (dew point depression) equation. These equations comprise a closed system which governs atmospheric motion within the model.

The horizontal resolution of the FSU GSM is determined from the triangular truncation of spherical harmonic waves. Each of the dependent variables in the model is expanded using spherical harmonics as basis functions that utilize Fourier

transformations in the zonal direction, and associated Legendre polynomials in the meridional direction. Experiments in this study were performed at T170 resolution. T170 resolution creates a 0.703125° latitude-longitude mesh grid, which corresponds to 512 points of longitude and 256 points of latitude. T170 was chosen to maximize resolution while minimizing extended computer processing time. Using only a single node of an IBM SP2, a three-day FSU GSM forecast run takes 25 hours to complete. Using two nodes of the IBM SP2 cuts this time in half.

The vertical structure of the FSU GSM is defined by the sigma ($\sigma = p / p_s$) coordinate, where p is the relevant pressure level and p_s is the surface pressure. For this experiment, 14 vertical levels were employed using vertical discretization based on Daley et al. (1976). In vertical discretization, temperature (T) and dewpoint depression (S) are defined at odd levels, while winds (u,v) and geopotential height (ϕ) are determined at even levels. Sigma (σ) is determined at each intermediate level according to $\sigma_i = \sqrt{\sigma_n \cdot \sigma_{n+1}}$. The vertical boundary conditions used in the model are defined as $\sigma = 0$ at both the top and bottom of the atmosphere.

Time integration of the FSU GSM is performed by a semi-implicit time differencing scheme utilizing an Asselin (1972) time filter. Horizontal differential terms in the governing equations are determined spectrally, while the vertical differential terms are determined using second order accuracy finite differencing. Centered differencing is used in the vertical for all variables except humidity.

The FSU GSM currently utilizes an envelope orography scheme following Wallace et al. (1983). In a global model the use of envelope orography reduces the systematic errors of the large-scale circulations, thus improving the steering motions of hurricanes. This is of particular importance for the medium range prediction of storm tracks (Krishnamurti et al., 1989). Finally, ECMWF level IIIa operational analyses datasets are used as the primary model input. A more detailed analysis of the elements of the FSU GSM can be found in *An Introduction to Global Spectral Modeling*, Krishnamurti et al., (1998).

All FSU GSM forecasts in this experiment begin with the use of SSM/I rain rate data and Outgoing Longwave Radiation (OLR) data to physically initialize the model environment. It is the physical initialization process which is affected most by differences in the Cal/Val, NESDIS, and GPROF SSM/I rain rates. The dependence of surface rain rates in the physical initialization of the FSU GSM is discussed next.

3.2 The Use of Rainfall Rates Within the Physical Initialization Process

In many previous tropical weather prediction experiments, available and accurate rainfall data has been sparse in coverage and limited in source. This problem is more pronounced over the oceans where buoys and ships provide observations which fail to achieve broad and consistent geographical coverage. Before the launch of satellites equipped with SSM/I technology, tropical weather prediction models relied solely on the elements of the World Weather Watch. According to Krishnamurti, et al. (1991), these models included surface-based networks of the radiosonde rawinsonde, pilot balloon distributions, commercial ships, aircraft observations, polar orbiting satellite-based

soundings, and geostationary satellite-based cloud tracked winds. In this decade, the precipitation estimates derived from SSM/I brightness temperatures have greatly enhanced the resolution and accuracy of the global rain rate field. Consequently, the inclusion of more accurate and more resolved rainfall rates within the physical initialization process of the Florida State University Global Spectral Model (FSU GSM) has produced improved hurricane forecasts.

While the addition of SSM/I based rain rate estimates has indeed provided data where no data existed before, it must be noted that not all SSM/I precipitation algorithms are effective. In fact, some perform quite poorly and clearly underestimate both the magnitude and geographical extent of significant rain events. Therefore it is crucial to use a sound precipitation algorithm within any prediction model in order to achieve valid results. This is the main purpose of my thesis: to incorporate the most accurate SSM/I rain rate algorithm which will in turn improve the physical initialization process, and ultimately improve the output of the FSU Global Spectral model.

It is estimated that two-thirds of all global precipitation falls in the tropics. In addition, three-fourths of the atmosphere's heat energy originates from the release of latent heat by precipitation processes. The energy release due to precipitation in the tropics, therefore, affects the *entire global circulation*. If the initialization of "observed" rainfall in a NWP model is too light, then the model-calculated energy release will be too weak, and inaccurate changes in the modeled, global circulation will result. In addition, if the rainfall in a NWP model is too robust, latent heat release will be too strong, and once again the modeled global circulation will be negatively affected. Consequently,

accurate initialization of the global rainfall field is critical. This underscores the necessity of a consistently accurate SSM/I rain rate algorithm in the physical initialization of a NWP model environment. The role of precipitation and its associated energy release (in the context of Dr. Krishnamurti's physical initialization process) will be detailed in this chapter.

Krishnamurti, et al. (1991) has stated that the sparsity of rainfall data contaminates the initialization of surface fluxes of moisture and sensible heat, precipitation, and clouds. While the quasi-geostrophic vertical motions produce a reasonable moisture field in the mid-latitudes, the deep convection in the tropics is poorly represented if large errors exist in the initial humidity distributions. This is in addition to the widely known "spin up" problem which hampers most global prediction models. Accurate rain rate values are a necessity in achieving the correct latent heating characteristics in any model's moisture profile. For example, if the lower troposphere is initialized too dry, this can result in enhancement of ocean evaporation and an ultimate reduction in a model's forecasted rain rates. An accurate, global rainfall initial state is essential for a productive, physically initialized model environment. Surface rain rate values which are either too light or too robust can lead to significant errors in the forecasted output of many numerical weather prediction models, to include the FSU Global Spectral model. This statement is validated by the results highlighted in subsequent chapters in this thesis.

Physical initialization assimilates satellite-based, surface rain rate estimations into the FSU Global Spectral model. These rain rate estimations are considered to be the "observed" values. According to Krishnamurti, et al. (1997), during the physical

initialization process the surface moisture flux, the apparent moisture sink, the surface pressure, and the vertical distributions of humidity, mass divergence, and convective heating undergo a “spin-up” consistent with the model physics and observed rain rates. Reverse physical algorithms are used in the process. The algorithms include a reverse similarity algorithm, a reverse cumulus parameterization algorithm, and an algorithm which restructures the vertical humidity distribution.

The SSM/I based rain rate estimations are a key element in both the reverse similarity algorithm and the reverse cumulus parameterization algorithm. Refer to the end of this chapter (Figure 3-2) for a flow chart incorporating reverse similarity theory and reverse cumulus parameterization in the physical initialization procedure. Reverse similarity theory will be explained first, while reverse cumulus parameterization will follow.

3.3 Reverse Similarity Theory

To highlight the role of SSM/I estimated surface rain rates within the reverse similarity algorithm, a description of Yanai fluxes $(F_S), (F_L)$ is necessary. The integral technique following Yanai et al. (1973), applies the vertically integrated equations for the apparent moisture sink (\hat{Q}_2) and the apparent heat source (\hat{Q}_1) . The surface flux of sensible heat (F_S) is expressed by:

$$F_S \uparrow = \hat{Q}_1 - \hat{Q}_R - LP \quad (1)$$

where (\hat{Q}_R) denotes the vertically integrated net radiative heating, and (\hat{Q}_1) is the vertically integrated apparent heat source according to:

$$Q_1 = \frac{\partial \bar{s}}{\partial t} + \nabla_{\sigma} \cdot \bar{s} \bar{v} + \frac{\partial}{\partial \sigma} \bar{s} \bar{\sigma} \quad (2)$$

where \bar{s} represents the large scale dry static energy.

The surface flux of latent heat (F_L) is expressed by:

$$F_L \uparrow = LP - \hat{Q}_2 \quad (3)$$

where \hat{Q}_2 is the vertically integrated apparent moisture sink according to:

$$Q_2 = -L \left(\frac{\partial \bar{q}}{\partial t} + \nabla_{\sigma} \cdot \bar{q} \bar{v} + \frac{\partial}{\partial \sigma} \bar{q} \bar{\sigma} \right) \quad (4)$$

and P is the measure of the “observed” surface rainfall rate.

The Yanai fluxes are essentially a moisture balance relation. Here the surface flux of latent heat exhibits an explicit dependence on the SSM/I based surface rain rates.

Consequently, the observed rain rates play a major role in determining an accurate

moisture balance relationship. In general, over rain free areas, \hat{Q}_2 is small and matches

the surface flux of humidity. On the other hand, over areas of rain, \hat{Q}_2 is a small

difference between the surface flux of latent heat and the observed precipitation. The

Yanai technique ultimately provides a reasonable estimate of the evaporation rates over global areas experiencing rainfall.

Reverse similarity theory is incorporated next to generate data sets of the above variables on top of the constant flux layer, consistent with the prescribed fluxes. Given the Yanai fluxes of sensible and latent heat as input to the reverse similarity theory, a solution for the potential temperature *and* the moisture variable on top of the constant

flux layer can be achieved. Following Chang (1978), the similarity fluxes of momentum, heat, and moisture can be expressed respectively by the relations:

$$F_M = \rho C_M (U_2 - U_1)^2 \quad (5)$$

$$F_H = \rho C_H c_p (U_2 - U_1)(\theta_2 - \theta_1) \quad (6)$$

$$F_Q = \rho C_q (U_2 - U_1)(q_2 - q_1)g_w \quad (7)$$

where the similarity exchange coefficients are given as follows:

(a) For the stable and neutral cases where $Ri_B > 0$

$$C_M = \frac{U_*^2}{(U_2 - U_1)^2} = \frac{k^2}{[\ln(Z_2 / Z_1)]^2} \cdot \frac{1}{(1 + 4.7 Ri_B)^2} \quad (8)$$

$$C_H = \frac{U_* \theta_*}{(U_2 - U_1)(\theta_2 - \theta_1)} = \frac{-1}{0.74} \cdot \frac{k^2}{[\ln(Z_2 / Z_1)]^2} \cdot \frac{1}{(1 + 4.7 Ri_B)^2} \quad (9)$$

$$C_q = 1.7 C_H \quad (10)$$

(b) For the unstable case where $Ri_B < 0$

$$C_M = \frac{U_*^2}{(U_1 - U_2)^2} = \frac{k^2}{[\ln(Z_2 / Z_1)]^2} \left(1 - \frac{9.4 Ri_B}{1 + C |Ri_B|^{1/2}}\right) \quad (11)$$

$$C_H = \frac{U_* \theta_*}{(U_2 - U_1)(\theta_2 - \theta_1)} = \frac{-1}{0.74} \cdot \frac{k^2}{[\ln(Z_2 / Z_1)]^2} \cdot \left(1 - \frac{9.4 Ri_B}{1 + C |Ri_B|^{1/2}}\right) \quad (12)$$

$$C_q = 1.7 C_H \quad (13)$$

C_M, C_H, C_q are the exchange coefficients of momentum, heat, and moisture.

$(U_1, U_2), (\theta_1, \theta_2)$ denote the wind and the potential temperature at the bottom and top of the surface layer. Z_1, Z_2 are the heights of the bottom and top of the constant flux layer.

The notation k is the Von Karman constant, and g_w is the ground wetness. Ri_B is the bulk Richardson number according to:

$$Ri_B \equiv \frac{g}{\bar{\theta}} \cdot \frac{(\theta_2 - \theta_1)(Z_2 - Z_1)}{(U_2 - U_1)^2} \quad (14)$$

The analysis of Louis (1979) is used to define C according to:

$$C = \frac{7.4 \cdot 9.4 k^2}{[\ln(Z_2 / Z_1)]^2} [Z_2 / Z_1]^{1/2} \quad (15)$$

for momentum, and

$$C = \frac{5.3 \cdot 9.4 k^2}{[\ln(Z_2 / Z_1)]^2} [Z_2 / Z_1]^{1/2} \quad (16)$$

for heat and moisture.

Given the surface fluxes of sensible and latent heat {equations (1) and (3)}, one can solve for θ_2 and q_2 according to equations (6) and (7). Since heat flux defines the stability, the only unknown in equations (9) and (12) is θ_2 . This can be solved for directly or iteratively.

An objective function can be defined for the unstable case, where $U_* \theta_* < 0$, according

$$\text{to:} \quad F \equiv \frac{U_* \theta_*}{(U_2 - U_1)(\theta_2 - \theta_1)} + \frac{k^2}{0.74 [\ln(Z_2 / Z_1)]^2} \cdot \left(1 - \frac{9.4 Ri_B}{1 + C |Ri_B|^{1/2}}\right) \quad (17)$$

where one searches for a value of θ_2 which minimizes F . The Newton-Rhapson iteration procedure is then used to obtain a final value of θ_2 , once it converges after three or four iterations.

For stable conditions, equation (9) can be rewritten as:

$$4.7^2 Ri_B^2 + (9.4 - A) Ri_B + 1 = 0, \quad (18)$$

where

$$A = \frac{1}{0.74} \cdot \frac{\bar{\theta}}{g\Delta z} \cdot \frac{(U_2 - U_1)^3}{U_* \theta_*} \cdot \frac{k^2}{[\ln(Z_2 / Z_1)]^2} \quad (19)$$

The signs of both roots of equation (18) are positive. The larger root is beyond the physical upper limit of Ri_B . Therefore, the solution used is the smaller root. θ_2 can then be computed from equation (14).

With a value for θ_2 , C_H and C_q can be computed using equations (9), (10), (12), and (13). Finally, q_2 can be obtained from equation (7). The outcome is a solution for the potential temperature and moisture on top of the constant flux layer.

3.4 Reverse Cumulus Parameterization

Reverse cumulus parameterization reanalyzes the vertical distribution of specific humidity in order that the rainfall implied by the cumulus parameterization algorithm resembles the SSM/I or "observed" rain rates (Krishnamurti, *et al.*, 1991). Reverse cumulus parameterization in this context was developed for a modified Kuo's scheme.

This modified Kuo scheme utilizes a moistening parameter, b , and a mesoscale convergence parameter, η . The large scale moisture supply is defined by:

$$I_L = \frac{-p_s}{g} \int_{\sigma=\sigma_T}^{\sigma=\sigma_B} \sigma \frac{\partial q}{\partial \sigma} d\sigma \quad (20)$$

where σ_B and σ_T refer to a sigma surface at the cloud base and cloud top. The total available moisture supply is expressed as:

$$I = I_L(1 + \eta) \quad (21)$$

while the total moistening and rainfall rates are expressed by the formulae:

$$M = I_L(1 + \eta)b \quad (22)$$

$$R = I_L(1 + \eta)(1 - b) \quad (23)$$

Both M and R are functions of large scale variables which ultimately control deep convection. If the Kuo scheme is reversed, the specific humidity q is modified and related to the rainfall rate R , by the following:

$$q_m = \frac{R \cdot q}{-\frac{p_s}{g} \int_{\sigma_T}^{\sigma_B} \sigma \frac{\partial q}{\partial \sigma} d\sigma} + \frac{\frac{1}{g} \int_{\sigma_T}^{\sigma_B} q d\sigma}{\frac{1}{g} \int_{\sigma_T}^{\sigma_B} d\sigma} \cdot \left[1 - \frac{R}{-\frac{p_s}{g} \int_{\sigma_T}^{\sigma_B} \sigma \frac{\partial q}{\partial \sigma} d\sigma} \right] \quad (24)$$

The moisture supply (expressed in terms of the modified specific humidity, q_m) matches the “observed” rainfall according to the relation:

$$R = -\frac{p_s}{g} \int_{\sigma_T}^{\sigma_B} \sigma \frac{\partial q_m}{\partial \sigma} d\sigma \quad (25)$$

Hence, reverse cumulus parameterization within the physical initialization process is directly affected by the SSM/I rain rates. “Observed” rain rates that are either too low or too robust will ultimately distort the deep convection parameterized in the FSU GSM.

3.5 Outgoing Longwave Radiation (OLR) Merging

The physical initialization scheme of the FSU GSM uses both SSM/I *and* outgoing longwave radiation (OLR) data to initialize the global rain rate distribution. OLR data is obtained from polar orbiting satellite(s) and this data is “sharpened” to match the SSM/I

rain rates (Krishnamurti *et al.*, 1997). In other words, regression based on a large volume of diverse rain rate datasets is used to statistically sharpen the OLR based rain to the SSM/I based rain. Figure 3-1 depicts a flow chart of this process.

OLR data is incorporated into the physical initialization process in order to fill in any SSM/I gaps (swaths) not available. In times and places (such as middle-latitude land areas) where SSM/I rain rates may be unreliable, OLR based rain rates can provide a consistent, alternative data source. However, as SSM/I rain rate algorithms continue to improve, less emphasis will be placed on the inclusion of OLR rain rate data.

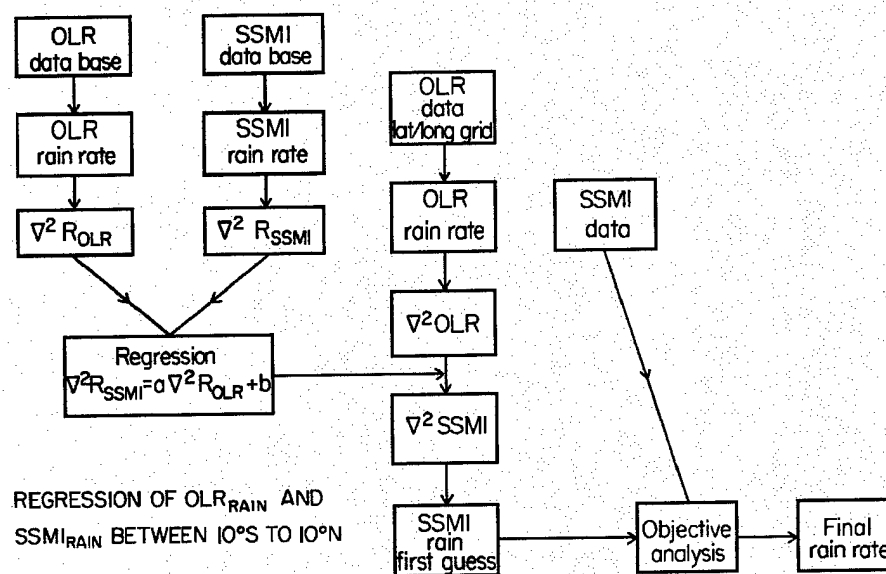


Figure 3-1: Rainfall estimation from a mix of outgoing longwave radiation (OLR) and SSM/I.

3.6 Newtonian Relaxation

Physical initialization is performed using Newtonian relaxation, otherwise known as nudging. The basic model variables are relaxed during a pre-integration phase corresponding to day -1 to day 0. Specifically, the vorticity, divergence, and pressure tendency equations undergo dynamic relaxation toward their observed state at the end of the initialization period. Since the divergence field evolves strongly from the imposed heating due to rainfall, this field is relaxed weakly as compared to the vorticity and surface pressure fields.

Newtonian “nudging” relaxes model forecast values to match the observed estimates. During the pre-integration phase, the model is integrated over a time interval preceding day 0 of the model run. Here, SSM/I rain rates from the prior day (day -1) are utilized. During this interval, assimilation of the products of the precipitation field, reverse similarity theory, OLR matching, and reverse cumulus parameterization takes place. The result is an improved, physically initialized model environment, where the precipitation distribution and associated surface fluxes of sensible and latent heat are in close agreement to the observed state (day 0). Figure 3-2 depicts a flow chart of the entire physical initialization procedure.

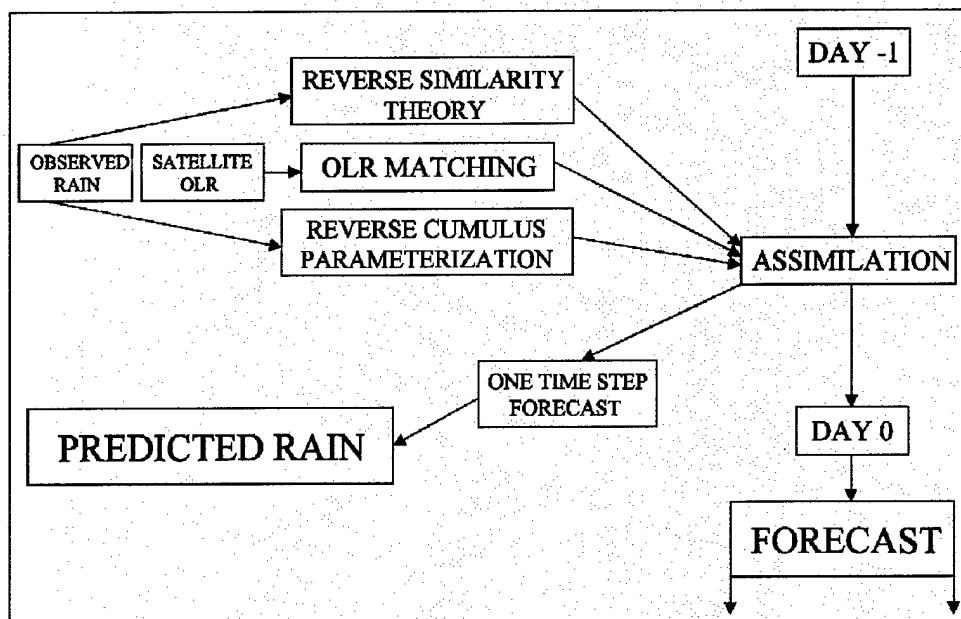


Figure 3-2: The physical initialization procedure.

CHAPTER 4

FSU GLOBAL SPECTRAL MODEL: HURRICANE FORECASTS

4.1 Overview

The Florida State University Global Spectral Model (FSU GSM) was used to generate both two and three day forecasts of hurricane track, wind intensity, and minimum central pressure. All model forecasts in this experiment include physical initialization and T170 resolution. No more than two nodes of an IBM SP2 were tasked to generate the forecasts. A three day forecast utilizing only one node took approximately 25 hours to complete, while the use of two nodes cuts the processing time in half.

This experiment focuses on four hurricanes from the 1998 Atlantic hurricane season: Hurricane Bonnie, Hurricane Danielle, Hurricane Georges, and Hurricane Mitch. Two and three day forecasts were generated for Hurricanes Bonnie, Danielle, and Mitch, while only a three day forecast was generated for Hurricane Georges. *Separate* model runs were initiated using *each* of the Cal/Val, NESDIS, and GPROF 4.0 SSM/I rain rates in the physical initialization of the model. In addition, model experiments using Tropical Rainfall Measuring Mission (TRMM) rain rates based upon the TMI – 2A12 rain rate algorithm were performed. These results, as well as the TMI – 2A12 rain rate algorithm, are highlighted in chapter five of this thesis. The results of 21 individual forecasts are

highlighted in this chapter, while seven additional TRMM based forecasts are the subject of chapter five.

FSU GSM hurricane track, wind intensity, and minimum central pressure forecasts using *each* of the SSM/I rain rate algorithms are compared to the official, observed data from the National Hurricane Center (NHC), Miami, Florida. Comparisons are highlighted in graphical formats. In addition, statistics (average deviations) are computed and presented. It is important to note that the observed data from the National Hurricane Center is the most recently published hurricane position and wind intensity data for the 1998 season. The observed, minimum central pressure data is taken directly from the original NHC storm advisories for each time period. If aircraft reconnaissance measurements of wind intensity and/or minimum central pressure are not available for a particular time period, the NHC estimates the winds and/or pressure based upon satellite data.

4.2.1 Hurricane Bonnie (72 hour forecast)

After a long trek across the Atlantic Ocean, Hurricane Bonnie maintained a northwesterly course toward North Carolina during the three days preceding landfall at Cape Fear. Figure 4-1 depicts three separate FSU GSM track forecasts for Hurricane Bonnie using either the Cal/Val, NESDIS, or GPROF 4.0 SSM/I rain rates as input to the physical initialization of the model. With the exception of the SSM/I rain rates, all other model parameters remained unchanged for each model experiment. Figure 4-1 shows

Bonnie 72 HR Fcst 0 Hr = 9823612 12Z

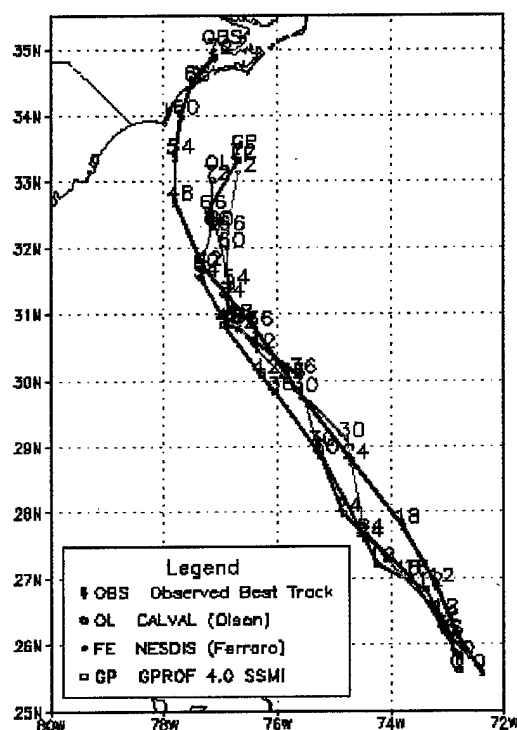


Figure 4-1: 72-hour track forecast(s) using three SSM/I rain rate algorithms for Hurricane Bonnie. Forecast tracks are compared to the official, NHC observed "best track" positions at 6 hour intervals.

that this particular three day forecast began at Julian date 9823612, which corresponds to 12Z on the 24th of August, 1998.

It is evident from Figure 4-1 that all three SSM/I rain rate algorithms contribute to fairly similar forecast storm tracks for Hurricane Bonnie. In addition, all three forecasts underestimate the northerly progress of the storm. While Hurricane Bonnie officially made landfall at the 66-hour point, the three forecasts predict the storm center is still a few hundred kilometers south of the North Carolina coast.

Great circle distance calculations were performed for Hurricane Bonnie, as well as for the other three hurricanes in this thesis. Great circle distance measures the average deviation of each six hourly *forecast* storm position from each official, six hourly *observed* “best track” storm position according to:

$$\sqrt{(lat - lato)^2 + [(lon - lono) \cdot \cos(0.5(lat + lato))]^2} \quad (1)$$

where *lat* and *lon* refer to the *forecast* storm position at each six hourly interval and where *lato* and *lono* refer to the *observed* “best track” storm position at each six hourly interval in the 72 hour duration. To obtain a single value of the average deviation of each six hourly, forecast storm position in terms of latitude *and* longitude, the *sum* of the latitude and longitude deviations at each forecast storm position is calculated according to equation (1) above. This measures how far away, on the average, each *forecast* latitude/longitude storm position is from the *observed* latitude/longitude storm position at *each* six hourly interval in the 72 hour forecast. The cosine term in equation (1) accounts for the curvature of the earth’s surface.

Table 4-1.1 shows the great circle distance deviation calculations for Figure 4-1. To obtain track deviation distances in units of kilometers, equation (1) above is simply multiplied by 111.1 (to convert degrees longitude to kilometers). For this particular three day forecast of Hurricane Bonnie, the Cal/Val based forecast produces the smallest track deviation for all time periods shown in Table 4-1.1. When comparing the NESDIS and GPROF 4.0 track deviations, the NESDIS based forecast maintains a smaller track deviation for the first 12 hours of the forecast. However, the GPROF based forecast produces a slightly smaller track deviation at the end of 72 hours.

Table 4-1.1: Forecast track deviations for Hurricane Bonnie (3 day forecast).

<i>Hours of Prediction</i>	<i>Cal/Val (Olson)</i>	<i>NESDIS (Ferraro)</i>	<i>GPROF 4.0</i>
12	24.54 km	36.70 km	46.32 km
24	57.88 km	65.15 km	64.02 km
36	70.40 km	76.96 km	77.66 km
48	92.67 km	102.75 km	107.72 km
60	118.72 km	128.75 km	127.64 km
72	135.49 km	144.06 km	138.43 km

To measure the variations of *forecast* wind intensity and *forecast* minimum central pressure (from the *observed* values), average deviation calculations were performed for Hurricane Bonnie and for the other three hurricanes highlighted in this thesis. The average deviation is a measure of variability. Average deviation (A.D.) can be expressed as:

$$A.D. = \frac{1}{N} \sum |x_i - \bar{x}| \quad (2)$$

where x_i represents the *forecast* wind intensity (or minimum central pressure) at each six hourly storm position, and \bar{x} is the official *observed* wind intensity (or minimum central pressure) at the appropriate six hourly storm position.

Figure 4-2 depicts FSU GSM wind intensity output for Hurricane Bonnie using the three different SSM/I rain rate algorithms as input to the physical initialization of the model. While the observed wind intensity remains fairly constant throughout the 72 hour forecast period, all three forecasts of wind intensity exhibit fluctuations. In addition, all three forecasts of wind intensity are greater in magnitude than the observed wind intensity. Figure 4-2 shows that forecast wind intensity fluctuations are the greatest using

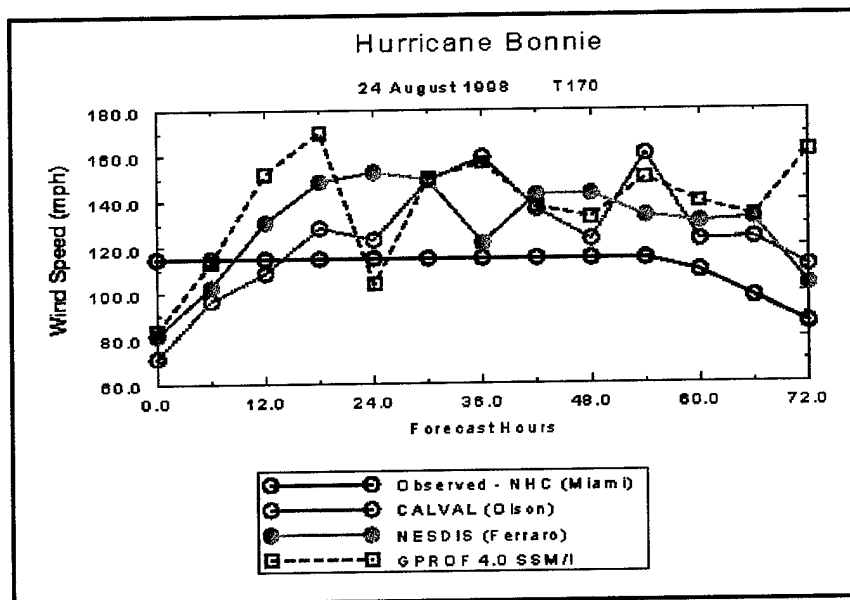


Figure 4-2: FSU GSM wind intensity output using three different SSM/I algorithms.

the GPROF 4.0 rain rates as input to the physical initialization of the model. Table 4-2.1 shows this as well. The average deviations for the GPROF based model experiment are indeed the greatest. With the exception of the first 12 hours of the forecast, the Cal/Val based experiment produces wind intensity output closest to the observed values.

Table 4-2.1: Forecast wind intensity deviations for Hurricane Bonnie (3 day forecast).

Hours of Prediction	Cal/Val (Olson)	NESDIS (Ferraro)	GPROF 4.0
12	22.87 mph	20.62 mph	23.48 mph
24	18.02 mph	26.57 mph	27.38 mph
36	24.04 mph	24.85 mph	30.55 mph
48	22.00 mph	25.56 mph	28.28 mph
60	23.39 mph	24.57 mph	29.08 mph
72	23.73 mph	24.74 mph	33.13 mph

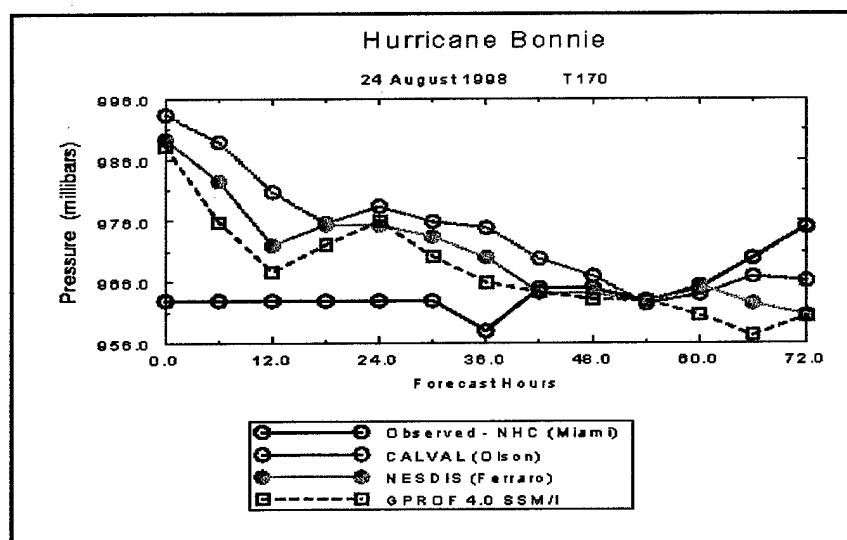


Figure 4-3: FSU GSM minimum central pressure output using three different SSM/I algorithms.

Figure 4-3 depicts FSU GSM minimum central pressure output for Hurricane Bonnie. It is apparent that all three forecasts do not come in line with the observed pressure until the 42 hour point. In addition, the GPROF and NESDIS model experiments fail to forecast an increase in Hurricane Bonnie's pressure after it made landfall. As both Figure 4-3 and Table 4-3.1 indicate, the GPROF based experiment produces the smallest pressure deviations from the observed values published by the NHC in Miami.

Table 4-3.1: Minimum central pressure deviations for Hurricane Bonnie (3 day forecast).

<i>Hours of Prediction</i>	<i>Cal/Val (Olson)</i>	<i>NESDIS (Ferraro)</i>	<i>GPROF 4.0</i>
12	24.67 mb	18.28 mb	14.22 mb
24	20.40 mb	15.90 mb	12.94 mb
36	18.83 mb	14.57 mb	11.42 mb
48	15.41 mb	11.50 mb	9.15 mb
60	12.75 mb	9.48 mb	7.89 mb
72	11.70 mb	9.71 mb	8.78 mb

4.2.2 Hurricane Bonnie (48 hour forecast)

A *second* experiment was conducted for Hurricane Bonnie in which two changes were introduced. First, the forecast began a day later. Second, the forecast only predicted 48 hours into the future. Figure 4-4 shows the forecast tracks for the two day forecast, beginning on August 25th, 1998, at 12Z. It is apparent that larger deviations exist between each of the three forecast tracks when compared to the 72 hour forecast(s). In addition, the GPROF forecast predicts Hurricane Bonnie will not make landfall, and the

Bonnie 48 HR Fcst 0 Hr = 9823712 12Z

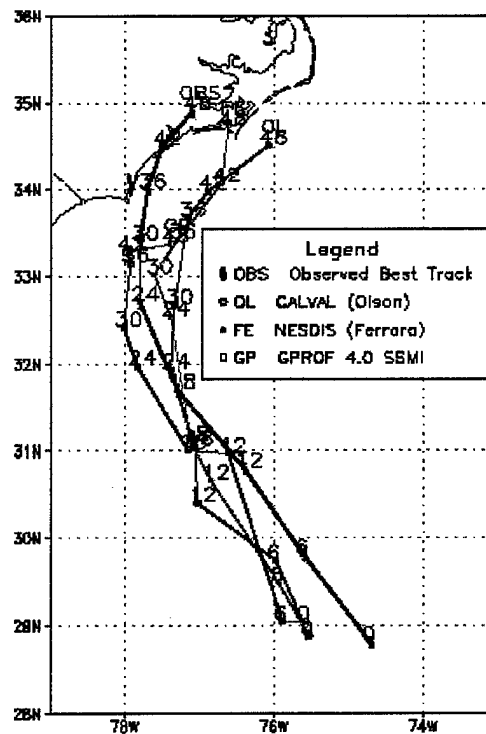


Figure 4-4: 48-hour track forecast(s) using three SSM/I rain rate algorithms for Hurricane Bonnie. Forecast tracks are compared to the official, NHC observed "best track" positions at 6 hour intervals.

Cal/Val forecast predicts the center of the storm will remain to the east of the North Carolina coast. Only the NESDIS based forecast track reasonably mimics the observed “best track”, with its 48 hour forecast location not far from where Hurricane Bonnie actually plagued North Carolina. Table 4-4.1 indicates that the storm track deviations are

Table 4-4.1: Forecast track deviations for Hurricane Bonnie (2 day forecast).

<i>Hours of Prediction</i>	<i>Cal/Val (Olson)</i>	<i>NESDIS (Ferraro)</i>	<i>GPROF 4.0</i>
12	64.42 km	58.42 km	68.95 km
24	72.50 km	57.27 km	73.17 km
36	73.64 km	58.06 km	82.07 km
48	77.63 km	60.10 km	98.80 km

significantly less using the NESDIS rain rates as input to the model. Moreover, the track deviations in this two day forecast are much improved when compared to the three day forecast(s) of Hurricane Bonnie.

Figure 4-5 depicts forecast wind intensity output for the two day forecast of Hurricane Bonnie. All three forecasts do not achieve the observed wind intensity until the 12 hour point. Visual inspection reveals that the NESDIS based wind intensity output exhibits the smallest fluctuations of the three forecasts. Table 4-5.1 validates this argument, showing that the smallest wind intensity deviations for the last three time periods are the product of the NESDIS based forecast.

Table 4-5.1: Forecast wind intensity deviations for Hurricane Bonnie (2 day forecast).

<i>Hours of Prediction</i>	<i>Cal/Val (Olson)</i>	<i>NESDIS (Ferraro)</i>	<i>GPROF 4.0</i>
12	37.68 mph	30.83 mph	30.02 mph
24	34.39 mph	26.46 mph	28.72 mph
36	29.26 mph	20.92 mph	22.59 mph
48	30.57 mph	19.57 mph	20.07 mph

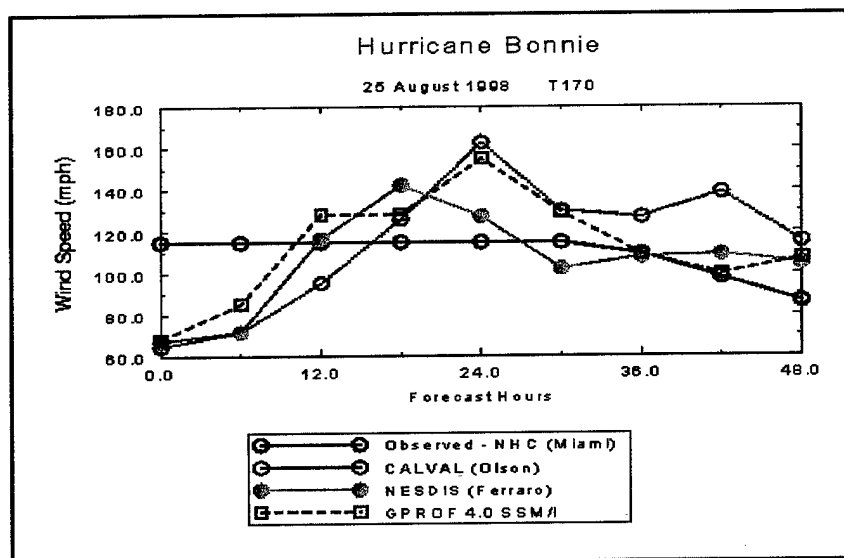


Figure 4-5: FSU GSM wind intensity output using three different SSM/I algorithms.

Table 4-6.1 and Figure 4-6 depict the FSU GSM minimum central pressure results for the 48 hour forecast of Hurricane Bonnie. Figure 4-6 shows that the forecast pressure for all three experiments is much higher than the observed pressure, and does not closely resemble the observed values until the 18 hour point. Table 4-6.1 shows that all three forecasts exhibit pressure deviations of the same order and magnitude.

Table 4-6.1: Minimum central pressure deviations for Hurricane Bonnie (2 day forecast).

<i>Hours of Prediction</i>	<i>Cal/Val (Olson)</i>	<i>NESDIS (Ferraro)</i>	<i>GPROF 4.0</i>
12	28.50 mb	25.14 mb	23.47 mb
24	17.99 mb	16.47 mb	15.03 mb
36	14.46 mb	14.29 mb	14.07 mb
48	11.78 mb	11.87 mb	11.84 mb

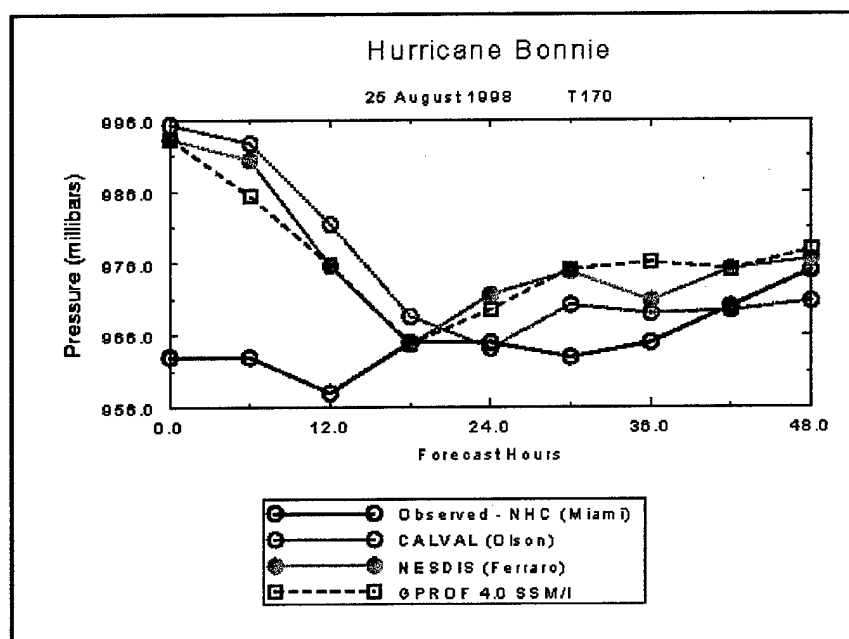


Figure 4-6: FSU GSM minimum central pressure output using three different SSM/I algorithms.

4.3.1 Hurricane Danielle (72 hour forecast)

Hurricane Danielle progressed on a west to northwest course from its point of origin until it experienced recurvature on August 31st, 1998, only 325 nautical miles east of Cape Canaveral, Florida. Despite the fact that Hurricane Danielle never made landfall, the storm is still worth studying in the context of this thesis. Figure 4-7 portrays a three day storm track forecast for Hurricane Danielle, beginning on August 29th, 1998. All three forecasts perform quite well in predicting the recurvature of Danielle around 48 hours into the period. Moreover, the forecast timing of the three experiments closely

Danielle 72 HR Fcst 0 Hr = 982411Z 12Z

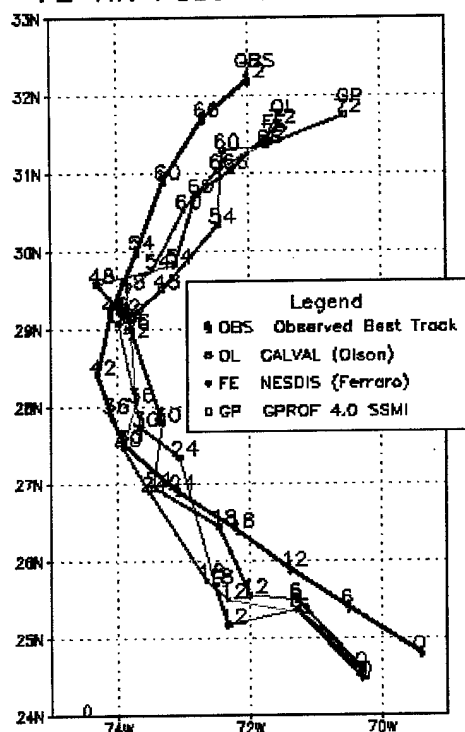


Figure 4-7: 72-hour track forecast(s) using three SSM/I rain rate algorithms for Hurricane Danielle. Forecast tracks are compared to the official, NHC observed "best track" positions at 6 hour intervals.

resembles the observed movement of the storm. However, both the Cal/Val and GPROF experiments exhibit some fluctuation in their forecast tracks. The NESDIS experiment, on the other hand, provides a more accurate forecast with the least amount of track fluctuation or deviation. Table 4-7.1 validates this claim. While the GPROF experiment produces the smallest forecast track deviation through the first 24 hours, the NESDIS experiment provides the best track forecast for the remaining two days in the forecast period. In addition, the Cal/Val experiment underperforms the NESDIS forecast, with

Table 4-7.1: Forecast track deviations for Hurricane Danielle (3 day forecast).

<i>Hours of Prediction</i>	<i>Cal/Val (Olson)</i>	<i>NESDIS (Ferraro)</i>	<i>GPROF 4.0</i>
12	99.69 km	86.80 km	81.08 km
24	86.92 km	77.71 km	61.31 km
36	85.53 km	61.97 km	70.92 km
48	82.09 km	60.79 km	74.46 km
60	77.18 km	57.63 km	80.90 km
72	77.88 km	61.82 km	87.28 km

track deviations as much as 23 km larger.

Table 4-8.1 and Figure 4-8 depict FSU GSM wind intensity results for the same three day forecast of Hurricane Danielle. While all three wind intensity forecasts are greater in

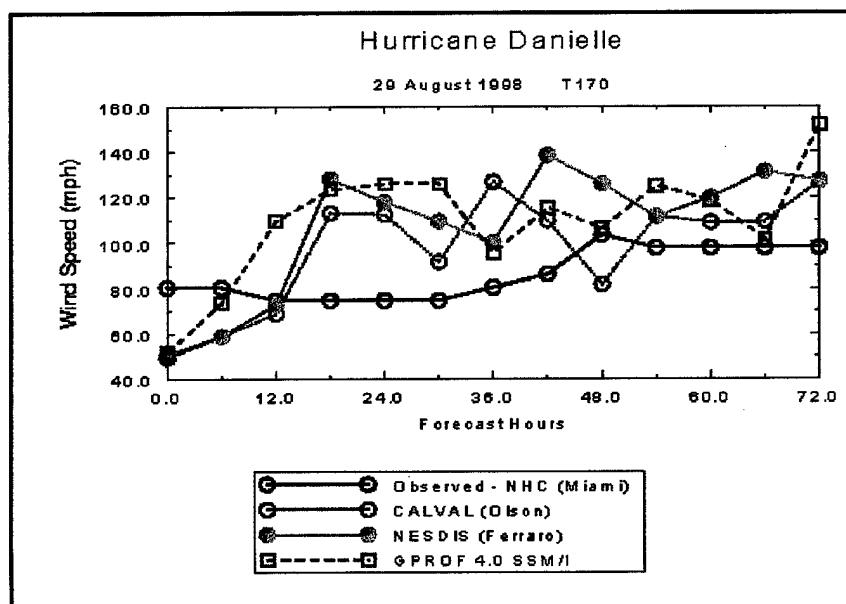


Figure 4-8: FSU GSM wind intensity output using three different SSM/I algorithms.

magnitude than the observed wind speeds, the Cal/Val experiment predicts slightly lower wind intensities throughout most of the forecast period. Consequently, Table 4-8.1 shows that the Cal/Val based forecast produces the smallest wind intensity deviations.

Table 4-8.1: Forecast wind intensity deviations for Hurricane Danielle (3 day forecast).

<i>Hours of Prediction</i>	<i>Cal/Val (Olson)</i>	<i>NESDIS (Ferraro)</i>	<i>GPROF 4.0</i>
12	19.57 mph	17.69 mph	23.48 mph
24	26.94 mph	29.95 mph	34.07 mph
36	28.28 mph	29.18 mph	33.76 mph
48	27.02 mph	31.00 mph	29.83 mph
60	24.38 mph	28.63 mph	28.80 mph
72	23.76 mph	29.07 mph	28.80 mph

Table 4-9.1 and Figure 4-9 show forecast minimum central pressure results for Hurricane Danielle. All three forecasts of minimum central pressure are outstanding after the 18 hour forecast point. The GPROF experiment, however, is slightly superior to the others. As indicated in Figure 4-9, the GPROF forecast pressures are almost identical to the observed pressures at each time increment.

Table 4-9.1: Minimum central pressure deviations for Hurricane Danielle (3 day forecast).

<i>Hours of Prediction</i>	<i>Cal/Val (Olson)</i>	<i>NESDIS (Ferraro)</i>	<i>GPROF 4.0</i>
12	15.17 mb	14.02 mb	11.04 mb
24	10.00 mb	9.97 mb	8.23 mb
36	8.13 mb	7.74 mb	6.21 mb
48	7.94 mb	6.71 mb	5.11 mb
60	7.11 mb	6.11 mb	4.43 mb
72	6.40 mb	5.63 mb	4.13 mb

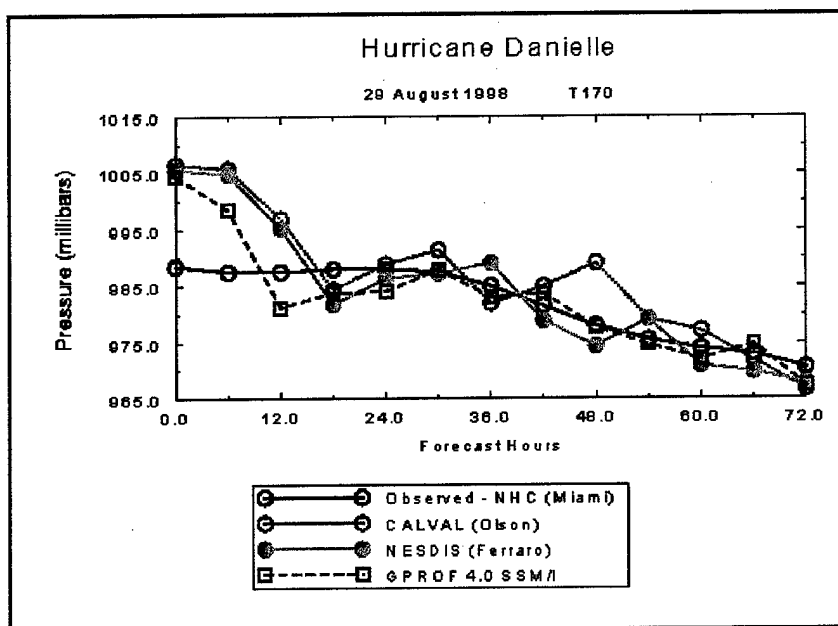


Figure 4-9: FSU GSM minimum central pressure output using three different SSM/I algorithms.

4.3.2 Hurricane Danielle (48 hour forecast)

A second forecast experiment of Hurricane Danielle was conducted, only this time the forecast began 24 hours later (August 30th, 1998) than the three day forecast. In addition, the forecast period is only 48 hours in duration. Figure 4-10 portrays the two day track forecast for Hurricane Danielle, beginning at 12Z on August 30th. While all three forecasts deviate significantly from the observed "best track" in the beginning, the NESDIS based storm track follows a very similar recurvature pattern (after 24 hours) as the observed track. The Cal/Val and GPROF forecasts, however, deviate considerably

Danielle 48 HR Fcst 0 Hr = 9824212 12Z

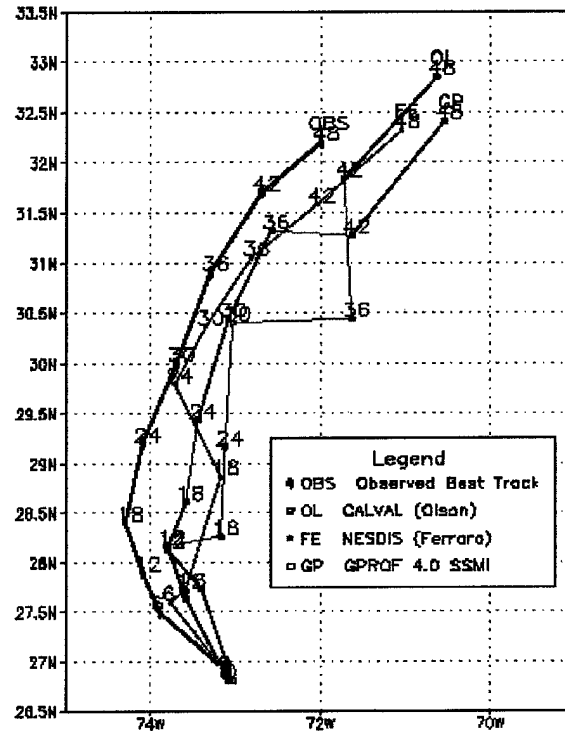


Figure 4-10: 48-hour track forecast(s) using three SSM/I rain rate algorithms for Hurricane Danielle. Forecast tracks are compared to the official, NHC observed “best track” positions at 6 hour intervals.

from the observed track throughout the entire 48 hour period. This is also shown in Table 4-10.1, where the NESDIS experiment produces the smallest track deviations from the observed for three of the four time periods.

Table 4-10.1: Forecast track deviations for Hurricane Danielle (2 day forecast).

<i>Hours of Prediction</i>	<i>Cal/Val (Olson)</i>	<i>NESDIS (Ferraro)</i>	<i>GPROF 4.0</i>
12	28.55 km	25.02 km	35.11 km
24	58.08 km	54.25 km	49.37 km
36	76.35 km	53.08 km	57.89 km
48	85.98 km	58.30 km	72.73 km

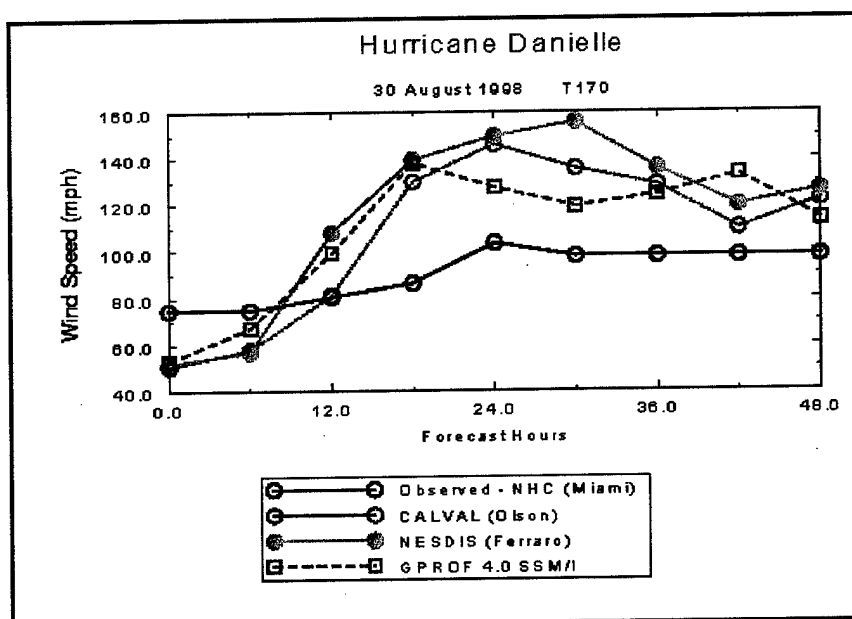


Figure 4-11: FSU GSM wind intensity output using three different SSM/I algorithms.

Figure 4-11 and Table 4-11.1 highlight the wind intensity results from the two day forecast of Hurricane Danielle. While all three forecasts overestimate the observed wind speeds after the twelve hour point, Table 4-11.1 shows that the GPROF experiment produces the smallest overestimation.

Table 4-11.1: Forecast wind intensity deviations for Hurricane Danielle (2 day forecast).

Hours of Prediction	Cal/Val (Olson)	NESDIS (Ferraro)	GPROF 4.0
12	13.94 mph	22.72 mph	15.94 mph
24	25.60 mph	33.46 mph	24.72 mph
36	28.12 mph	37.60 mph	24.51 mph
48	25.89 mph	34.85 mph	24.77 mph

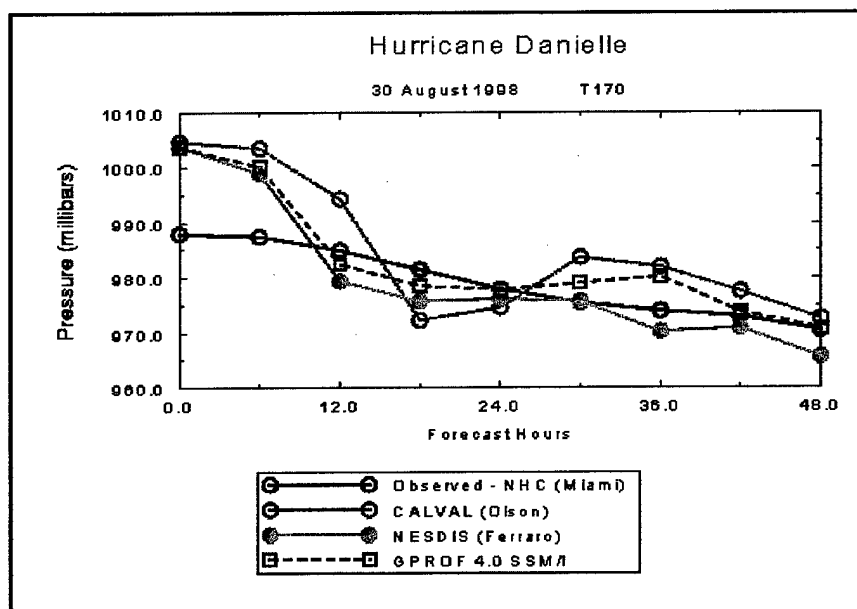


Figure 4-12: FSU GSM minimum central pressure output using three different SSM/I algorithms.

Figure 4-12 and Table 4-12.1 depict forecast minimum central pressure results from the same two day experiment for Hurricane Bonnie. Once again it takes 12 hours for the forecasts to mimic the observed pressures. Figure 4-12 shows that both the GPROF and the NESDIS experiments closely follow the observed pressure curve. However, Table 4-12.1 proves that the GPROF experiment gives the smallest pressure deviations.

Table 4-12.1: Minimum central pressure deviations - Hurricane Danielle (2 day forecast).

Hours of Prediction	Cal/Val (Olson)	NESDIS (Ferraro)	GPROF 4.0
12	13.98 mb	10.91 mb	10.28 mb
24	10.89 mb	8.06 mb	6.79 mb
36	10.10 mb	6.32 mb	6.24 mb
48	8.60 mb	5.69 mb	4.99 mb

4.4.1 Hurricane Georges (72 hour forecast)

After crossing the Florida Keys, Hurricane Georges initiated a northwesterly course toward the U.S. Gulf Coast States of Louisiana and Mississippi. A weak trough developing in the central United States presented the possibility that Hurricane Georges might recurve into the Florida Panhandle. However, as most of the model guidance suggested, Georges made landfall near Gulfport, Mississippi, on the 28th of September. Figure 4-13 shows the three day storm track forecast(s) for Hurricane Georges, beginning on September 25th, 1998. It is apparent from the figure that the experiments did not

Georges 72 HR Fcst 0 Hr = 9826812 12Z

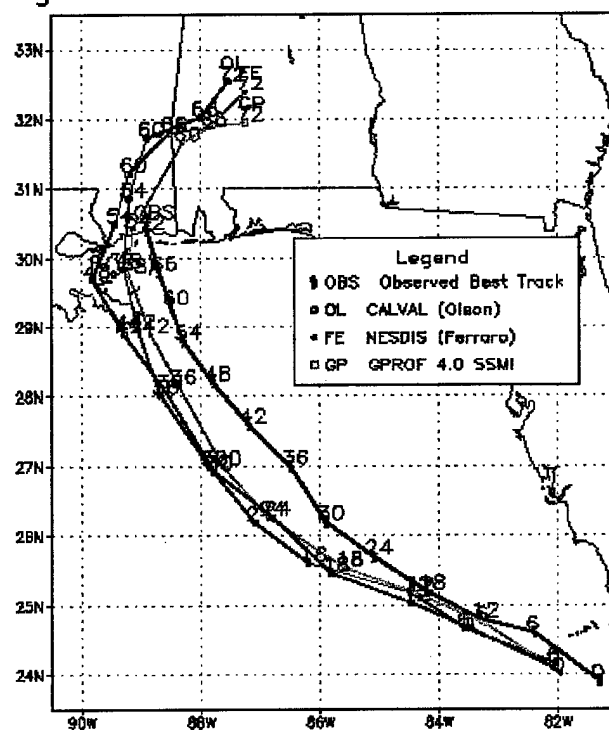


Figure 4-13: 72-hour track forecast(s) using three SSM/I rain rate algorithms for Hurricane Georges.

predict the fact that Georges stalled as it approached Gulfport. However, the NESDIS experiment predicts a track closest to the observed “best track.” This claim is substantiated in Table 4-13.1, in which the NESDIS based experiment has the smallest forecast track deviations for every time increment.

Table 4-13.1: Forecast track deviations for Hurricane Georges (3 day forecast).

<i>Hours of Prediction</i>	<i>Cal/Val (Olson)</i>	<i>NESDIS (Ferraro)</i>	<i>GPROF 4.0</i>
12	107.40 km	91.18 km	102.54 km
24	147.02 km	121.36 km	130.81 km
36	170.15 km	146.48 km	156.83 km
48	184.48 km	162.39 km	178.27 km
60	198.02 km	174.70 km	186.00 km
72	207.88 km	187.48 km	192.44 km

Figure 4-14 and Table 4-14.1 show the forecast wind intensity results for Hurricane Georges. In a departure from the wind intensity results highlighted earlier in this chapter, Figure 4-14 exhibits a severe *underestimation* of the wind speeds by all three forecasts, most notably in the latter half of the forecast period. The quick decrease in the forecast winds toward the end of the three day period can be attributed to the rapid storm movement forecast over land (vs. the observed stall of Georges at the coast). Table 4-14.1 highlights the fact that the Cal/Val experiment produces the smallest wind

Table 4-14.1: Forecast wind intensity deviations for Hurricane Georges (3 day forecast).

<i>Hours of Prediction</i>	<i>Cal/Val (Olson)</i>	<i>NESDIS (Ferraro)</i>	<i>GPROF 4.0</i>
12	27.63 mph	30.18 mph	28.85 mph
24	17.73 mph	23.92 mph	25.19 mph
36	17.98 mph	22.59 mph	25.85 mph
48	22.55 mph	25.04 mph	28.47 mph
60	25.97 mph	28.08 mph	30.90 mph
72	28.80 mph	30.29 mph	31.86 mph

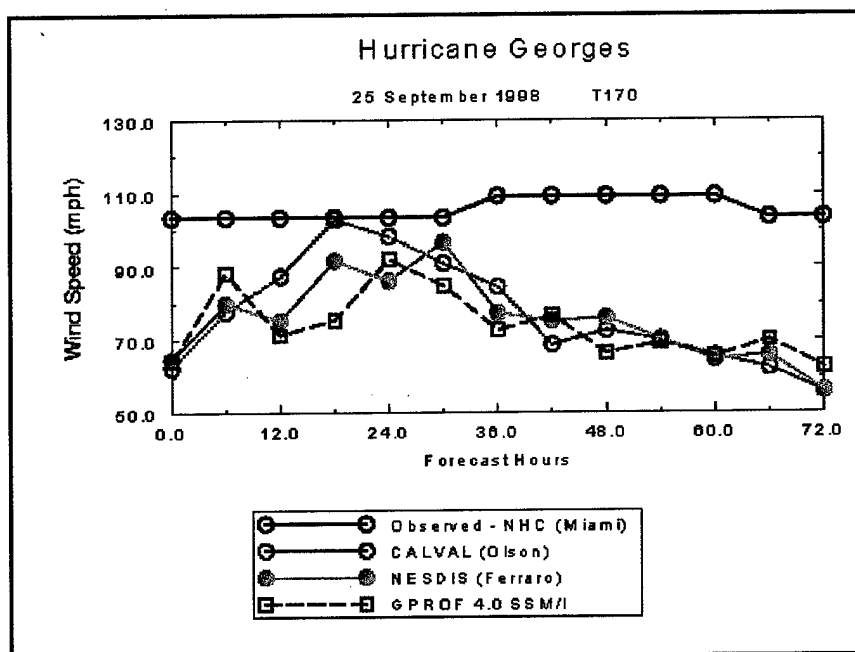


Figure 4-14: FSU GSM wind intensity output using three different SSM/I algorithms.

intensity deviations for every time step in the forecast.

Table 4-15.1 and Figure 4-15 depict the forecast minimum central pressure results for Hurricane Georges. Table 4-15.1 shows that all three forecasts of minimum central

Table 4-15.1: Minimum central pressure deviations for Hurricane Georges (3 day forecast).

<i>Hours of Prediction</i>	<i>Cal/Val (Olson)</i>	<i>NESDIS (Ferraro)</i>	<i>GPROF 4.0</i>
12	11.20 mb	9.28 mb	10.79 mb
24	7.44 mb	6.95 mb	6.68 mb
36	6.64 mb	6.47 mb	6.19 mb
48	8.35 mb	7.95 mb	8.38 mb
60	11.53 mb	11.06 mb	11.31 mb
72	13.94 mb	13.37 mb	13.44 mb

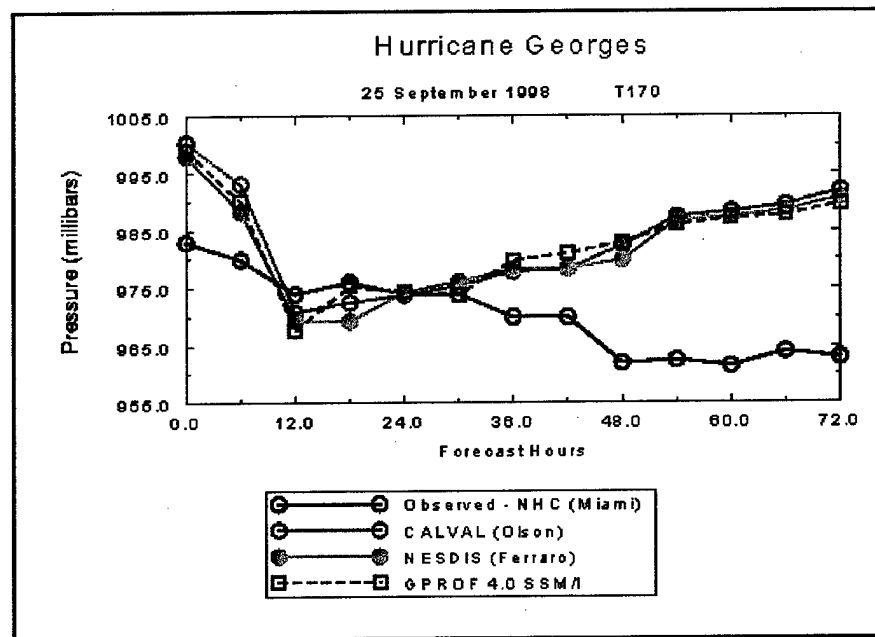


Figure 4-15: FSU GSM minimum central pressure output using three different SSM/I algorithms.

pressure produce almost identical pressure deviations. The rapid rise in the forecasted pressure depicted in Figure 4-15 is once again indicative of the fact that the model accelerates Hurricane Georges too quickly over land, whereas in reality the storm stalled just off the Gulf Coast.

4.5.1 Hurricane Mitch (72 hour forecast)

Hurricane Mitch proved to be a prime example of the limits of numerical weather prediction. While most of the model guidance predicted that Mitch would continue its northwesterly movement toward the Yucatan Peninsula, the storm stalled just north of the

Honduran coast. After 24 hours, Hurricane Mitch reversed direction and assumed a slow drift to the south, ultimately moving inland over Honduras.

Figure 4-16 highlights the fact that all three FSU GSM forecasts did not predict Mitch's unusual drift toward Honduras. After 48 hours into the forecast, all three track predictions show a storm acceleration to the northwest. As both Figure 4-16 and Table 4-16.1 indicate, the GPROF experiment produces the most accurate storm track for the

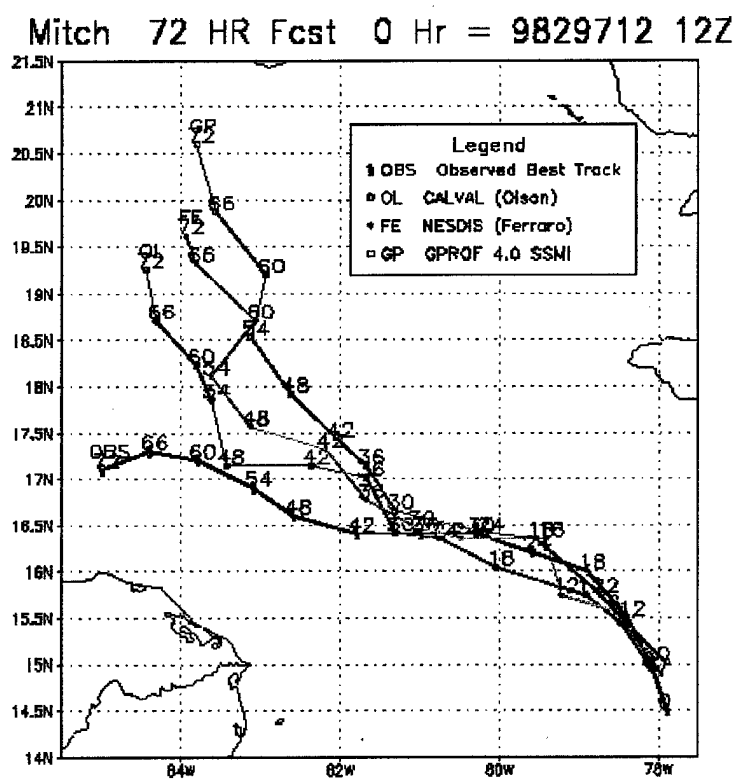


Figure 4-16: 72-hour track forecast(s) using three SSM/I rain rate algorithms for Hurricane Mitch.

first 24 hours, the NESDIS experiment provides the most accurate track for the *next* 24 hours, and the Cal/Val experiment gives the most accurate forecast track for the *last* 24 hours in the period.

Table 4-16.1: Forecast track deviations for Hurricane Mitch (3 day forecast).

<i>Hours of Prediction</i>	<i>Cal/Val (Olson)</i>	<i>NESDIS (Ferraro)</i>	<i>GPROF 4.0</i>
12	59.92 km	71.59 km	59.66 km
24	85.07 km	75.78 km	64.72 km
36	90.31 km	77.49 km	77.74 km
48	93.54 km	85.93 km	89.97 km
60	97.90 km	100.34 km	111.90 km
72	113.90 km	125.95 km	149.05 km

Figure 4-17 and Table 4-17.1 portray forecast wind intensity results for the three day forecast of Hurricane Mitch. As Table 4-17.1 shows, the NESDIS experiment provides the smallest wind intensity deviations for all but the first 12 hours of the forecast. Moreover, as Figure 4-17 indicates, the NESDIS curve mimics Mitch's observed wind speed curve extremely well from 18 to 48 hours into the forecast.

Table 4-17.1: Forecast wind intensity deviations for Hurricane Mitch (3 day forecast).

<i>Hours of Prediction</i>	<i>Cal/Val (Olson)</i>	<i>NESDIS (Ferraro)</i>	<i>GPROF 4.0</i>
12	22.60 mph	19.41 mph	15.13 mph
24	24.42 mph	13.35 mph	18.51 mph
36	23.97 mph	10.80 mph	17.48 mph
48	25.40 mph	13.16 mph	19.65 mph
60	27.98 mph	17.57 mph	21.97 mph
72	28.18 mph	16.48 mph	22.66 mph

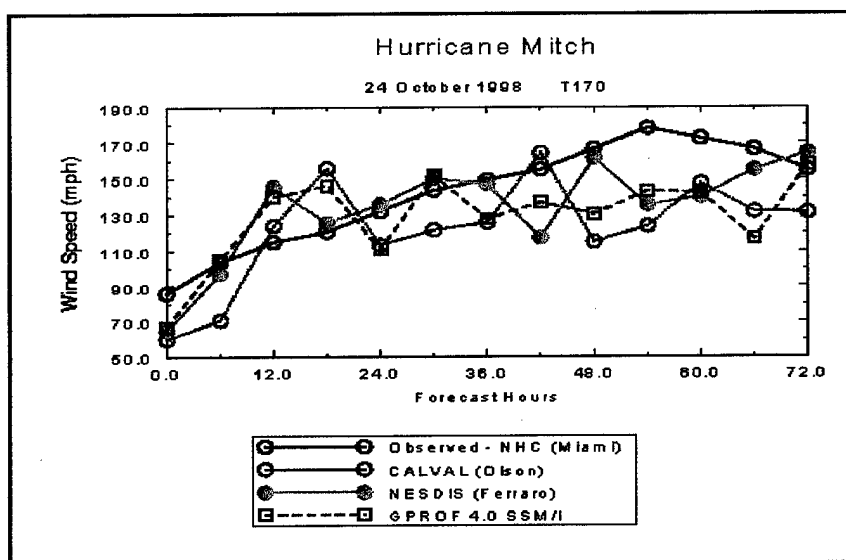


Figure 4-17: FSU GSM wind intensity output using three different SSM/I algorithms.

Table 4-18.1 and Figure 4-18 depict forecast minimum central pressure results for Hurricane Mitch. It is clearly evident that the FSU GSM poorly predicted the rapid decrease in Mitch's pressure after the 12 hour point. Table 4-18.1 shows pressure deviations on the order of 40 millibars for all three forecasts. While not much better than

Table 4-18.1: Minimum central pressure deviations for Hurricane Mitch (3 day forecast).

Hours of Prediction	Cal/Val (Olson)	NESDIS (Ferraro)	GPROF 4.0
12	14.32 mb	8.39 mb	6.92 mb
24	21.83 mb	18.74 mb	18.23 mb
36	32.78 mb	28.73 mb	28.13 mb
48	38.23 mb	34.48 mb	33.79 mb
60	44.26 mb	40.67 mb	40.73 mb
72	46.24 mb	42.94 mb	43.60 mb

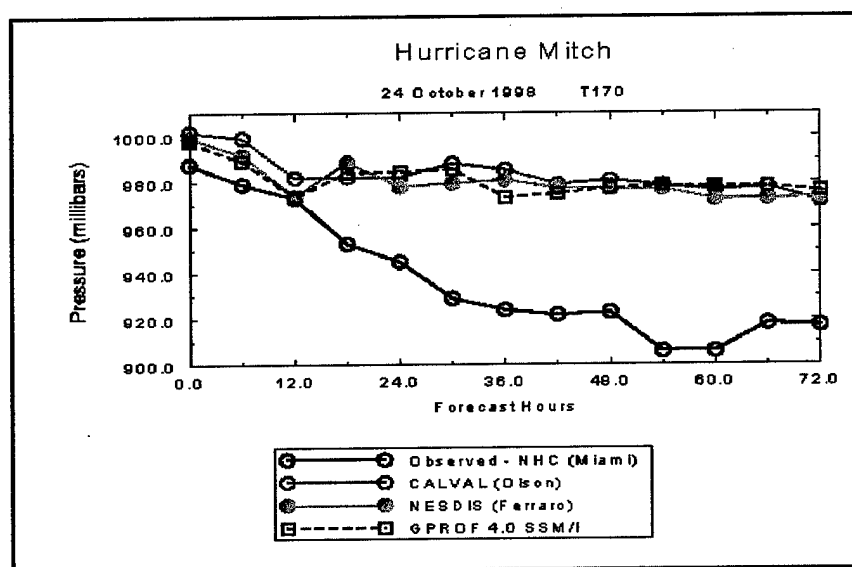


Figure 4-18: FSU GSM minimum central pressure output using three different SSM/I algorithms.

the Cal/Val and NESDIS experiments, the GPROF experiment once again produced the smallest minimum central pressure deviations for most of the forecast period.

4.5.2 Hurricane Mitch (48 hour forecast)

A second forecast experiment of Hurricane Mitch was performed to determine if the FSU GSM could better predict the southerly drift of the storm. This forecast began 24 hours later than the three day forecast and only ran for 48 hours into the future. As Figure 4-19 depicts, all three forecasts once again fail to predict Hurricane Mitch's slow drift toward Honduras. Despite the poor forecasts, the NESDIS based experiment

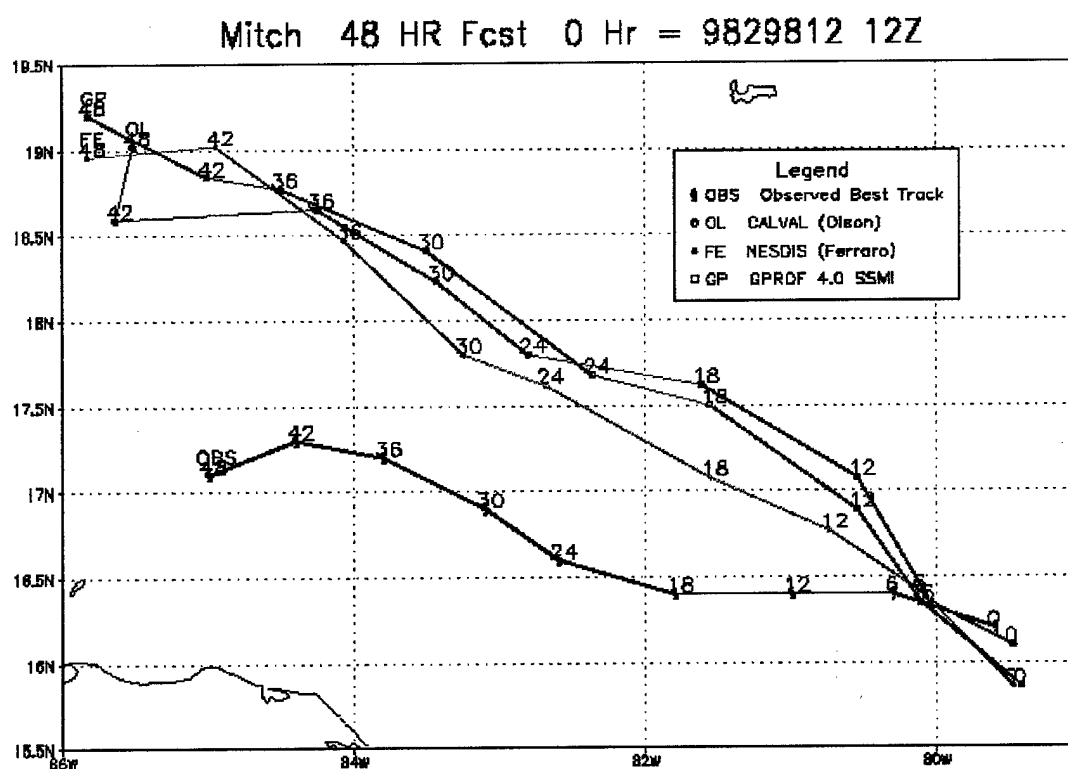


Figure 4-19: 48-hour track forecast(s) using three SSM/I rain rate algorithms for Hurricane Mitch.

proves to be the most accurate of the three, with track deviations 10 to 22 kilometers less than the Cal/Val and GPROF experiments.

Table 4-19.1: Forecast track deviations for Hurricane Mitch (2 day forecast).

<i>Hours of Prediction</i>	<i>Cal/Val (Olson)</i>	<i>NESDIS (Ferraro)</i>	<i>GPROF 4.0</i>
12	44.54 km	36.58 km	45.30 km
24	81.13 km	60.64 km	76.64 km
36	103.72 km	78.34 km	106.62 km
48	126.72 km	108.07 km	130.93 km

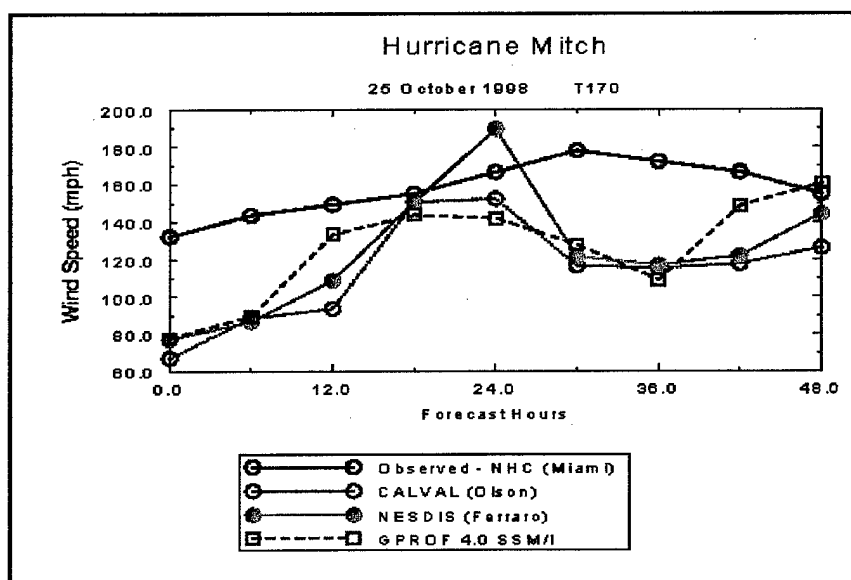


Figure 4-20: FSU GSM wind intensity output using three different SSM/I algorithms.

Figure 4-20 and Table 4-20.1 present forecast wind intensity results from the two day model run of Hurricane Mitch. Figure 4-20 shows how all three forecasts reach Mitch's observed wind intensity at the 18 hour point, but then quickly lose that intensity only 12 hours later. Table 4-20.1 indicates the GPROF model run has the smallest deviations.

Table 4-20.1: Forecast wind intensity deviations for Hurricane Mitch (2 day forecast).

<i>Hours of Prediction</i>	<i>Cal/Val (Olson)</i>	<i>NESDIS (Ferraro)</i>	<i>GPROF 4.0</i>
12	58.61 mph	50.82 mph	41.50 mph
24	38.91 mph	36.01 mph	32.11 mph
36	44.70 mph	41.74 mph	39.15 mph
48	43.43 mph	38.64 mph	33.06 mph

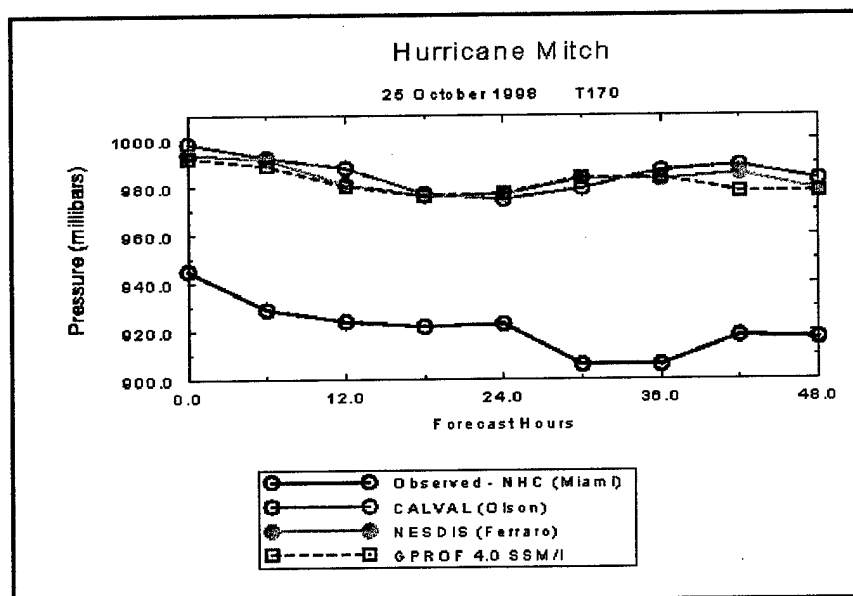


Figure 4-21: FSU GSM minimum central pressure output using three different SSM/I algorithms.

Figure 4-21 and Table 4-21.1 highlight the FSU GSM's poor prediction of Hurricane Mitch's decreasing pressure. Average deviations from the observed values are as high as 64 millibars. While all three forecasts of minimum central pressure appear identical, Table 4-21.1 shows that the GPROF experiment has slightly smaller pressure deviations for the entire period.

Table 4-21.1: Minimum central pressure deviations - Hurricane Mitch (2 day forecast).

<i>Hours of Prediction</i>	<i>Cal/Val (Olson)</i>	<i>NESDIS (Ferraro)</i>	<i>GPROF 4.0</i>
12	60.03 mb	56.03 mb	54.37 mb
24	57.36 mb	55.17 mb	54.26 mb
36	62.94 mb	61.44 mb	61.00 mb
48	64.17 mb	62.10 mb	60.87 mb

CHAPTER 5

TROPICAL RAINFALL MEASURING MISSION (TRMM)

TMI – 2A12 RAIN RATE ALGORITHM

5.1 TRMM Overview

The Tropical Rainfall Measuring Mission (TRMM) is solely dedicated to the passive and active measurement of tropical and subtropical rainfall. The TRMM satellite hosts microwave, visible, and infrared sensors, as well as the first ever spaceborne rain radar. With the use of modern, state-of-the-art instruments and a low-altitude orbit of 217 miles (350 km), both more accurate *and* higher resolution measurements can be provided to the meteorological community. According to Kummerow et al. (1998), the main objective of TRMM is to measure rainfall and its associated energy exchange between the tropical and subtropical regions of the world.

The TRMM satellite orbit range is between 35 degrees north and 35 degrees south of the equator. Unlike SSM/I satellites, TRMM does not achieve entire, global coverage. However, between 35 degrees north and 35 degrees south, TRMM covers each position on the earth's surface at a different local time each day. This enables rain variation calculations over a 24 hour period. Figure 5-1 shows the orbit of the TRMM satellite.

Since 75% of the tropics is ocean, very little surface-based measurement of rainfall is

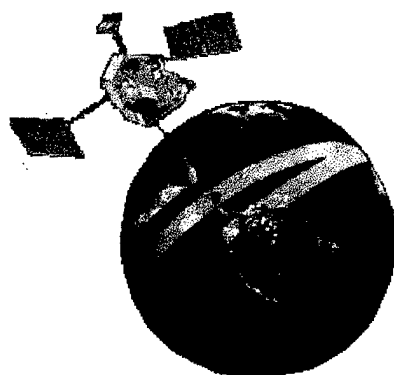


Figure 5-1: TRMM satellite orbit.

available. Consequently, large-scale tropical precipitation measurements can only be achieved through remote, space-based sensing. This is TRMM's main advantage over other remote sensing platforms: the fact that it concentrates its measurements solely over the tropics and subtropics. In time, more TRMM satellites will be placed in orbit and more continuous sensing of the tropical oceans will take place. It has been proposed that once validation of TRMM's numerous instruments is complete, other platforms such as SSM/I satellites will become obsolete. While this may become truth for the tropics, other satellites will still be needed for *complete* global coverage, such as the polar orbiters.

5.2 TRMM Microwave Imager (TMI)

It is important to note that the rain rates used within this study were measured solely by the TRMM Microwave Imager (TMI). Rain rate data from the other TRMM instruments, such as the TRMM Precipitation Radar (PR), was not used in order to

maintain similarities between TRMM and the SSM/I rain rate data highlighted earlier. The TRMM Microwave Imager (TMI) is a nine-channel passive radiometer based upon the SSM/I. According to Kummerow et al. (1998), two main differences exist between the TMI and the SSM/I. First, the TMI benefits from the addition of a pair of 10.7 GHz channels (both horizontal and vertical polarizations). Second, the TMI changes the frequency of the water vapor channel from 22.235 GHz to 21.3 GHz. Kummerow et al. (1998) states that this adjustment off the center of the water vapor "line" was made in order to avoid saturation in the tropical orbit of TRMM. While increased spatial resolution is characteristic of TMI versus SSM/I, this is not due to the sensor changes described above. It is due to the lower earth orbit of the TRMM satellite.

Figure 5-2 shows the TMI scan geometry, in addition to the scan geometries of the two other rainfall sensors (PR and VIRS). The TMI antenna is an offset parabola which

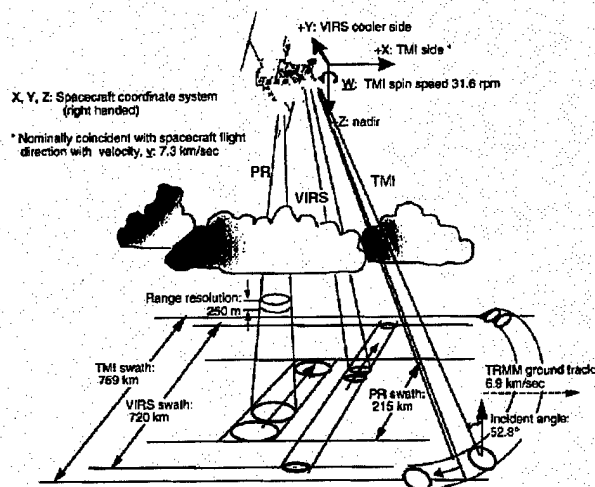


Figure 5-2: TMI scan geometry.

“sees” the earth’s surface with an incident angle of 52.8° . The TMI antenna rotates about an axis at a speed of 31.6 rpm. This rotation traces a “circle” on the earth’s surface. However, only 130° of this circle is used for acquiring data. This 130° scanned area creates a swath width of 758.5 km. Using the 85.5 GHz channel, the smallest “footprint” size the TMI samples is 6.9 km by 4.6 km. Larger footprints exist for the other channels (Kummerow *et al.*, 1998).

5.3 TRMM / TMI - 2A12 Rain Rate Algorithm

As previously written in Chapter 1, section 1.4, the GPROF 4.0 *SSM/I* rain rate algorithm was originally developed in anticipation of its adaptation to the future, operational applications of TRMM. Now that TRMM is operational, the original GPROF 4.0 SSM/I rain rate algorithm (with minor modifications) is indeed being used to calculate rain rates from the raw TMI data (brightness temperatures). This modified GPROF algorithm is known as TMI – 2A12. Figure 5-3 depicts a flow chart of the 2A12

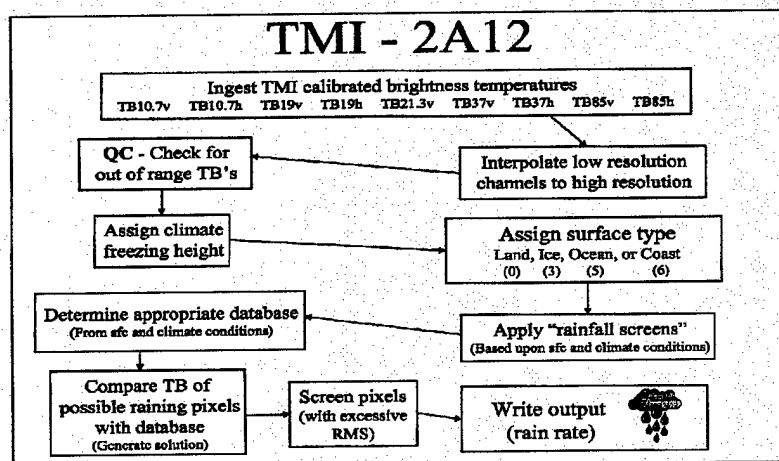


Figure 5-3: TRMM / TMI – 2A12 rain rate algorithm flow chart.

rain rate algorithm. For a complete, detailed analysis of the TMI – 2A12 algorithm (GPROF), refer back to chapter 1, section 1.4. The main difference between GPROF 4.0 for SSM/I and TMI – 2A12 can be seen in Figure 5-3. It is here that the brightness temperature data from the 10.7v, 10.7h, 21.3v, and 85v GHz channels are added to the 2A12 algorithm. This enables the 2A12 algorithm to calculate rain rates from nine different channels, whereas the original GPROF 4.0 algorithm only ingested data from six different channels.

A post-launch validation of the TMI sensor was conducted soon after the launch of the TRMM satellite. TMI brightness temperatures were compared to SSM/I brightness temperatures from DMSP F14. Biases between the two were discovered. Specifically, the TMI tended to yield warmer brightness temperatures than the SSM/I at the lower end of the brightness temperature range (~150K). In addition, the TMI also yielded warmer brightness temperatures in the higher end range. As this paper is being written, validation by comparing to ground-truth rain rates is continuing. Validation of the TMI, therefore, is a function of both the sensor itself *and* the 2A12 rain rate algorithm. The remainder of this chapter will focus on both validating the TMI – 2A12 algorithm and applying the TMI – 2A12 rain rate data to the physical initialization of the FSU GSM. Validation studies identical to the SSM/I validation studies (Chapter 2) are highlighted in section 5.4. In addition, hurricane track, wind intensity, and minimum central pressure forecasts using the TMI – 2A12 rain rates as input to the physical initialization of the FSU GSM are compared to the previous SSM/I (Chapter 4) results.

5.4 TMI – 2A12 Rain Rate Validation

Before the TMI – 2A12 rain rate algorithm is utilized in the physical initialization of the FSU GSM, the accuracy of the algorithm must be determined. Three ground validation studies are presented to determine if the TMI – 2A12 algorithm performs better or worse than the SSM/I rain rate algorithms. Three of the case studies used to validate the SSM/I rain rates also evaluate TMI – 2A12 accuracy.

5.4.1 Case 1: July 13, 1998 (Julian Day 194)

Figure 5-4 depicts TMI – 2A12 estimated rain rates for the same thunderstorm event described in Chapter 2. The most glaring difference between the TMI and SSM/I rain in

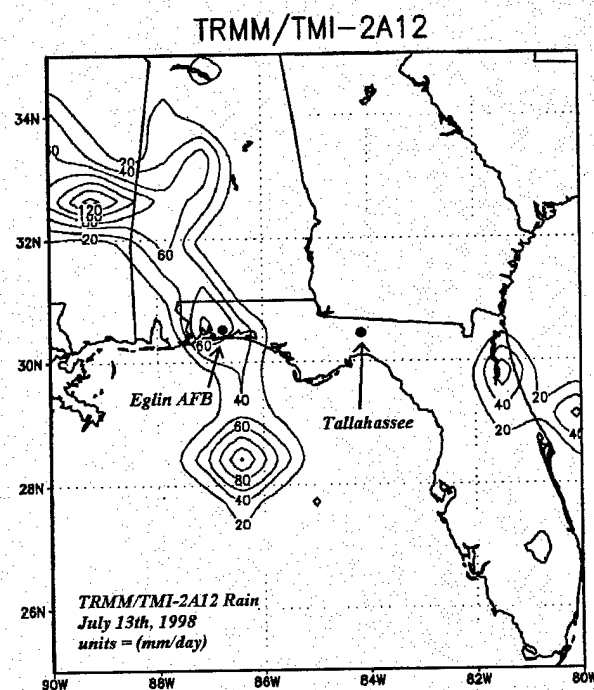


Figure 5-4: TMI – 2A12 rain rates, July 13th, 1998 (mm/day)

this case is the fact that no rain whatsoever is present in Tallahassee. This can be attributed to the lack of daily coverage by the TRMM satellite. Since the thunderstorms which flooded Tallahassee on July 13th were short-lived (3 hours), the TRMM platform most likely missed the event altogether. However, the TRMM satellite *did* capture the more persistent rain in the vicinity of Pensacola, Florida. Figure 5-4 shows that the TMI – 2A12 rain rate algorithm estimates 70 mm of precipitation fell on Eglin AFB. The official, 24-hour observation for Eglin AFB was 43.25 mm. The TMI – 2A12 algorithm provides a much higher rain rate than all three of the SSM/I algorithms for this case in particular.

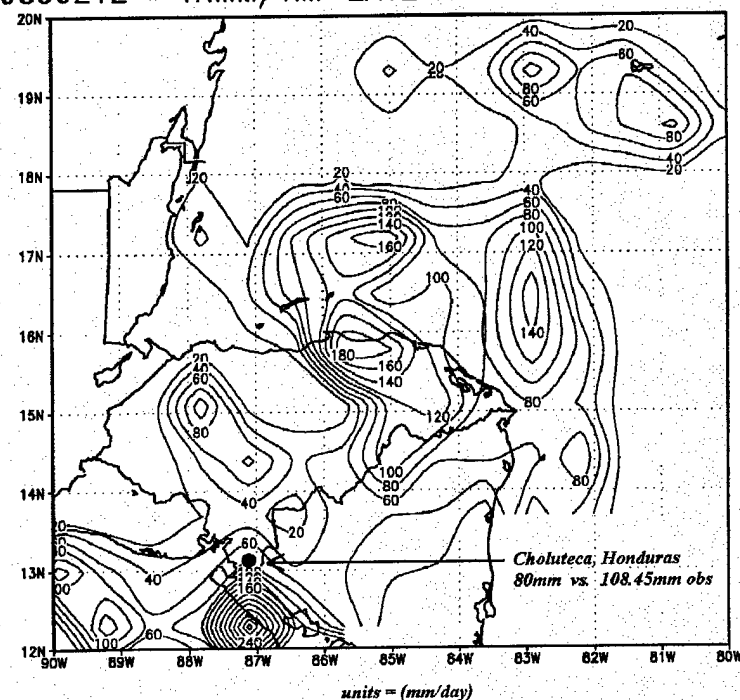
5.4.2 Case 2: October 29, 1998 (Julian Day 302)

As noted in Chapter 2, only the NESDIS SSM/I rain rate algorithm provided a reasonable estimate of the precipitation which fell on Choluteca, Honduras (Hurricane Mitch). Figure 5-5 portrays rain rates as estimated by the TMI – 2A12 algorithm for the same 24-hour period highlighted in Chapter 2. While not as accurate as the NESDIS SSM/I algorithm (110 mm), the TMI estimate of 80 mm is quite reasonable. Moreover, the TMI estimate is closer to the observed value when compared to the Cal/Val and GPROF 4.0 SSM/I rain rate results.

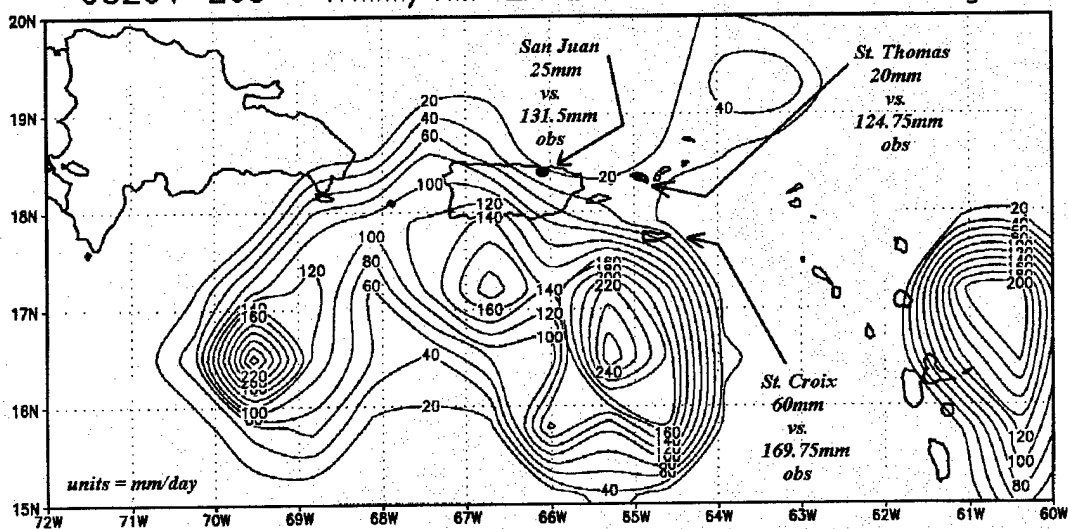
5.4.3 Case 3: September 21-22, 1998 (Julian Days 264-265)

Figure 5-6 shows TMI – 2A12 estimated rain rates for the same two day period of Hurricane Georges (as presented in Chapter 2). It is evident that the TMI algorithm

9830212 TRMM/TMI-2A12 Rain Hurricane Mitch

Figure 5-5: TMI - 2A12 rain rates for Hurricane Mitch, October 29th, 1998.

98264-265 TRMM/TMI-2A12 Rain Hurricane Georges

Figure 5-6: TMI - 2A12 rain rates for Hurricane Georges, Sep 21st - 22nd, 1998.

grossly underestimates the observed rain for Hurricane Georges as it swept through St. Croix, St. Thomas, and San Juan. In fact, the TMI estimated rain rates are not much greater than the Cal/Val SSM/I rain rates (Chapter 2). As shown in Chapter 2, only the NESDIS SSM/I rain rate algorithm provides an accurate and reasonable estimate of the rain generated by Hurricane Georges.

5.5 TRMM / TMI – 2A12 Hurricane Forecasts

Identical to the SSM/I forecast experiments in Chapter 4, the FSU GSM was used to generate forecasts of hurricane track, wind intensity, and minimum central pressure. However, rain rates as estimated by the TMI – 2A12 algorithm were used to physically initialize the model. Due to the fact that the TRMM satellite does not provide global coverage, NESDIS SSM/I rain rate data was inserted into all grid points on the globe where TRMM / TMI data was not available. This is referred to in the following figures as *TRMM/NESDIS Blend*. This blended set of rain rate data provides mostly TMI – 2A12 estimated rain rates for the tropics, and NESDIS SSM/I estimated rain rates for the middle and upper latitudes. While this procedure is still in its experimental stages, it provides a reasonable solution to the lack of global TRMM coverage.

5.6.1 Hurricane Bonnie (72 hour forecast)

Figure 5-7 depicts a FSU GSM track forecast for Hurricane Bonnie using the TRMM/NESDIS blended rain rates as input to the physical initialization of the model. The SSM/I based forecasts from Chapter 4 are also included for comparison purposes.

Bonnie 72 HR Fcst 0 Hr = 9823812 12Z

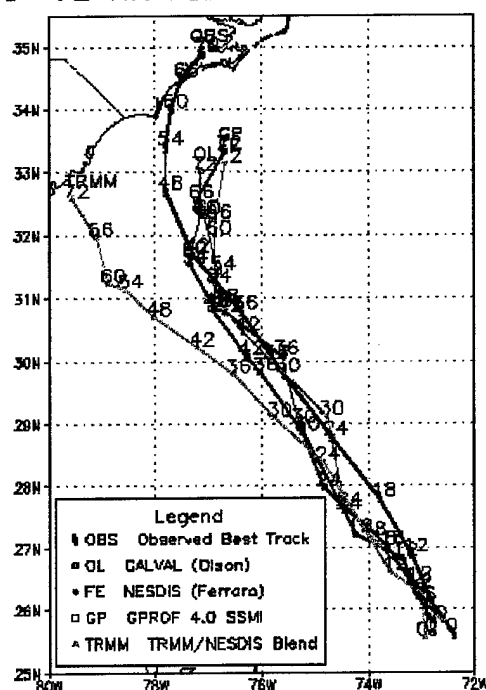


Figure 5-7: 72-hour track forecast using TRMM/NESDIS blended rain rates. SSM/I based model experiments are included for comparison purposes.

It is evident in both Figure 5-7 and Table 5-7.1 that the TRMM based forecast is very similar to the SSM/I based forecasts through the first 36 hours. However, the TRMM based forecast deviates significantly after this time period.

Table 5-7.1: Forecast track deviations for Hurricane Bonnie (3 day forecast).

Hours of Prediction	Cal/Val (Olson)	NESDIS (Ferraro)	GPROF 4.0	TRMM/NESDIS Blend
12	24.54 km	36.70 km	46.32 km	44.15 km
24	57.88 km	65.15 km	64.02 km	50.76 km
36	70.40 km	76.96 km	77.66 km	63.87 km
48	92.67 km	102.75 km	107.72 km	92.77 km
60	118.72 km	128.75 km	127.64 km	129.36 km
72	135.49 km	144.06 km	138.43 km	160.38 km

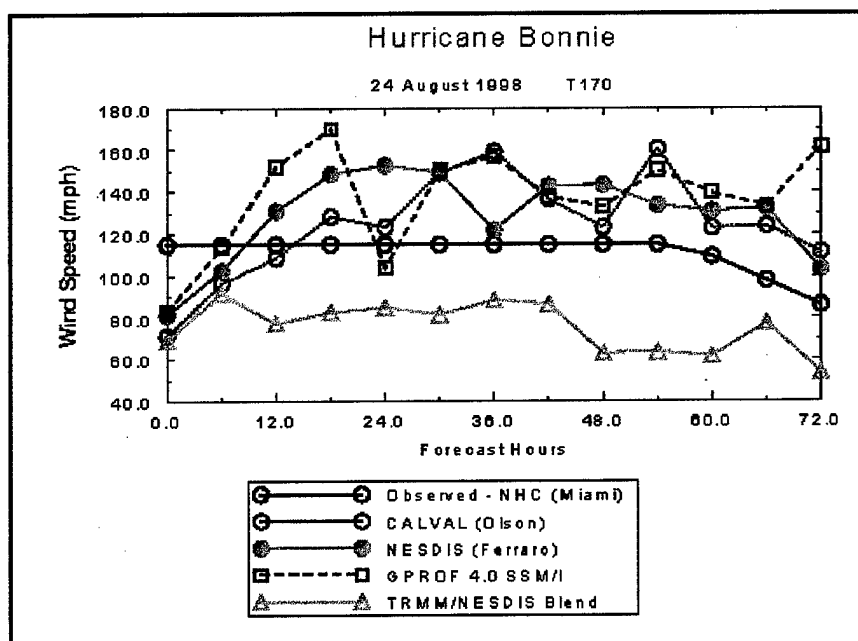


Figure 5-8: FSU GSM wind intensity output using TRMM/NESDIS blended rain rates. SSM/I based forecasts are included for comparison purposes.

Figure 5-8, Figure 5-9, Table 5-8.1, and Table 5-9.1 show forecast wind intensity and minimum central pressure results for Hurricane Bonnie using the TRMM/NESDIS blended rain rates as input to the physical initialization of the model. While Figure 5.9

Table 5-8.1: Forecast wind intensity deviations for Hurricane Bonnie (3 day forecast).

Hours of Prediction	Cal/Val (Olson)	NESDIS (Ferraro)	GPROF 4.0	TRMM/NESDIS Blend
12	22.87 mph	20.62 mph	23.48 mph	35.58 mph
24	18.02 mph	26.57 mph	27.38 mph	33.81 mph
36	24.04 mph	24.85 mph	30.55 mph	32.69 mph
48	22.00 mph	25.56 mph	28.28 mph	34.33 mph
60	23.39 mph	24.57 mph	29.08 mph	37.07 mph
72	23.73 mph	24.74 mph	33.13 mph	35.41 mph

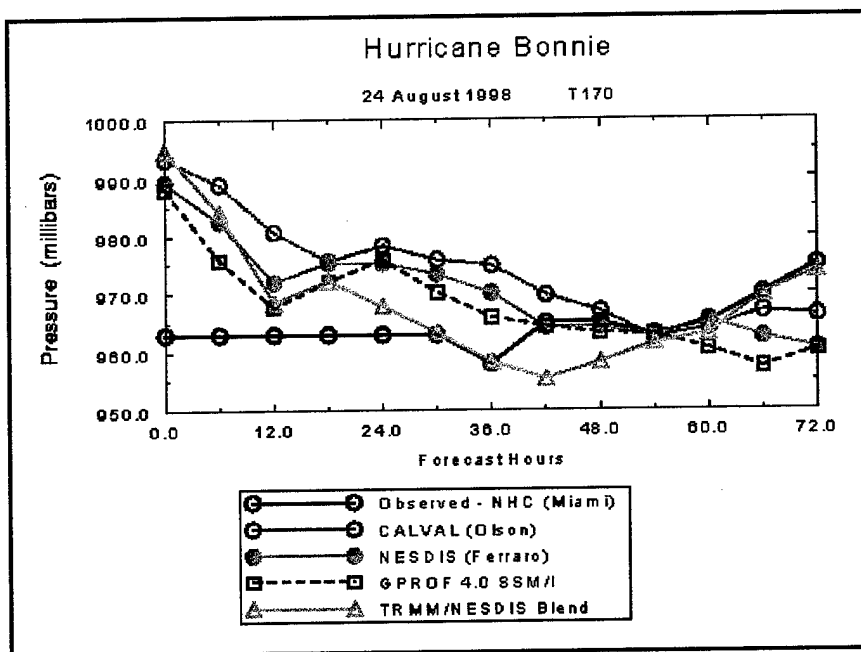


Figure 5-9: FSU GSM minimum central pressure output using TRMM/NESDIS blended rain rates. SSM/I based forecasts are included for comparison purposes.

Table 5-9.1: Minimum central pressure deviations for Hurricane Bonnie (3 day forecast).

<i>Hours of Prediction</i>	<i>Cal/Val (Olson)</i>	<i>NESDIS (Ferraro)</i>	<i>GPROF 4.0</i>	<i>TRMM/ NESDIS Blend</i>
12	24.67 mb	18.28 mb	14.22 mb	19.45 mb
24	20.40 mb	15.90 mb	12.94 mb	14.50 mb
36	18.83 mb	14.57 mb	11.42 mb	10.45 mb
48	15.41 mb	11.50 mb	9.15 mb	9.94 mb
60	12.75 mb	9.48 mb	7.89 mb	8.44 mb
72	11.70 mb	9.71 mb	8.78 mb	7.24 mb

and Table 5-9.1 indicate the TRMM based forecast pressure is comparable to the SSM/I based output, Figure 5-8 and Table 5-8.1 depict a deviation between the TRMM based

and SSM/I based forecast wind intensity. While all three SSM/I experiments overestimate the observed wind speed, the TRMM experiment severely *underestimates* Hurricane Bonnie's wind intensity.

5.6.2 Hurricane Bonnie (48 hour forecast)

The TMI - 2A12 rain rate algorithm was also used to physically initialize a two day forecast for Hurricane Bonnie, beginning one day later. Figure 5-10 portrays the TRMM based forecast as compared to the SSM/I based output. A more reasonable TRMM based

Bonnie 48 HR Fcst 0 Hr = 9823712 12Z

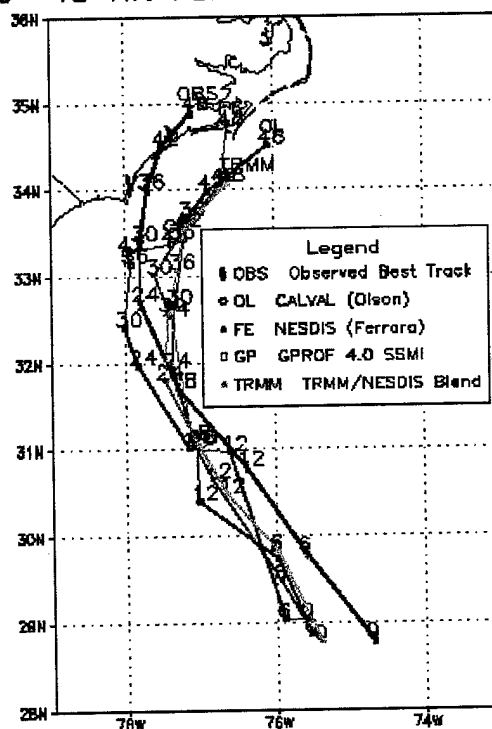


Figure 5-10: 48-hour track forecast using TRMM/NESDIS blended rain rates. SSM/I based model experiments are included for comparison purposes.

forecast track is evident when compared to the previous three day forecast. Table 5-10.1 depicts track deviations for the two day forecast. The TRMM based deviations are similar in magnitude to the SSM/I based track deviations.

Table 5-10.1: Forecast track deviations for Hurricane Bonnie (2 day forecast).

<i>Hours of Prediction</i>	<i>Cal/Val (Olson)</i>	<i>NESDIS (Ferraro)</i>	<i>GPROF 4.0</i>	<i>TRMM/ NESDIS Blend</i>
12	64.42 km	58.42 km	68.95 km	49.15 km
24	72.50 km	57.27 km	73.17 km	65.70 km
36	73.64 km	58.06 km	82.07 km	76.52 km
48	77.63 km	60.10 km	98.80 km	82.96 km

The remaining tables and figures in this section highlight the forecast wind intensity and pressure results from the two day forecast of Hurricane Bonnie. While no notable

Table 5-11.1: Forecast wind intensity deviations for Hurricane Bonnie (2 day forecast).

<i>Hours of Prediction</i>	<i>Cal/Val (Olson)</i>	<i>NESDIS (Ferraro)</i>	<i>GPROF 4.0</i>	<i>TRMM/ NESDIS Blend</i>
12	37.68 mph	30.83 mph	30.02 mph	41.96 mph
24	34.39 mph	26.46 mph	28.72 mph	34.43 mph
36	29.26 mph	20.92 mph	22.59 mph	30.42 mph
48	30.57 mph	19.57 mph	20.07 mph	27.93 mph

Table 5-12.1: Minimum central pressure deviations for Hurricane Bonnie (2 day forecast).

<i>Hours of Prediction</i>	<i>Cal/Val (Olson)</i>	<i>NESDIS (Ferraro)</i>	<i>GPROF 4.0</i>	<i>TRMM/ NESDIS Blend</i>
12	28.50 mb	25.14 mb	23.47 mb	20.59 mb
24	17.99 mb	16.47 mb	15.03 mb	13.95 mb
36	14.46 mb	14.29 mb	14.07 mb	10.98 mb
48	11.78 mb	11.87 mb	11.84 mb	9.31 mb

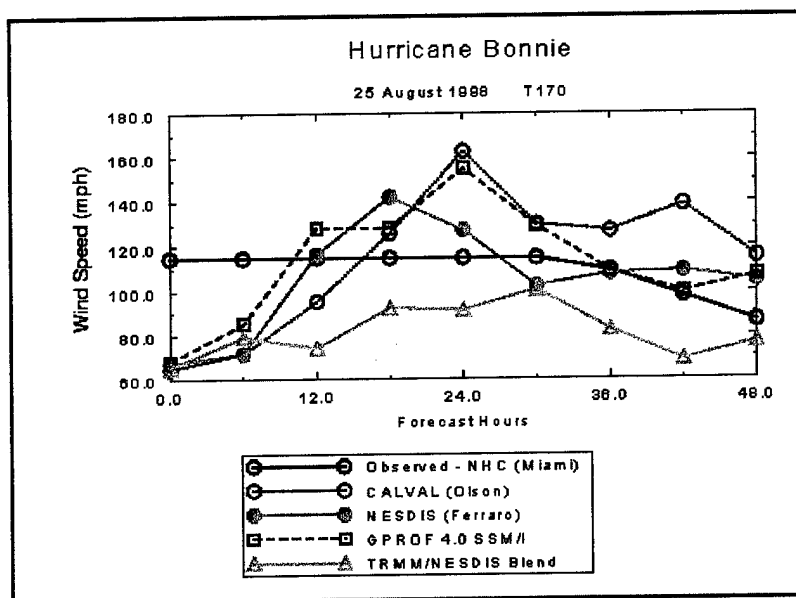


Figure 5-11: FSU GSM wind intensity output using TRMM/NESDIS blended rain rates. SSM/I based forecasts are included for comparison purposes.

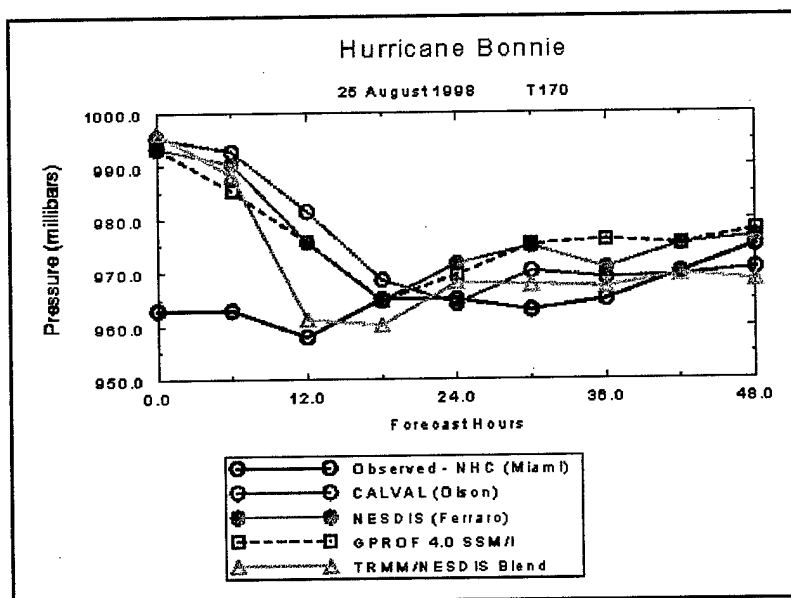


Figure 5-12: FSU GSM minimum central pressure output using TRMM/NESDIS blended rain rates. SSM/I based forecasts are included for comparison.

improvements are evident in the forecast wind intensity, the TRMM based experiment does produce the most accurate minimum central pressure forecast.

5.7.1 Hurricane Danielle (72 hour forecast)

The following figures and tables show the TRMM based results for the same three day forecast of Hurricane Danielle presented in Chapter 4. While no improvements are

Danielle 72 HR Fcst 0 Hr = 982411Z 12Z

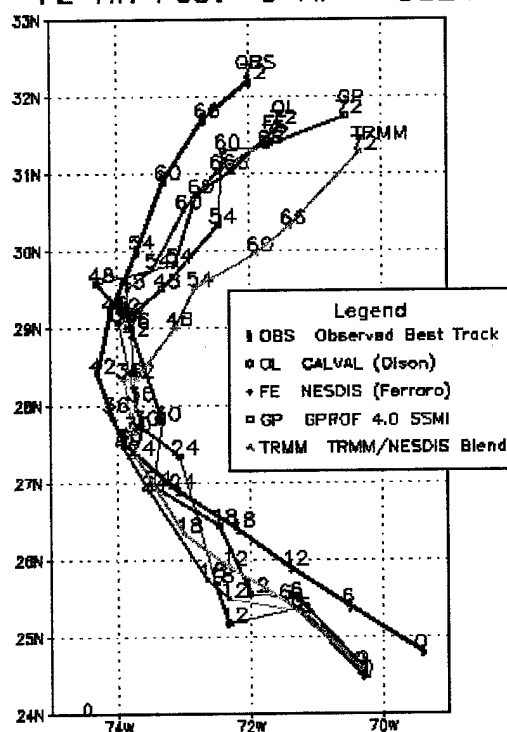


Figure 5-13: 72-hour track forecast using TRMM/NESDIS blended rain rates. SSM/I based model experiments are included for comparison purposes.

Table 5-13.1: Forecast track deviations for Hurricane Danielle (3 day forecast).

<i>Hours of Prediction</i>	<i>Cal/Val (Olson)</i>	<i>NESDIS (Ferraro)</i>	<i>GPROF 4.0</i>	<i>TRMM/ NESDIS Blend</i>
12	99.69 km	86.80 km	81.08 km	95.17 km
24	86.92 km	77.71 km	61.31 km	88.79 km
36	85.53 km	61.97 km	70.92 km	73.82 km
48	82.09 km	60.79 km	74.46 km	74.51 km
60	77.18 km	57.63 km	80.90 km	85.46 km
72	77.88 km	61.82 km	87.28 km	102.00 km

Table 5-14.1: Forecast wind intensity deviations for Hurricane Danielle (3 day forecast).

<i>Hours of Prediction</i>	<i>Cal/Val (Olson)</i>	<i>NESDIS (Ferraro)</i>	<i>GPROF 4.0</i>	<i>TRMM/ NESDIS Blend</i>
12	19.57 mph	17.69 mph	23.48 mph	16.72 mph
24	26.94 mph	29.95 mph	34.07 mph	16.42 mph
36	28.28 mph	29.18 mph	33.76 mph	15.41 mph
48	27.02 mph	31.00 mph	29.83 mph	14.56 mph
60	24.38 mph	28.63 mph	28.80 mph	16.83 mph
72	23.76 mph	29.07 mph	28.80 mph	18.21 mph

Table 5-15.1: Minimum central pressure deviations for Hurricane Danielle (3 day forecast).

<i>Hours of Prediction</i>	<i>Cal/Val (Olson)</i>	<i>NESDIS (Ferraro)</i>	<i>GPROF 4.0</i>	<i>TRMM/ NESDIS Blend</i>
12	15.17 mb	14.02 mb	11.04 mb	13.97 mb
24	10.00 mb	9.97 mb	8.23 mb	12.27 mb
36	8.13 mb	7.74 mb	6.21 mb	12.35 mb
48	7.94 mb	6.71 mb	5.11 mb	10.76 mb
60	7.11 mb	6.11 mb	4.43 mb	9.20 mb
72	6.40 mb	5.63 mb	4.13 mb	8.35 mb

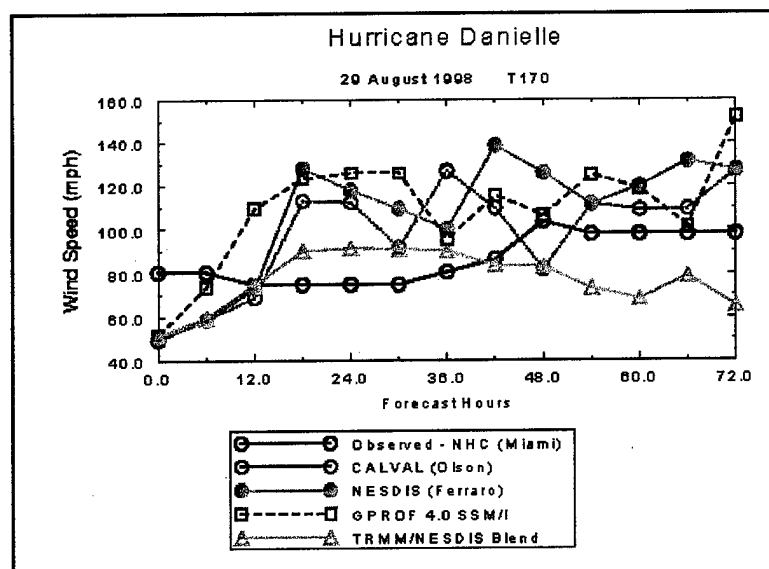


Figure 5-14: FSU GSM wind intensity output using TRMM/NESDIS blended rain rates. SSM/I based forecasts are included for comparison purposes.

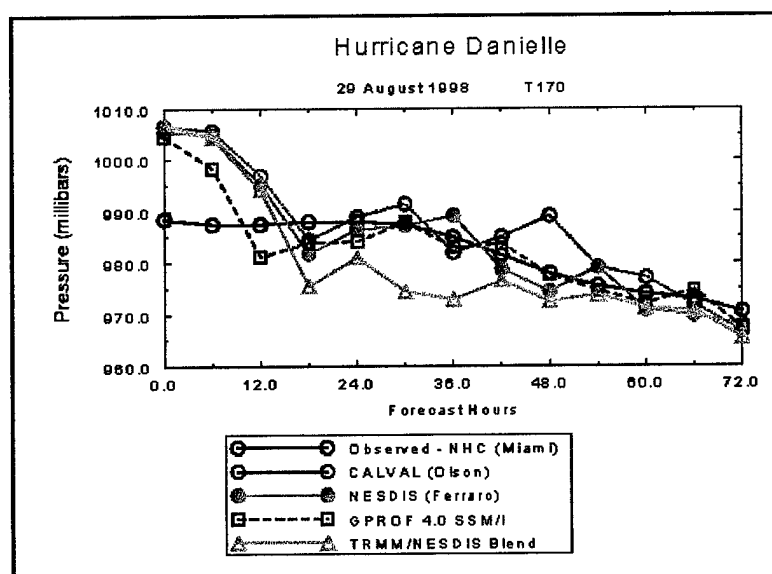


Figure 5-15: FSU GSM minimum central pressure output using TRMM/NESDIS blended rain rates. SSM/I based forecasts are included for comparison.

achieved in terms of forecast track or pressure, the TRMM based experiment does produce a superior forecast of Hurricane Danielle's wind intensity. The accuracy of the TRMM based wind intensity output is most evident in the first 42 hours of the forecast.

5.7.2 Hurricane Danielle (48 hour forecast)

The following figures and tables show the TRMM based results for the same two day forecast of Hurricane Danielle presented in Chapter 4. Once again the TRMM based

Danielle 48 HR Fcst 0 Hr = 9824212 12Z

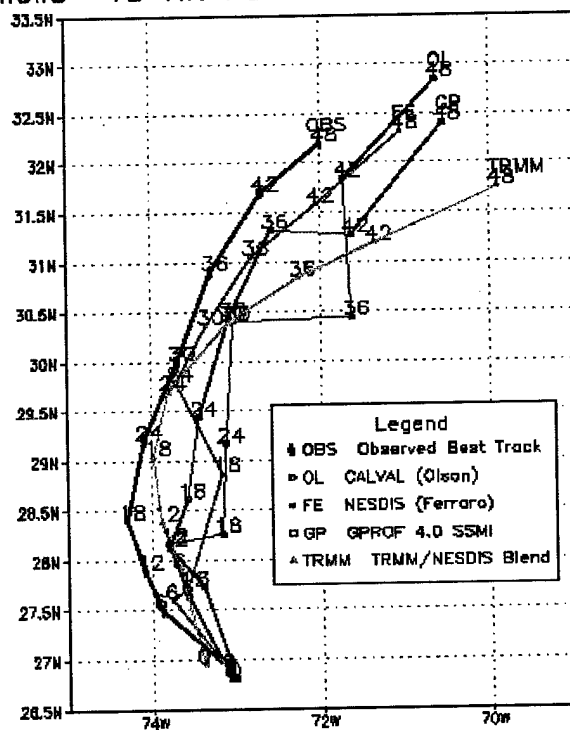


Figure 5-16: 48-hour track forecast using TRMM/NESDIS blended rain rates. SSM/I based model experiments are included for comparison purposes.

Table 5-16.1: Forecast track deviations for Hurricane Danielle (2 day forecast).

<i>Hours of Prediction</i>	<i>Cal/Val (Olson)</i>	<i>NESDIS (Ferraro)</i>	<i>GPROF 4.0</i>	<i>TRMM/ NESDIS Blend</i>
12	28.55 km	25.02 km	35.11 km	46.17 km
24	58.08 km	54.25 km	49.37 km	55.60 km
36	76.35 km	53.08 km	57.89 km	64.28 km
48	85.98 km	58.30 km	72.73 km	87.83 km

Table 5-17.1: Forecast wind intensity deviations for Hurricane Danielle (2 day forecast).

<i>Hours of Prediction</i>	<i>Cal/Val (Olson)</i>	<i>NESDIS (Ferraro)</i>	<i>GPROF 4.0</i>	<i>TRMM/ NESDIS Blend</i>
12	13.94 mph	22.72 mph	15.94 mph	12.68 mph
24	25.60 mph	33.46 mph	24.72 mph	10.29 mph
36	28.12 mph	37.60 mph	24.51 mph	9.35 mph
48	25.89 mph	34.85 mph	24.77 mph	12.83 mph

Table 5-18.1: Minimum central pressure deviations - Hurricane Danielle (2 day forecast).

<i>Hours of Prediction</i>	<i>Cal/Val (Olson)</i>	<i>NESDIS (Ferraro)</i>	<i>GPROF 4.0</i>	<i>TRMM/ NESDIS Blend</i>
12	13.98 mb	10.91 mb	10.28 mb	12.21 mb
24	10.89 mb	8.06 mb	6.79 mb	12.08 mb
36	10.10 mb	6.32 mb	6.24 mb	8.91 mb
48	8.60 mb	5.69 mb	4.99 mb	7.11 mb

experiment produces an outstanding wind intensity forecast for Hurricane Danielle.

Figure 5-17 shows that the forecast winds closely mimic the observed winds for the first 36 hours of prediction. In addition, the TRMM based experiment provides similar forecast pressure output when compared to the three SSM/I experiments.

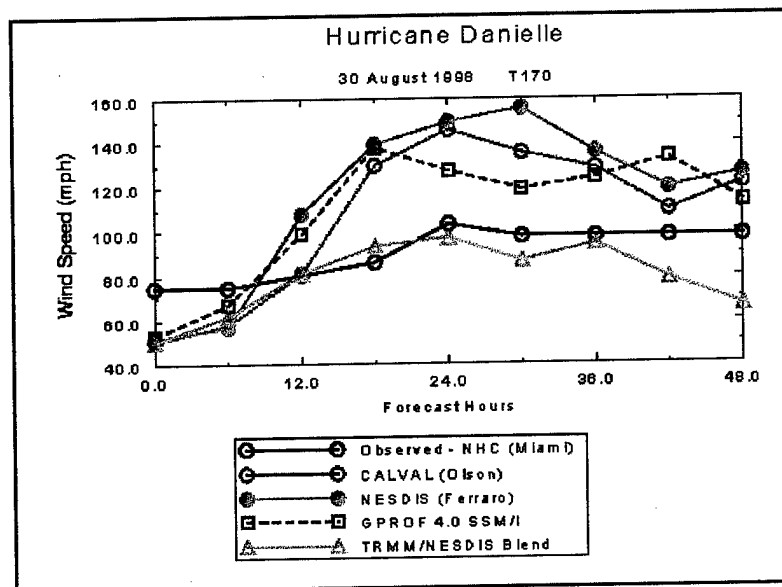


Figure 5-17: FSU GSM wind intensity output using TRMM/NESDIS blended rain rates. SSM/I based forecasts are included for comparison purposes.

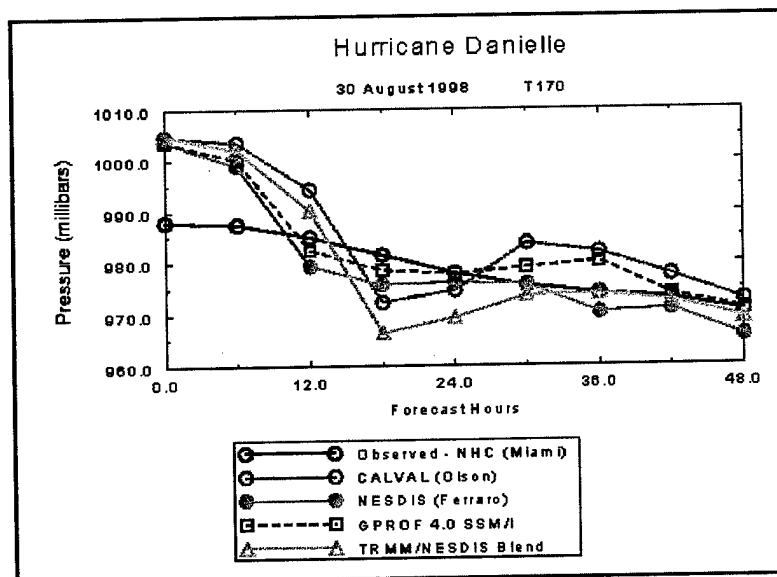


Figure 5-18: FSU GSM minimum central pressure output using TRMM/NESDIS blended rain rates. SSM/I based forecasts are included for comparison.

5.8.1 Hurricane Georges (72 hour forecast)

The following figures and tables show the TRMM based results for the same three day forecast of Hurricane Georges presented in Chapter 4. No improvements in forecast track, wind intensity, or minimum central pressure are realized by using the TRMM/NESDIS blended rain rates to initialize the model. The FSU GSM output is quite similar for both the TRMM and SSM/I rain rate experiments.

Georges 72 HR Fcst 0 Hr = 9826812 12Z

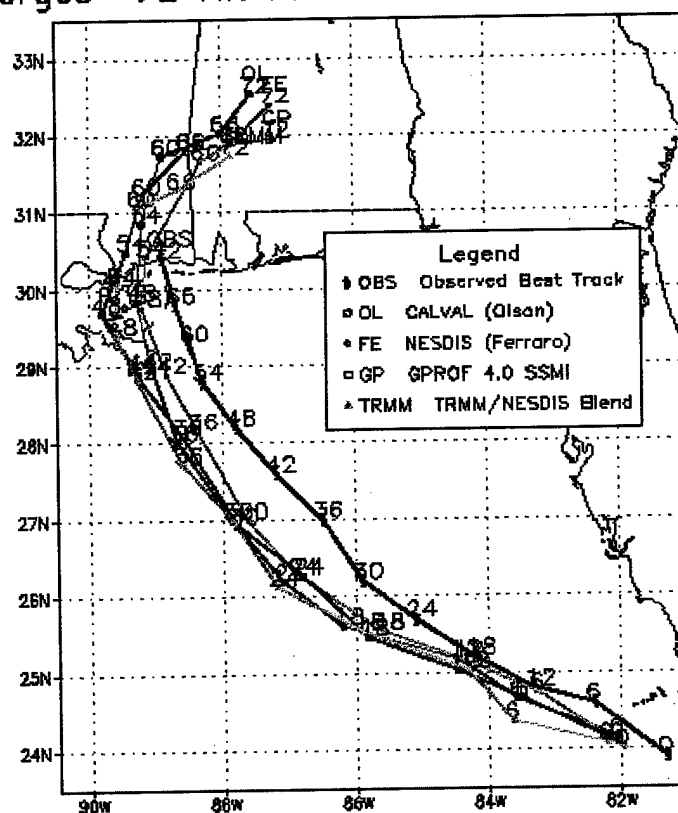


Figure 5-19: 72-hour track forecast using TRMM/NESDIS blended rain rates. SSM/I based model experiments are included for comparison purposes.

Table 5-19.1: Forecast track deviations for Hurricane Georges (3 day forecast).

<i>Hours of Prediction</i>	<i>Cal/Val (Olson)</i>	<i>NESDIS (Ferraro)</i>	<i>GPROF 4.0</i>	<i>TRMM/ NESDIS Blend</i>
12	107.40 km	91.18 km	102.54 km	108.47 km
24	147.02 km	121.36 km	130.81 km	142.45 km
36	170.15 km	146.48 km	156.83 km	164.12 km
48	184.48 km	162.39 km	178.27 km	179.30 km
60	198.02 km	174.70 km	186.00 km	182.84 km
72	207.88 km	187.48 km	192.44 km	181.12 km

Table 5-20.1: Forecast wind intensity deviations for Hurricane Georges (3 day forecast).

<i>Hours of Prediction</i>	<i>Cal/Val (Olson)</i>	<i>NESDIS (Ferraro)</i>	<i>GPROF 4.0</i>	<i>TRMM/ NESDIS Blend</i>
12	27.63 mph	30.18 mph	28.85 mph	32.14 mph
24	17.73 mph	23.92 mph	25.19 mph	27.85 mph
36	17.98 mph	22.59 mph	25.85 mph	26.09 mph
48	22.55 mph	25.04 mph	28.47 mph	28.35 mph
60	25.97 mph	28.08 mph	30.90 mph	31.32 mph
72	28.80 mph	30.29 mph	31.86 mph	33.00 mph

Table 5-21.1: Minimum central pressure deviations for Hurricane Georges (3 day forecast).

<i>Hours of Prediction</i>	<i>Cal/Val (Olson)</i>	<i>NESDIS (Ferraro)</i>	<i>GPROF 4.0</i>	<i>TRMM/ NESDIS Blend</i>
12	11.20 mb	9.28 mb	10.79 mb	12.98 mb
24	7.44 mb	6.95 mb	6.68 mb	8.01 mb
36	6.64 mb	6.47 mb	6.19 mb	7.52 mb
48	8.35 mb	7.95 mb	8.38 mb	9.62 mb
60	11.53 mb	11.06 mb	11.31 mb	12.73 mb
72	13.94 mb	13.37 mb	13.44 mb	15.03 mb

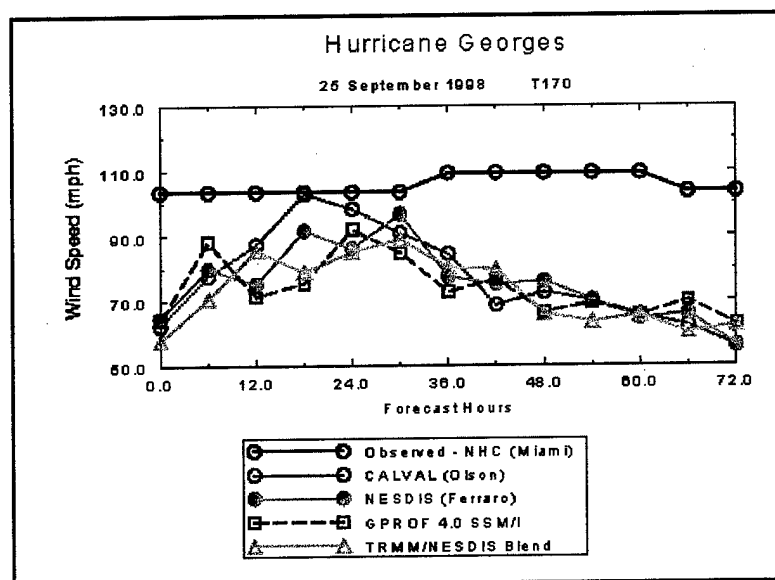


Figure 5-20: FSU GSM wind intensity output using TRMM/NESDIS blended rain rates. SSM/I based forecasts are included for comparison purposes.

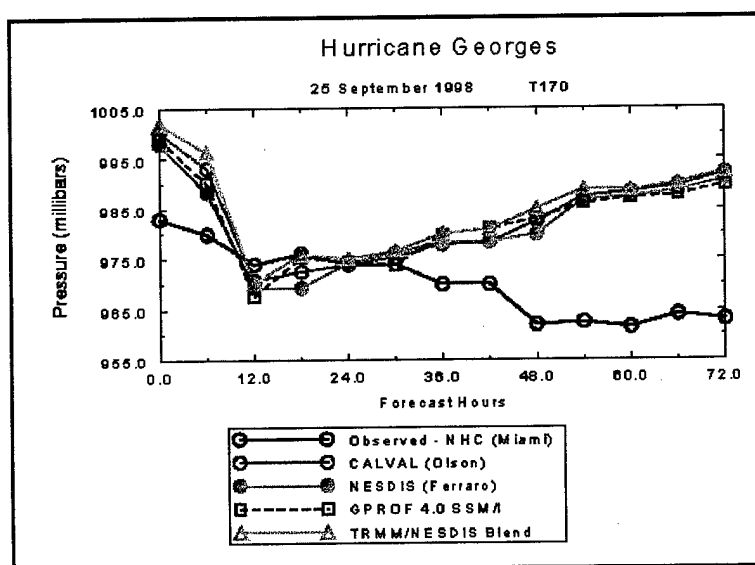


Figure 5-21: FSU GSM minimum central pressure output using TRMM/NESDIS blended rain rates. SSM/I based forecasts are included for comparison.

5.9.1 Hurricane Mitch (72 hour forecast)

The following figures and tables show the TRMM based results for the same three day forecast of Hurricane Mitch presented in Chapter 4. While no improvement is achieved in terms of forecast wind intensity and minimum central pressure, a significant improvement in the predicted track of Mitch can be seen in Figure 5-22. The TRMM based forecast is the only experiment which predicts storm movement to the west after the 48 hour point. All three SSM/I based tracks incorrectly forecast Mitch will head to the north after 48 hours, sparing the Honduran coast. Unfortunately Mitch did not spare Honduras, as the observed "best track" shows and the TRMM based track predicts.

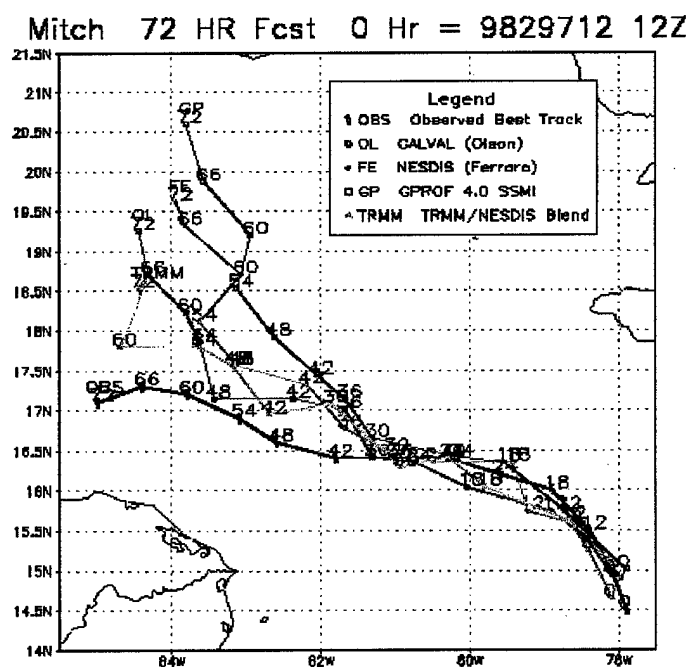


Figure 5-22: 72-hour track forecast using TRMM/NESDIS blended rain rates. SSM/I based model experiments are included for comparison purposes.

Table 5-22.1: Forecast track deviations for Hurricane Mitch (3 day forecast).

<i>Hours of Prediction</i>	<i>Cal/Val (Olson)</i>	<i>NESDIS (Ferraro)</i>	<i>GPROF 4.0</i>	<i>TRMM/ NESDIS Blend</i>
12	59.92 km	71.59 km	59.66 km	34.12 km
24	85.07 km	75.78 km	64.72 km	55.35 km
36	90.31 km	77.49 km	77.74 km	66.36 km
48	93.54 km	85.93 km	89.97 km	77.88 km
60	97.90 km	100.34 km	111.90 km	84.73 km
72	113.90 km	125.95 km	149.05 km	96.77 km

Table 5-23.1: Forecast wind intensity deviations for Hurricane Mitch (3 day forecast).

<i>Hours of Prediction</i>	<i>Cal/Val (Olson)</i>	<i>NESDIS (Ferraro)</i>	<i>GPROF 4.0</i>	<i>TRMM/ NESDIS Blend</i>
12	22.60 mph	19.41 mph	15.13 mph	33.02 mph
24	24.42 mph	13.35 mph	18.51 mph	22.03 mph
36	23.97 mph	10.80 mph	17.48 mph	27.93 mph
48	25.40 mph	13.16 mph	19.65 mph	30.63 mph
60	27.98 mph	17.57 mph	21.97 mph	34.70 mph
72	28.18 mph	16.48 mph	22.66 mph	37.96 mph

Table 5-24.1: Minimum central pressure deviations for Hurricane Mitch (3 day forecast).

<i>Hours of Prediction</i>	<i>Cal/Val (Olson)</i>	<i>NESDIS (Ferraro)</i>	<i>GPROF 4.0</i>	<i>TRMM/ NESDIS Blend</i>
12	14.32 mb	8.39 mb	6.92 mb	20.61 mb
24	21.83 mb	18.74 mb	18.23 mb	25.41 mb
36	32.78 mb	28.73 mb	28.13 mb	34.70 mb
48	38.23 mb	34.48 mb	33.79 mb	40.31 mb
60	44.26 mb	40.67 mb	40.73 mb	47.03 mb
72	46.24 mb	42.94 mb	43.60 mb	49.45 mb

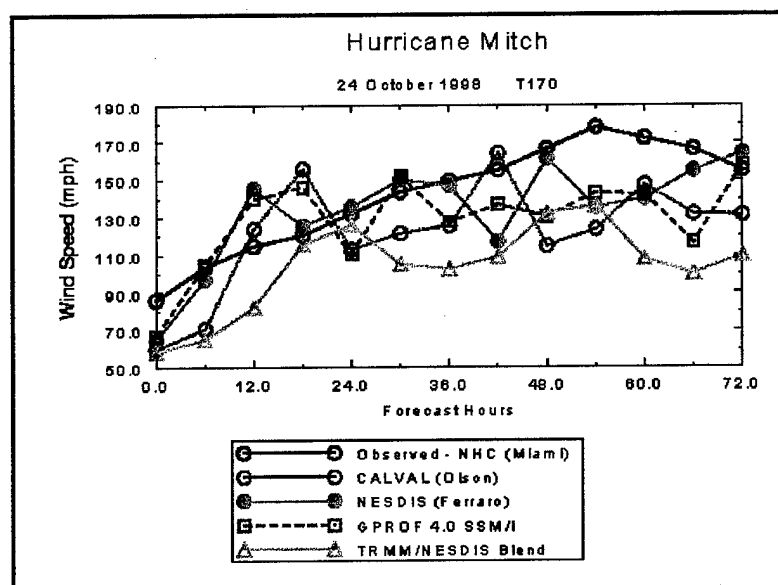


Figure 5-23: FSU GSM wind intensity output using TRMM/NESDIS blended rain rates. SSM/I based forecasts are included for comparison purposes.

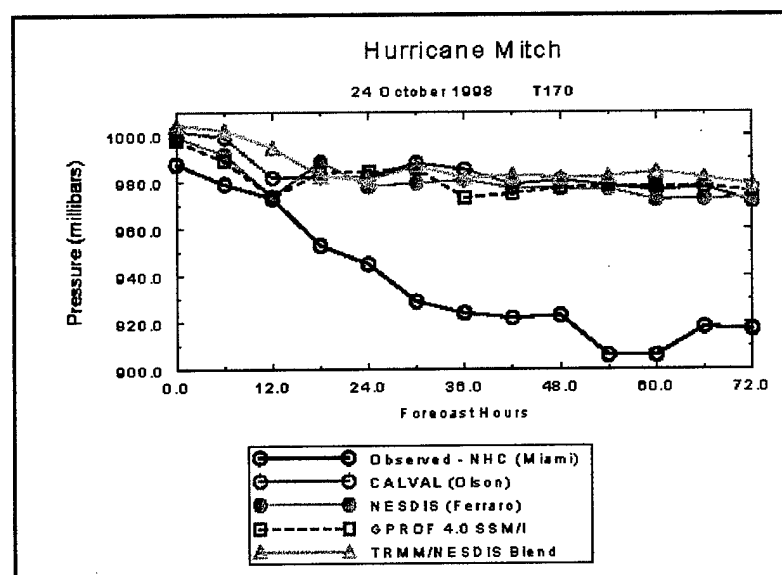


Figure 5-24: FSU GSM minimum central pressure output using TRMM/NESDIS blended rain rates. SSM/I based forecasts are included for comparison.

5.9.2 Hurricane Mitch (48 hour forecast)

The following figures and tables show the TRMM based results for the same two day forecast of Hurricane Mitch presented in Chapter 4. No improvement is achieved by using the TRMM/NESDIS blended rain rates to initialize the model. The forecast track, wind intensity, and minimum central pressure for the TRMM based experiment are very similar to the SSM/I based output.

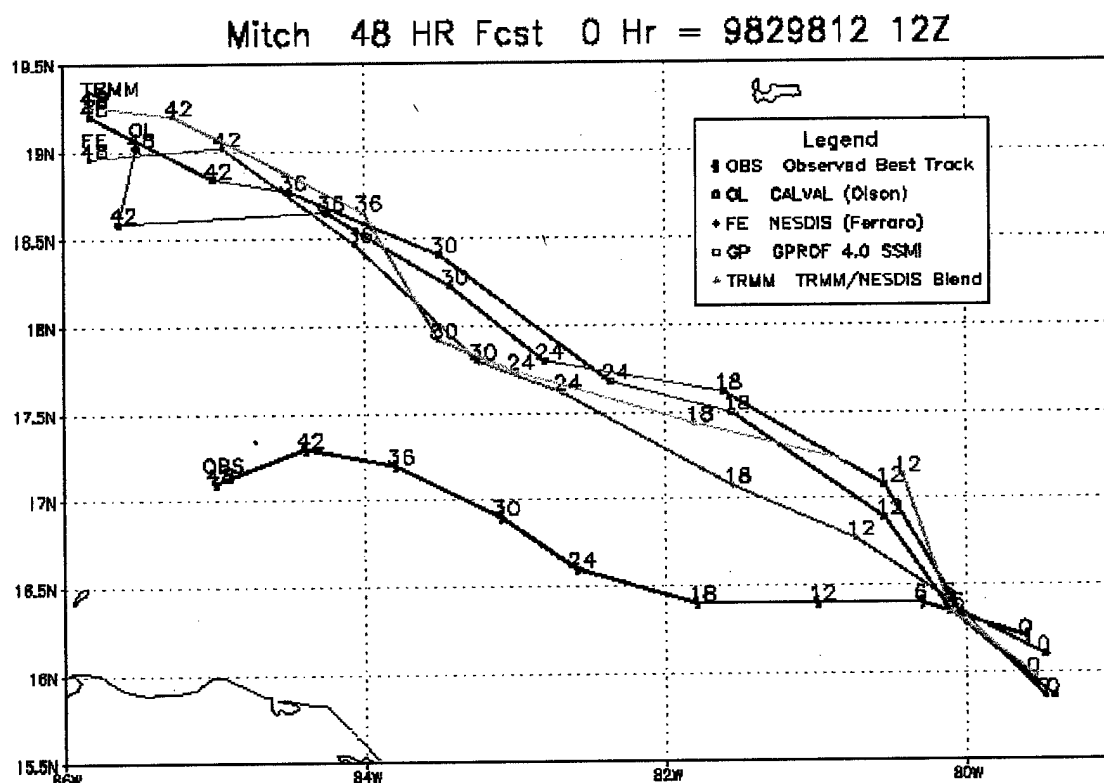


Figure 5-25: 48-hour track forecast using TRMM/NESDIS blended rain rates. SSM/I based model experiments are included for comparison purposes.

Table 5-25.1: Forecast track deviations for Hurricane Mitch (2 day forecast).

<i>Hours of Prediction</i>	<i>Cal/Val (Olson)</i>	<i>NESDIS (Ferraro)</i>	<i>GPROF 4.0</i>	<i>TRMM/ NESDIS Blend</i>
12	44.54 km	36.58 km	45.30 km	49.39 km
24	81.13 km	60.64 km	76.64 km	79.46 km
36	103.72 km	78.34 km	106.62 km	97.33 km
48	126.72 km	108.07 km	130.93 km	129.66 km

Table 5-26.1: Forecast wind intensity deviations for Hurricane Mitch (2 day forecast).

<i>Hours of Prediction</i>	<i>Cal/Val (Olson)</i>	<i>NESDIS (Ferraro)</i>	<i>GPROF 4.0</i>	<i>TRMM/ NESDIS Blend</i>
12	58.61 mph	50.82 mph	41.50 mph	60.24 mph
24	38.91 mph	36.01 mph	32.11 mph	46.72 mph
36	44.70 mph	41.74 mph	39.15 mph	49.55 mph
48	43.43 mph	38.64 mph	33.06 mph	44.71 mph

Table 5-27.1: Minimum central pressure deviations - Hurricane Mitch (2 day forecast).

<i>Hours of Prediction</i>	<i>Cal/Val (Olson)</i>	<i>NESDIS (Ferraro)</i>	<i>GPROF 4.0</i>	<i>TRMM/ NESDIS Blend</i>
12	60.03 mb	56.03 mb	54.37 mb	62.69 mb
24	57.36 mb	55.17 mb	54.26 mb	61.71 mb
36	62.94 mb	61.44 mb	61.00 mb	67.27 mb
48	64.17 mb	62.10 mb	60.87 mb	67.53 mb

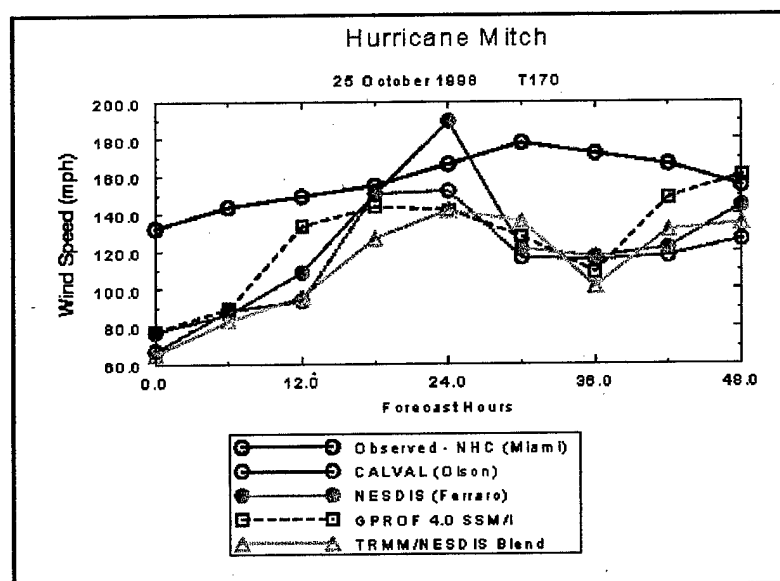


Figure 5-26: FSU GSM wind intensity output using TRMM/NESDIS blended rain rates. SSM/I based forecasts are included for comparison purposes.

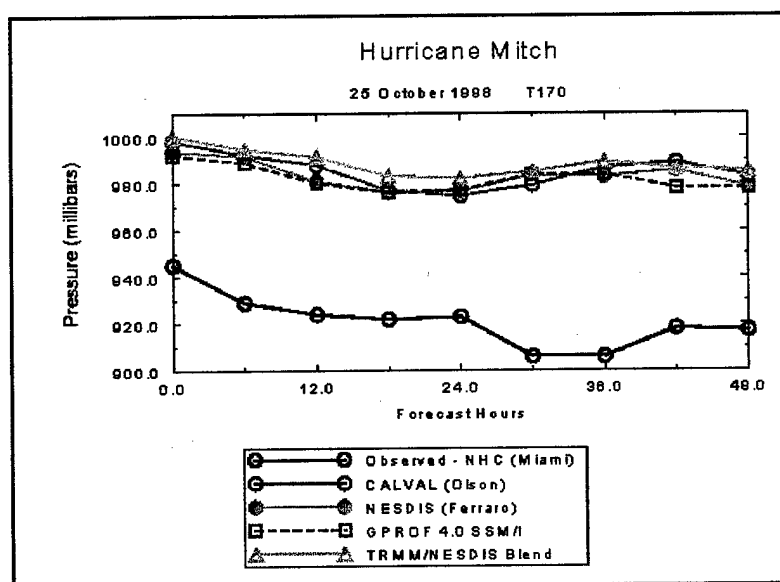


Figure 5-27: FSU GSM minimum central pressure output using TRMM/NESDIS blended rain rates. SSM/I based forecasts are included for comparison.

CHAPTER 6

CONCLUSIONS

In the past four decades, numerical weather prediction has produced remarkable improvements in forecast skill and accuracy. However, this development did not occur overnight. Throughout the short history of NWP, numerous, small improvements have contributed to the overall picture. In other words, many small steps add up to a giant stride over time. The research highlighted in this paper is a prime example of one of those steps.

This thesis has demonstrated notable improvements in the FSU GSM's hurricane forecasting ability. By introducing more credible SSM/I and TMI rain rate algorithms into the physical initialization of the model, advances in the prediction of hurricane tracks have been achieved. In addition, small improvements in forecast wind intensity and minimum central pressure have also been presented. Table 6-1.1 depicts a compilation of forecast track data for all four hurricanes highlighted in this paper. Track deviations for all four storms were averaged (at each 12 hour forecast interval) for *each* of the rain rate algorithms. A *total* track deviation average was computed for each rain rate algorithm. This value(s) encompasses the average of all six time increments for all four hurricanes studied, from a total of seven separate experiments.

Table 6-1.1: Average forecast track deviations for a total of four hurricanes and seven different experiments.

<i>Hours of Prediction</i>	<i>12</i>	<i>24</i>	<i>36</i>	<i>48</i>	<i>60</i>	<i>72</i>	<i>total</i>
<i>Cal/Val (Olson)</i>	61.29	84.09	95.73	106.16	122.96	133.79	100.67
<i>NESDIS (Ferraro)</i>	52.80	73.17	78.91	91.19	115.36	129.83	90.21
<i>GPROF 4.0</i>	62.71	74.29	89.96	107.55	126.61	141.80	100.49
<i>TRMM/NESDIS Blend</i>	60.95	76.87	86.61	103.56	120.60	135.07	97.28

units = km

As Table 6-1.1 indicates, the NESDIS SSM/I rain rate algorithm is best suited for use in the physical initialization of the FSU GSM. When compared to the rain rate algorithm (Cal/Val) which had been previously used for real-time, operational hurricane forecasts, **the NESDIS algorithm has demonstrated an overall 10.46 km forecast track deviation improvement.** As a direct result of this study, the Florida State University Real-Time Hurricane Forecast Center (FSU RTHFC) has retired the Cal/Val rain rate algorithm in favor of the NESDIS algorithm.

While not as significant as the hurricane track forecasts, small improvements in both wind intensity and minimum central pressure were also realized as a direct result of this research project. Table 6-2.1 shows forecast wind intensity deviation averages for all seven hurricane experiments. When compared to the Cal/Val algorithm, the NESDIS

Table 6-2.1: Average forecast wind intensity deviations for a total of four hurricanes and seven different experiments.

<i>Hours of Prediction</i>	<i>12</i>	<i>24</i>	<i>36</i>	<i>48</i>	<i>60</i>	<i>72</i>	<i>total</i>
<i>Cal/Val (Olson)</i>	28.99	26.57	28.05	28.30	25.43	26.12	27.24
<i>NESDIS (Ferraro)</i>	27.47	27.10	26.81	26.83	24.71	25.15	26.35
<i>GPROF 4.0</i>	25.49	27.24	27.70	26.30	27.69	29.11	27.26
<i>TRMM/NESDIS Blend</i>	33.19	27.36	27.35	27.62	29.98	31.15	29.44

units = mph

rain rate algorithm has achieved approximately a 1 mph wind deviation improvement. The large wind intensity deviations exhibited by all four rain rate algorithms indicate the need for further modifications to the FSU GSM. In addition to the large wind intensity output fluctuations inherent between forecast time intervals, the FSU GSM is prone to overestimate hurricane wind speeds.

Table 6-3.1 depicts forecast pressure deviation averages for all seven hurricane experiments. It is clear that both the GPROF and NESDIS algorithms have achieved a significant improvement in forecast minimum central pressure. While the NESDIS rain rate algorithm produces an overall pressure deviation improvement of 2.27 mb, the GPROF algorithm is even more impressive with an overall 3.24 mb improvement. Further work is also needed to produce more accurate FSU GSM minimum central pressure forecasts. Nonetheless, a small improvement has been noted as a direct result of this research.

Table 6-3.1: Average forecast minimum central pressure deviations for a total of four hurricanes and seven different experiments.

<i>Hours of Prediction</i>	<i>12</i>	<i>24</i>	<i>36</i>	<i>48</i>	<i>60</i>	<i>72</i>	<i>total</i>
<i>Cal/Val (Olson)</i>	23.98	20.84	21.98	22.07	18.91	19.57	21.23
<i>NESDIS (Ferraro)</i>	20.29	18.75	19.94	20.04	16.83	17.91	18.96
<i>GPROF 4.0</i>	18.73	17.45	19.04	19.16	16.09	17.49	17.99
<i>TRMM/NESDIS Blend</i>	23.21	21.13	21.74	22.08	19.35	20.02	21.26

units = mb

Finally, with the exception of the 72 hour forecast track of Hurricane Mitch and the forecast wind intensity of Hurricane Danielle, no significant forecast improvement was achieved in this research by using TRMM / TMI rain rate data. This is most likely the

result of three reasons. First, the TRMM / TMI sensor's brightness temperature biases need to be corrected. Second, the TMI - 2A12 rain rate algorithm is in need of modification. Future, updated versions of the algorithm will hopefully provide more consistent rain rate estimations. Third, the TRMM / NESDIS blended data set needs further work to prevent possible asymmetries in the global rain rate field. While highly accurate, NESDIS calculated rain rate values were used in place of the missing TRMM data, this method still requires modification. The FSU GSM requires a complete, *global* rain rate field for proper physical initialization. A different method must be developed which incorporates TRMM rain rates and also completes the initial, global rain rate field. This will be the subject of further hurricane prediction research.

REFERENCES

- Asselin, R., 1972: Frequency filter for time integrations. *Mon. Wea. Rev.*, **100**, 487-490.
- Berg, W., W. Olson, R. Ferraro, S.J. Goodman, and F.J. LaFontaine, 1998: An assessment of the first- and second-generation navy operational precipitation retrieval algorithms. *J. Atmos. Sci.*, **55**, 1558-1575.
- Chang, L. W., 1978: Determination of surface flux of sensible heat, latent heat, and Momentum utilizing the bulk Richardson number. *Papers Meteor. Res.* **1**, 16-24.
- Daley, R. C., C. Girard, J. Henderson, and I. Simmonds, 1976: Short-term forecasting with a multi-level spectral primitive equation model. Part I: Model formulation. *Atmosphere*, **14**, 98-116.
- Ferraro, R. R., N.C. Grody, J.C. Alishouse, and G. Marks, 1992: The calibration of an SSM/I scattering index for rain rate retrievals using RADAP-II and AMeDAS radar data. *Proc. Sixth Conf. On Satellite Meteorology and Oceanography*, Atlanta, GA, Amer. Meteor. Soc., 290-295.
- Ferraro, R. R., N.C. Grody, and G.F. Marks, 1994: Effects of surface conditions on rain identification using the SSM/I. *Remote Sens. Rev.*, **11**, 195-210.
- Ferraro, R. R., and G. F. Marks, 1995: The development of SSM/I rain-rate retrieval algorithms using ground-based radar measurements. *J. Atmos. Oceanic Technol.*, **12**, 755-770.
- Ferraro, R. R., 1997: Special sensor microwave imager derived global rainfall estimates for climatological applications. *J. Geophys. Res.*, **102**, 16715-16735.
- Ferraro, R.R., E. A. Smith, W. Berg, and G. Huffman, 1998: A review of screening techniques for passive microwave precipitation retrieval algorithms. *J. Atmos. Sci.*, **55**, 1583-1600.
- Grody, N.C., 1991: Classification of snow cover and precipitation using the Special Sensor Microwave/Imager (SSM/I). *J. Geophys. Res.*, **96**, 7423-7435.

- Hakkarinen, I.M., and R.F. Adler, 1988: Observations of precipitating convective systems at 92 and 183 GHz: Aircraft results. *Meteor. Atmos. Phys.*, **38**, 164-182.
- Krishnamurti, T. N., D. Oosterhof, and Nancy Dignon, 1989: Hurricane prediction with a high resolution global model. *Mon. Wea. Rev.*, **117**, 631-669.
- Krishnamurti, T. N., J. Xue, H.S. Bedi, K. Ingles, and D. Oosterhof, 1991: Physical initialization for numerical weather prediction over the tropics. *Tellus*, **43**, 53-81.
- Krishnamurti, T.N., H.S. Bedi, G.D. Rohaly, D.K. Oosterhof, R.C. Torres, E. Williford, and N. Surgi, 1997: Physical initialization. *Atmos-Ocean Special.*, **35**, 369-398.
- Krishnamurti, T.N., H. S. Bedi, and V. M. Hardiker, 1998: An Introduction to Global Spectral Modeling. Oxford University Press., 253 pp.
- Kummerow, C., L. Giglio, 1994: A passive microwave technique for estimating rainfall and vertical structure information from space. Part I: algorithm description. *J. Appl. Meteor.*, **33**, 3-18.
- Kummerow, C., W. S. Olson, and L. Giglio, 1996: A simplified scheme for obtaining precipitation and vertical hydrometeor profiles from passive microwave sensors. *IEEE Trans. Geosci. Remote Sens.*, **34**, 1213-1232.
- Kummerow, C., W. Barnes, T. Kozu, J. Shiue, and J. Simpson, 1998: The Tropical Rainfall Measuring Mission (TRMM) sensor package. *J. Atmos. Ocean. Tech.*, **15**, 809-817.
- Liebe, H. J., 1985: An updated model for millimeter wave propagation in moist air. *Radio Sci.*, **20**, 1069-1089.
- Louis, J. F., 1979: A parametric model of the vertical eddy fluxes in the atmosphere. *Bound. Layer Meteo.*, **17**, 187-202.
- Manabe, S., J. Smagorinsky, and R. F. Strickler, 1965: Simulated climatology of a general circulation model with a hydrologic cycle. *Mon. Wea. Rev.*, **93**, 769-798.
- Olson, W. S., F. J. LaFontaine, W. L. Smith, and T. H. Achtor, 1990: Recommended algorithms for the retrieval of rainfall rates in the tropics using the SSM/I (DMSP-8). Manuscript. University of Wisconsin, Madison, 10 pp.
- Olson, W. S., C. Kummerow, G. M. Heymsfield, and L. Giglio, 1996: A method for combined passive-active microwave retrievals of cloud and precipitation profiles. *J. Appl. Meteor.*, **35**, 1763-1789.

- Roberti, L., J. Haferman, and C. Kummerow, 1994: Microwave radiative transfer through horizontally inhomogeneous precipitating clouds. *J. Geophys. Res.*, **99**, 16707-16718.
- Smith, E. A., J. E. Lamm, R. Adler, J. Alishouse, K. Aonashi, E. Barrett, P. Bauer, W. Berg, A. Chang, R. Ferraro, J. Ferriday, S. Goodman, N. Grody, C. Kidd, D. Kniveton, C. Kummerow, G. Liu, F. Marzano, A. Mugnai, W. Olson, G. Petty, A. Shibata, R. Spencer, F. Wentz, T. Wilheit, and E. Zipser, 1998: Results of WetNet PIP-2 project. *J. Atmos. Sci.*, **55**, 1483-1536.
- Tao, W. K., and J. Simpson, 1993: Goddard cumulus ensemble model. Part I: Model description. *TAO*, **4**, 35-72.
- Wallace, J. M., S. Tibaldi, and A. J. Simmons, 1983: Reduction of systematic forecast errors in the ECMWF model through the introduction of envelope orography. *Quart. J. Roy. Meteor. Soc.*, **109**, 683-718.
- Weng, F., and N. C. Grody, 1994: Retrieval of cloud liquid water using the special sensor microwave imager (SSM/I). *J. Geophys. Res.*, **99**, 25535-25551.
- Wentz, F. J., 1990: West coast storm forecasting with SSM/I, Vol. 1, final technical report, Remote Sens. Syst., Santa Rosa, Calif., 42 pp.
- Wentz, F. J., 1991: User's Manual – SSM/I Antenna Temperature Tapes (Revision 1). Remote Sens. Syst., Santa Rosa, Calif., 70 pp.
- Wilheit, T. T., 1979: A model for the microwave emissivity of the ocean's surface as a function of wind speed. *IEEE Trans. Geosci. Electron.*, **GE-17**, 244-249.
- Yanai, M., S. Esbensen, and J. H. Chu, 1973: Determination of bulk properties of tropical cloud clusters from large-scale heat and moisture budgets. *J. Atmos. Sci.*, **30**, 611-627.

BIOGRAPHICAL SKETCH

Captain R. Thomas Tibbetts was born on April 8th, 1971, in Naples, Florida. On May 1st, 1993, Tom graduated with a bachelor's degree in meteorology from The Florida State University, Tallahassee, Florida. On that same day he completed the Air Force ROTC program at FSU and was commissioned as a 2nd Lieutenant, United States Air Force.

For his first assignment (1994-1995), Tom served as both a Wing Weather Officer and Weather Flight Chief, 93rd Operations Support Squadron, Castle AFB, California. In his second active-duty assignment (1995-1997), Tom filled the role of a Weather Liaison Officer, 78th Operations Support Squadron, Robins AFB, Georgia. During his tour of duty at Robins, Tom deployed in support of Operation Deny Flight, Istres Air Base, France (1995). He also served as the Weather Flight Commander of Riyadh Air Base, Kingdom of Saudi Arabia (1996).

In 1997, Tom was accepted into the Air Force Institute of Technology (AFIT) graduate degree program in meteorology. He subsequently enrolled in The Florida State University to pursue his graduate studies. Upon completion of his thesis, Tom will be reassigned to 12th Air Force, Davis-Monthan AFB, Arizona, where he will develop and provide tropical weather support for the Air Force's Caribbean and South American missions.